ADVANCED MATERIALS
www.advmat.de

Multifunctional Photonic Nanomaterials for Diagnostic, Therapeutic, and Theranostic Applications

Hyemin Kim, Songeun Beack, Seulgi Han, Myeonghwan Shin, Taehyung Lee, Yoonsang Park, Ki Su Kim, Ali K. Yetisen, Seok Hyun Yun, Woosung Kwon, and Sei Kwang Hahn**

The last decade has seen dramatic progress in the principle, design, and fabrication of photonic nanomaterials with various optical properties and functionalities. Light-emitting and light-responsive nanomaterials, such as semiconductor quantum dots, plasmonic metal nanoparticles, organic carbon, and polymeric nanomaterials, offer promising approaches to low-cost and effective diagnostic, therapeutic, and theranostic applications. Reasonable endeavors have begun to translate some of the promising photonic nanomaterials to the clinic. Here, current research on the state-of-the-art and emerging photonic nanomaterials for diverse biomedical applications is reviewed, and the remaining challenges and future perspectives are discussed.

1. Introduction

Fluorescent molecules have been traditionally used for bioimaging to visualize biomolecules from the cellular to the integrative levels.[1] The most conventional imaging agents are fluorophores with a few aromatic rings with several π bonds.[2,3] Small-molecular fluorophores have the advantage of easy chemical modification to tune their optical properties and biological behaviors by altering the molecular structures.[4,5] Diverse fluorescent dyes over a wide range of excitation/emission wavelengths have been synthesized and developed for laboratory usage.[6,7] Despite the extensive investigation of molecular fluorophores, there are significant limitations for further clinical applications due to the low photobleaching threshold, poor stability, and long-term safety issues.[8] To date, only two fluorophores, indocyanine green (ICG)[9] and methylene blue,[10] have been approved for intraoperative imaging by the US Food and Drug Administration (FDA).[11] In this context, one compelling motivation for the development of photonic nanomaterials is to circumvent the current limitation of fluorophores.

The electronic and optical properties of materials on a nanometer scale are significantly influenced by the quantum-confinement effect of the electronic wave functions.[12] In nanoscale semiconductor systems, the energy bands are modified to discrete molecular electronic levels. In noble metals, free electrons in the conduction band can oscillate collectively and form resonance in metallic nanoparticles. The plasmonic oscillation can interact with photons strongly at the metallic surface,[13] enabling the optical properties of nanomaterials to be easily tuned by changing the particle size and shape. A variety of nanomaterials have been widely investigated over the past few decades, for applications toward diagnostics, therapeutics, and theranostics (**Figure 1**). Colloidal semiconductor quantum dots (QDs) have been regarded as potential alternatives to molecular fluorophores owing to their long-term photostability and narrow emission bands.[14] Colloidal gold nanomaterials are the typical example of metal nanomaterials for biophotonic applications in the forms of gold nanospheres, gold nanorods, and hollow gold nanospheres (HAuNSs).[15] Carbon nanomaterials including fullerene, graphene, and carbon nanotubes have also been considered for applications such as biosensors, bioimaging agents, and photothermal therapy.[16] Despite the numerous studies on these nanomaterials, they have suffered from safety issues. To address the safety concerns, biocompatible, biodegradable, and excretable photonic nanomaterials are actively pursued.

Dr. H. Kim
PHI BIOMED Co., #613
12 Gangnam-daero 65-gil, Seocho-gu, Seoul 06612, South Korea
S. Beack, S. Han, M. Shin, Prof. S. K. Hahn
Department of Materials Science and Engineering
Pohang University of Science and Technology (POSTECH)
77 Cheongam-ro, Nam-gu, Pohang, Gyeongbuk 37673, South Korea
E-mail: skhanb@postech.ac.kr
T. Lee, Y. Park
Department of Chemical Engineering
POSTECH
77 Cheongam-ro, Nam-gu, Pohang, Gyeongbuk 37673, South Korea
Dr. K. S. Kim, Dr. A. K. Yetisen, Prof. S. H. Yun
Wellman Center for Photomedicine
Massachusetts General Hospital
65 Landsdowne St., UP-5, Cambridge, MA 02139, USA
Prof. W. Kwon
Department of Chemical and Biological Engineering
Sookmyung Women's University
100 Cheongpa-ro 47-gil, Seoul 04310, South Korea
E-mail: wkwon@sookmyung.ac.kr

DOI: 10.1002/adma.201701460

Here, we chronologically review the development of various photonic nanomaterials, including colloidal semiconductor quantum dots, gold nanomaterials, carbon nanomaterials, polymeric melanoidin,[17] transition-metal dichalcogenides (TMDs),[18] and upconversion nanoparticles (UCNPs).[19] We then describe current research efforts to test and validate their diagnostic and therapeutic utilities. The applications being pursued include fluorescence imaging, plasmon-resonance-based sensing and imaging, photoacoustic imaging, photothermal therapy, photodynamic therapy, and optogenetic therapy. Furthermore, we describe novel, emerging photonic nanomaterials for theranostic applications combining the diagnostic and therapeutic platform technologies. Finally, we discuss several important strategies to improve the clinical feasibility of photonic nanomaterials for the applications to futuristic photomedicine.

2. Photonic Nanomaterials

2.1. Semiconductor Quantum Dots

From the early stage, QDs have been considered as one of the most popular nanomaterials for biophotonic applications. QDs are defined as particles composed of periodic groups of II–VI or III–V semiconductor elements with physical dimensions smaller than the Bohr radius.[20] QDs typically have core–shell or core-only structures with a diameter of 1–10 nm. The core materials are usually inorganic semiconductors, such as CdSe, CdTe, CdS, ZnS, ZnSe, PbS, and PbSe, as well as InP and InGaP without toxic heavy-metal ions.[21] The shell materials are often inorganic semiconductors with a wider bandgap such as ZnS and CdS.[22] The passivation of the core surface with shell materials can protect the core from oxidation and harsh biological environments. In particular, a ZnS shell has been used to prevent the leaching of heavy-metal ions to the surrounding solution.[23] Additionally, the shell capping causes the tunneling of charge carriers into the shell layers. In accordance, absorption and emission are redshifted compared with the core QDs.[24]

Several attractive properties of QDs distinguish them from typical fluorophores for biomedical applications. First, QDs have a relatively high quantum yield over a wide range of absorption and emission wavelengths from the visible to the near-infrared (NIR) range.[25] Second, QDs have a long fluorescence lifetime, ≈10–100 ns, which can be distinguished from short fluorescence signals like cellular autofluorescence in time-gated detection.[26] The typical organic fluorophores have a fluorescence time shorter than 10 ns. Third, the emission bands of QDs are mostly narrow and symmetrical, whereas most fluorophores have red-tailed emission spectra.[27] Fourth, the optical properties of QDs, including the absorption and emission wavelengths, can be controlled by changing their composition, size, size distribution, shape, and surface chemistry.[8] In addition, the size and shape of QDs can be precisely tuned by changing the synthesis temperature and time, and the ligand molecules.

Several kinds of QDs prepared with CdSe, CdS, ZnSe, CdTe, PbS, InP, and InGaP are now commercially available for laboratory or preclinical usage.[28] A robust and reproducible method to synthesize high-quality CdSe/ZnS QDs was developed by Bawendi and co-workers.[29] The synthesis of CdSe cores was

Seok Hyun Yun is a Professor at Harvard University and an affiliated faculty member at MIT (Health Sciences and Technology). He received his Ph.D. degree in physics from KAIST in 1997. His thesis research in fiber optics has led to a $68M-funded startup, Novera Optics, Inc., and he worked for this company as a founding member and engineering manager from 1999 to 2003. In 2003, he moved to the biomedical sector and joined the Wellman Center for Photomedicine at Massachusetts General Hospital and Harvard Medical School. His research interests lie in developing optical techniques and applying them to significant biomedical problems.

Woosung Kwon is an Assistant Professor at Sookmyung Women's University. He received his B.S. in chemical engineering with a minor in Physics (2010) and Ph.D. in chemical engineering (2013) from Pohang University of Science and Technology (POSTECH). He carried out postdoctoral research at Stanford University in 2014. His research interests include (i) development of biocompatible nanomaterials for theragnostic applications, (ii) advancement of functionality of nanomaterials through chemical modification, and (iii) study of the effect of nanomaterials on physiological biochemical processes in living organisms to address nanotoxicological issues.

Sei Kwang Hahn is a SeAh Young Chair Professor in the Department of Materials Science and Engineering at POSTECH. He obtained his B.S. in 1991, M.S. in 1993, and Ph.D. in 1996 from the Department of Chemical and Biomolecular Engineering at KAIST. After working at the LG Chemical group, he carried out postdoctoral research with Prof. Allan Hoffman at the University of Washington. After that, he worked at the Hoffman-La Roche group, Chugai Pharmaceutical Co., in Japan. He was a visiting professor at the Harvard Medical School. His research interests are biomaterials for nanomedicines.

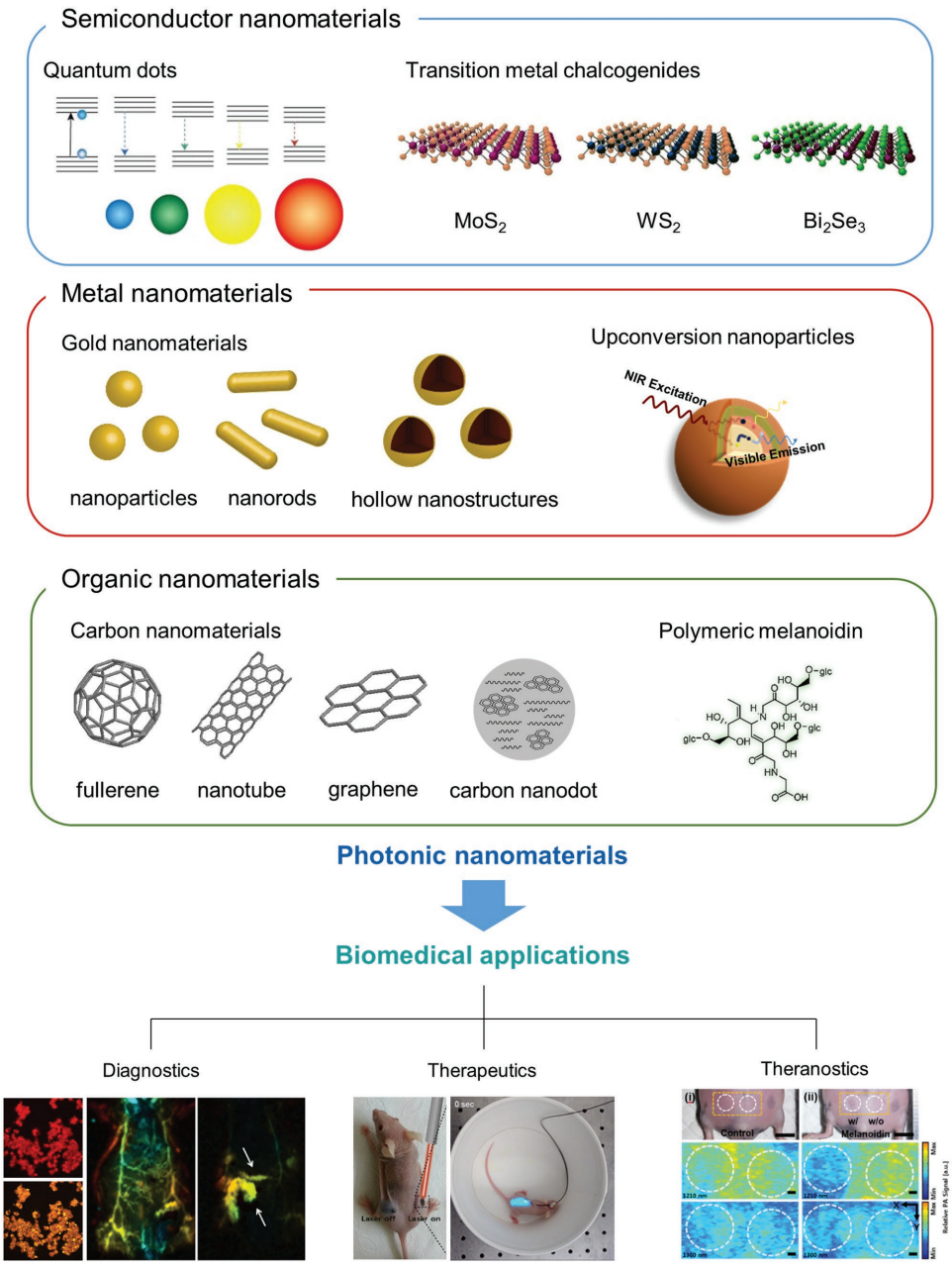

Figure 1. Photonic nanomaterials for diagnostic, therapeutic, and theranostic applications. Theranostics: Reproduced with permission.[17] Copyright 2016, American Chemical Society. Diagnostics: Reproduced with permission.[190] Copyright 2014, American Chemical Society. Therapeutics: Reproduced with permission.[349] Copyright 2013, Nature Publishing Group.

based on the pyrolysis of organometallic precursors, dimethylcadmium and trioctyl phosphine selenide, in a mixture of trioctyl phosphine (TOP) and trioctyl phosphine oxide (TOPO) at high temperature. After reaction, highly crystalline CdSe cores were synthesized with a narrow size distribution of 8–11%.[30] The reproducible reaction to control the size of QDs can contribute to the fine-tuning of optical properties. The CdSe QDs with a wide range of absorption and emission wavelengths, which is dependent on the core size, are shown in **Figure 2**.[28] A ZnS layer can be coated on the surface of QDs by the same growth reaction as that of CdSe cores in TOP/TOPO.[30] The ZnS shells not only protect the core from the surrounding environment, but also improve the yield of photoluminescence (PL).[28]

Because QDs have superior optical properties, including resistance to photobleaching and high/narrow light emission, they are suitable for various bioimaging applications. The QDs synthesized by pyrolysis are hydrophobic and require adequate surface modification for phase transfer to aqueous solution. The surface of QDs can easily be functionalized with hydrophilic ligands by cap exchange. These ligands can facilitate both the solubilization of QDs in aqueous media and the chemical modification with biomolecules.[31] An alternative strategy to achieve

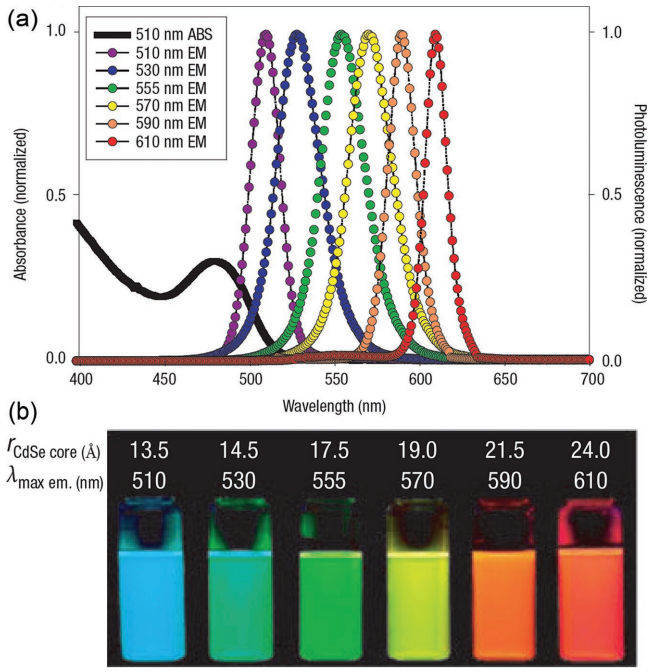

Figure 2. a) Absorption and emission spectra and b) a photograph of six different QDs with different sizes of CdSe cores. In the photograph, all samples were excited at 365 nm with a ultraviolet light source. Reproduced with permission.[28] Copyright 2005, Nature Publishing Group.

high water solubility, stability, and biocompatibility of QDs is silica coating. QDs can be embedded in a siloxane shell and functionalized with groups such as thiol and amine.[32] They exhibit high stability in the aqueous environment and thus have been used as multimodal bioimaging contrast agents, including fluorescence detection of fixed cell and tissue sections,[33] ex vivo live cell imaging,[34] and in vivo imaging in animals.[35] In recent years, QDs have been used as two-photon imaging agents with their very large cross-sections for two-photon action. Moreover, FACS analysis[36] and biosensors using biomolecule-conjugated QDs[37] have been investigated extensively due to the narrow fluorescence emission and easy functionalization of QDs.

Despite the unique optical properties and feasibility of QDs, the cytotoxicity caused by the constituent materials is a major concern for clinical applications. InP and InGaP QDs have been considered as promising candidates without using heavy-metal ions, but have suffered from relatively low PL yields.[38] Thick overcoating with shell materials and efficient surface capping have been attempted to prevent the leakage of heavy-metal ions and the generation of reactive oxygen species (ROS).[39,40] However, core materials detrimental to health and environment have ultimately precluded the FDA approval of QDs for further clinical applications. Recently, various alternatives to QDs have been investigated for biomedical applications as described in the following sections.

2.2. Gold Nanomaterials

The medicinal use of gold has a long history. Gold salts and red colloidal gold have been traditionally used for the treatment of rheumatoid arthritis and nerve diseases since 2500 BC.[41,42] Gold as a nanomaterial was used in decorative art, stained glass, and alchemy in the Middle Ages. An early investigation of colloidal gold as a nanomaterial was reported by Michael Faraday.[43] He reduced gold salts with phosphorous in carbon disulfide and reported that the resulting gold colloidal solution showed a ruby red color, which could be distinguished from the golden yellow color of bulk gold. Since then, gold nanomaterials have been extensively investigated to identify the unique electrical and optical properties. The phenomena appear to be caused by (localized) surface plasmon resonance (SPR).[44] Gold nanoparticles and heavily doped semiconductors have free electrons. Under light irradiation, the electric field causes the collective coherent oscillation of conduction-band electrons on the surface of the nanoparticles. The resonance can cause light scattering, a surface plasmon absorption converting the incident light to heat, and a strong local electromagnetic field enhancing the optical signals of fluorescence and Raman scattering.[15] In particular, SPR peaks in the NIR region are important in biomedical applications due to the deep tissue-penetration depth.[10] The optical properties of gold nanomaterials are governed by the position and shape of SPR peaks, and the peaks can be controlled by changing the size, shape, and aspect ratio of the nanostructures.

Gold nanomaterials possess particular advantages that support their suitability as a nanoscale platform for biomedical applications. First, the synthesis methods of gold nanostructures are robust with a high yield.[45] Second, the reactions can be generally performed in aqueous solution, which does not require further phase transfer to water for biomedical applications. The simple and fast preparation of gold nanostructures has enabled relevant studies in the early stage. Moreover, the surface of gold has an affinity to compounds containing S, P, or N. Accordingly, gold nanomaterials can be readily modified with ligands having functional groups such as thiols, phosphines, and amines.[46] Gold nanomaterials modified with bioinert polymers, such as poly(ethylene glycol) (PEG) and hyaluronic acid (HA), can be stabilized in the biological environment.[47] In the case of conjugation with biologically functional moieties such as antibodies, oligonucleotides, and peptides, the nanomaterials can efficiently interact with biological systems, rendering applications toward biosensors[48] and targeted delivery.[49] The bioinert nature of gold is also beneficial for biomedical applications. Although there are toxicological concerns about the effect of gold nanomaterials on the induction of oxidative stress and genotoxicity, they are still considered highly biocompatible and less cytotoxic than other nanomaterials.[50] The synthesis, optical properties, and biomedical applications of several representative gold nanostructures are reviewed in the following sections.

2.2.1. Gold Nanoparticles

There are three kinds of gold nanostructures that are round in shape: gold nanoclusters, gold nanoparticles, and gold nanospheres.[15] Gold nanoclusters are molecular species composed of a few to several hundred Au atoms with a size smaller than 2 nm. Gold nanospheres are spherical nanocrystals with a single-crystal structure without a sharp corner or edge on the surface.

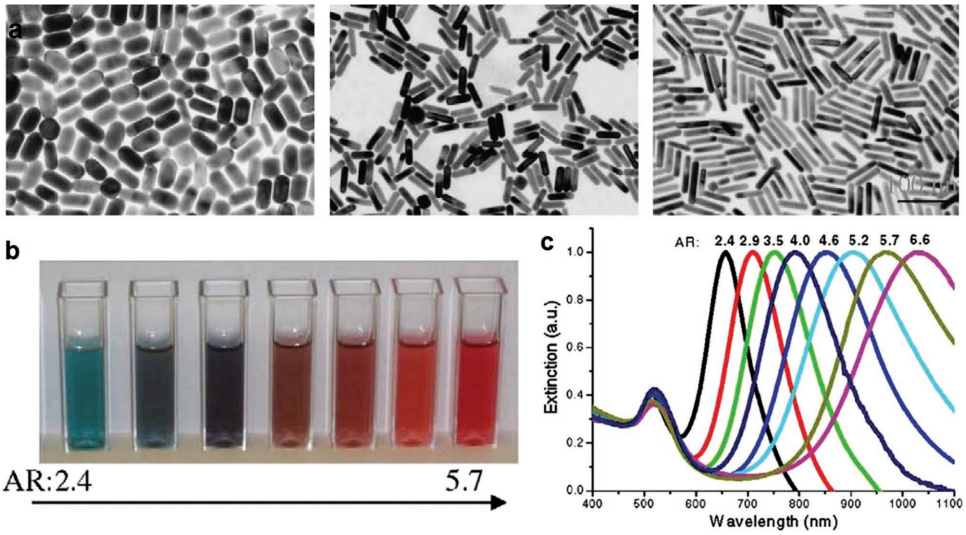

Figure 3. Tunable optical properties of gold nanorods achieved by changing the aspect ratio. Gold nanorods with different aspect ratios exhibit different dimensions as shown by a) TEM, b) different colors, and c) different SPR bands (scale bar: 100 nm; AR: aspect ratio). Reproduced with permission.[60] Copyright 2010, Elsevier.

Herein, we describe gold nanoparticles with polycrystalline nanostructures in a quasispherical shape as the most common gold nanomaterials for biomedical applications. Gold nanoparticles can be synthesized by reduction of $HAuCl_4$ in the solution phase. There are two representative methods: the Turkevich method and the Brust–Schiffrin method. Turkevich used citrate as both a reducing agent and a capping agent to synthesize 20 nm particles.[51] Frens reported the control of the particle size by changing the citrate to gold ratio.[52] In the Brust–Schiffrin method, $HAuCl_4$ is reduced with sodium borohydride ($NaBH_4$) using alkanethiol as a capping agent.[53] The particle size can be controlled by changing the ratio of $HAuCl_4$ to thiol. Gold nanoparticles with a size of 10–100 nm have SPR peaks at 520–570 nm in the visible region, which is the origin of ruby red color of the gold solution.[54] Gold nanoparticles exhibiting SPR in the visible region can be used as colorimetric biosensors to detect DNAs, metal ions, proteins, and small molecules.[55] In addition, they can be used for dark-field light-scattering imaging by delivering the nanoparticles to the target region.[56]

2.2.2. Gold Nanorods

Despite the wide applications of gold nanoparticles, the presence of SPR bands only in the visible region has been the major drawback for further development. Remarkably, the SPR bands can be extended to the NIR region by changing the shape and aspect ratio of the gold nanomaterials. Gold nanorods were developed as one of the resulting achievements. Gold nanorods have an anisotropic shape and free electrons can oscillate along both the long and short axes. Thus, gold nanorods have two SPR bands: a weaker one in the visible region and a stronger one in the NIR region.[57] The band position in the NIR region is very sensitive to the aspect ratio. Murphy and co-workers and El-Sayed and Nikoobakht reported a typical synthesis method by the seed-mediated growth using hexadecyltrimethylammonium bromide (CTAB) as a capping agent.[58,59] CTAB can preferentially bind to specific crystal facets on spherical gold seed particles and induce the formation of nanorods. The aspect ratio can be controlled by changing the concentration of silver ions, and the resulting gold nanorods show color changes from blue to red (**Figure 3**).[60] The SPR bands of gold nanorods in the NIR region show a deep penetration into biological tissues, enabling in vivo biomedical applications, such as surface-enhanced Raman scattering (SERS) imaging[57] and photothermal therapy (PTT).[61]

2.2.3. Other Gold Nanomaterials

A variety of gold nanostructures have been developed, including gold nanoplates with different 2D shapes, including triangles (**Figure 4**a), hexagons (Figure 4b), truncated triangles, and circles.[62] Gold nanoplates are enclosed by two relatively large basal planes with low aspect ratios. They can be synthesized by wet-chemical methods using the two-stage mechanism of nucleation and growth. In the nucleation step, various surfactants like poly(vinylpyrrolidone),[63] CTAB,[64] and aspartate[65] act as crystal-face-blocking ligands and seeds are generated with planar defects. Then, lateral growth of the seeds can be induced to form plates with different edge lengths. The SPR peaks of gold nanoplates are in the visible and the NIR range, and the optical properties of the nanoplates can be tuned by changing the edge length, thickness, and corner sharpness.[62]

Other types are hollow gold nanostructures (HAuNSs) (Figure 4c) and gold nanocages (Figure 4d). HAuNSs have been considered as potential theranostic agents due to the capacity for carrying other molecules and the strong absorption of NIR light for photothermal applications.[66] The most popular synthesis method for HAuNSs is the galvanic replacement reaction. HAuNSs are generally prepared by the galvanic

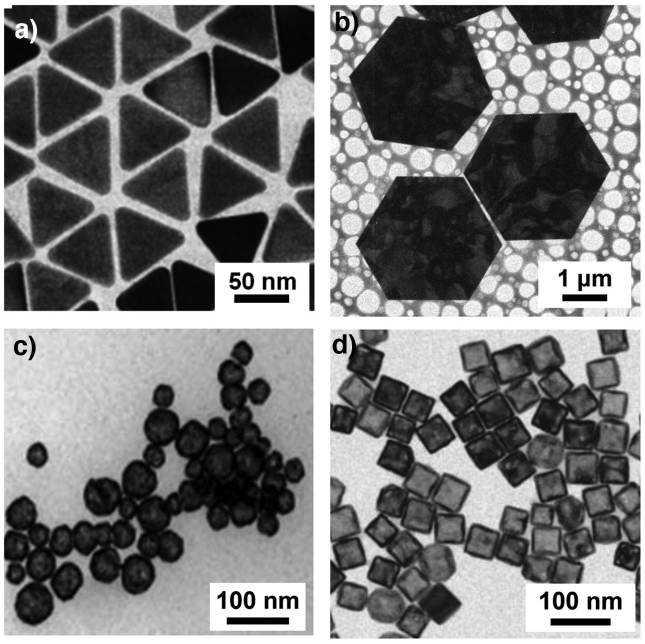

Figure 4. TEM images of a) triangular gold nanoplates, b) hexagonal gold nanoplates, c) hollow gold nanospheres, and d) gold nanocages. a) Reproduced with permission.[15] Copyright 2010 American Chemical Society. b) Reproduced with permission.[64] Copyright 2010, Hindawi. c) Reproduced with permission.[68] Copyright 2011, Royal Society of Chemistry. d) Reproduced with permission.[70] Copyright 2010, John Wiley&Sons.

replacement reaction between cobalt nanoparticles and chloroauric acid.[67,68] The position of the surface plasmon band can be tuned between 550 and 820 nm by changing the particle size and wall thickness with reducing and capping agents.[69] Gold nanocages with hollow interior and porous walls can be prepared using silver nanocubes as sacrificial templates and Au(III) or Au(I) as precursors to form gold shells.[70] The shapes and dimensions of the resulting nanostructures can be controlled by varying the ratio of gold precursor to silver nanocube. A diverse nanocage has a different SPR peak at wavelengths between 400 and 1200 nm.[71]

2.3. Carbon Nanomaterials

Since the incidental discovery of fullerene by Smalley and coworkers in 1985,[72] carbon nanomaterials have been widely investigated for various applications. Further studies realized the discovery of other nanosized carbon allotropes, such as carbon nanotubes (CNTs), graphene, carbon dots (C-dots), and nanodiamonds.[73–76] Each carbon nanomaterial exhibits a unique structure owing to the versatile carbon sp^2- and sp^3-hybridized orbitals. The sp^2-hybridized orbitals enable fullerene, CNTs, and graphene to form hollow spheres, pipes, and 2D honeycomb structures, respectively. In contrast, C-dots are carbon nanoparticles less than 10 nm that consist of a mixture of sp^2 and sp^3 carbons. Nanodiamonds comprise sp^3 carbon atoms on a nanometer scale. Due to the quantum-confinement effect caused by the nanoscale size, carbon nanomaterials exhibit some distinct electrical, magnetic, optical, mechanical, and chemical properties. These properties allow the applications toward energy storage, catalysis, and biomedicine.[77–79] In the following, we describe the structures and properties of each carbon material especially in terms of photonic applications.

2.3.1. Fullerene

Fullerene is a carbon molecule in the forms of hollow spheres, ellipsoids, and tubes. Among the fullerenes, C_{60} is the famous structure, honored with a Nobel Prize in 1996. C_{60} is a hollow sphere composed of 12 pentagonal and 20 hexagonal carbon rings with a van der Waals' diameter of 1.1 nm. C_{60} is synthesized by the evaporation of graphite using laser and heat or by the organic method using aromatic precursors.[72,80] The synthesized C_{60} can be renovated by posttreatments, which include functionalization and encapsulation. The functionalization involves the covalent bridging with ligands, which confer water solubility or biocompatibility to C_{60}.[81,82] The encapsulation is performed by noncovalent surrounding of C_{60} with amphiphilic host molecules.[83] Posttreatments have provided C_{60} with biocompatibility and enabled selective targeting to certain biomarkers, both of which are necessary for theranostic applications. Posttreatments are known to improve the fluorescence quantum yield. After stirring with tetraethylene glycol and lithium hydroxide as a catalyst, C_{60} becomes soluble in water with increased photoluminescence, which is tunable by changing the amount of C_{60}.[84]

2.3.2. Carbon Nanotubes

As a pipe-type fullerene, CNTs show cylindrical nanostructures that are a roll of single or multiple graphitic sheets. Because these carbon allotropes have unusual mechanical, electrical, optical, and thermal properties, they have been investigated for biomedical, electronic, and electrochemical applications.[85] CNTs are also appropriate for theranostic applications owing to their unique photonic properties. CNTs can be synthesized by arc discharge, laser ablation, plasma torch, and chemical vapor deposition.[73,86–88] CNTs with a single rolled graphitic layer are called single-walled CNTs (SWCNTs) and CNTs with several rolled graphitic layers are called multiwalled CNTs (MWCNTs). The diameter of the cylinder and the direction of the rolling up of the graphitic layers determine the bandgap of the CNT, which varies from 0 to 2 eV and influences the electronic behaviors of metallic or semiconducting CNTs. For semiconducting nanotubes, it has been simulated and proven that the bandgap energy is inversely proportional to the tube diameter.[89–91]

Semiconducting SWCNTs are photoresponsive due to their bandgaps. They can absorb light in the visible (400–750 nm) and NIR-I (750–1000 nm) regions, and then emit NIR-II light (1000–1700 nm) with nonradiative relaxation in the form of heat.[92] The NIR-I and NIR-II windows are important for biomedical imaging because the radiation in these windows has high transparency, low absorption, reduced scattering, and minimal autofluorescence from biological tissues in the body.[93] SWCNTs have been used as photosensitizers (PSs)

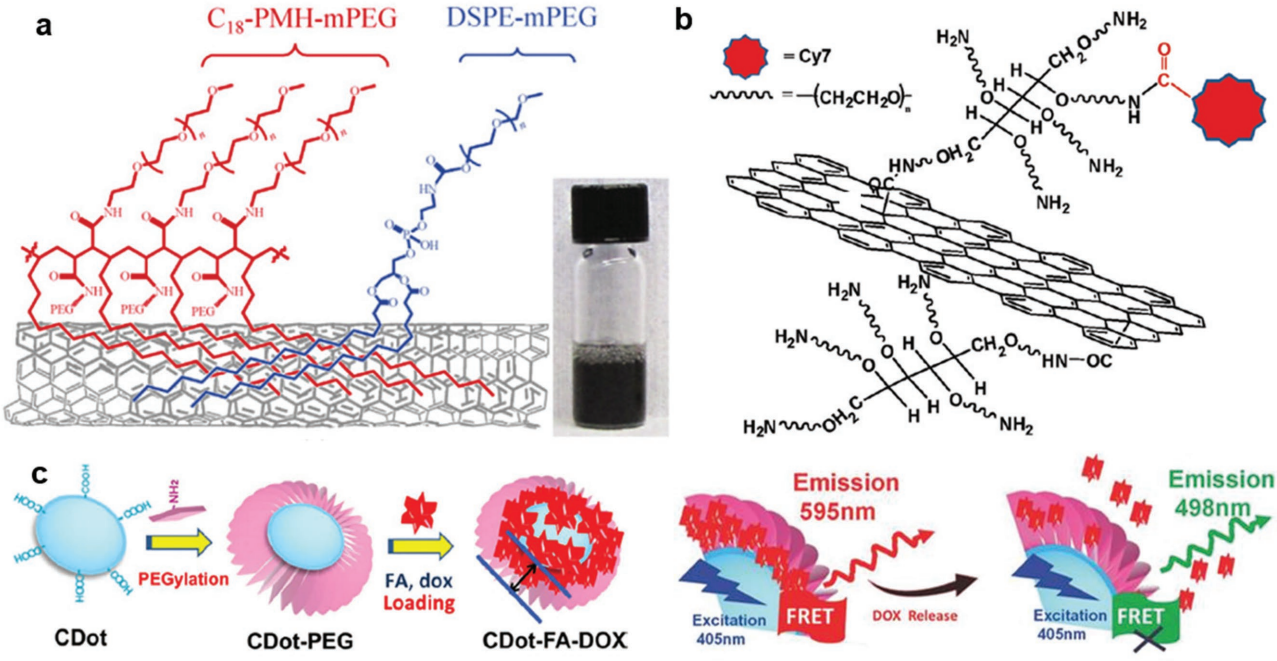

Figure 5. a) Schematic illustration of SWCNTs functionalized with poly(maleic anhydride-*alt*-1-octadecene)-methyl-PEG (C_{18}-PMH-mPEG) and 1,2-distearoyl-phosphatidylethanol amine-methyl-PEG (DSPE-mPEG) in a suspension (inset: a photo of a functionalized-SWCNT suspension in water). Reproduced with permission.[94] Copyright 2010, Springer. b) A scheme of nanographene sheets with PEG functionalization and Cy7 labeling. Reproduced with permission.[118] Copyright 2010 American Chemical Society. c) A schematic illustration for the surface coupling chemistry (left) and proposed FRET mechanism (right) for FRET-C-dot-drug delivery system. Reproduced with permission.[139] Copyright 2013, John Wiley&Sons.

for photothermal and photodynamic therapy (PDT).[94,95] Welsher et al. synthesized SWCNTs functionalized with PEGylated phospholipids, which were biologically nontoxic and long circulating with intrinsic NIR photoluminescence (**Figure 5**a).[96] SWCNTs have also been used as fluorophores to visualize the targeted structural and molecular features of living systems.[97,98] CNTs have been used for conjugation with bioactive molecules through π–π stacking for chemotherapy and gene therapy.[99–101] Despite these advantages of CNTs, the critical safety issue is still controversial with conflicting opinions.[102]

2.3.3. Graphene Oxide

Graphene is a 2D material composed of honeycomb hexagonal carbon atoms with sp^2 hybridization. Since the first mechanical exfoliation with a Scotch tape to find graphene,[74] numerous preparation methods have been developed including mechanical and chemical exfoliation,[74,103,104] unzipping of CNTs,[105,106] bottom-up epitaxial growth,[107,108] and chemical synthesis.[109] Graphene is known to have a zero bandgap.[110] Dirac fermions are defined as massless and ultrarelativistic charge carriers that move within the graphene layers and result in high carrier mobility,[111,112] high thermal conductivity,[113] ambipolar electric field effect,[74] and quantum Hall effect at room temperature.[114] The large surface area, high mechanical flexibility, and chemical versatility are also the important advantages of graphene.

While graphene is less suitable for theranostic applications, graphene oxide (GO) has been extensively exploited for theranostic applications due to its strong fluorescence emission by the heterogeneous atoms of GO. The fluorescence emission range of GO is very wide from the ultraviolet to NIR. The origin of GO fluorescence is electronic transitions in the non-oxidized sp^2 carbon atom region and the boundary of oxidized carbon atom region.[115] Additionally, GO has been used for target cell imaging with the NIR-I fluorescence,[116] photoacoustic (PA) imaging with acoustic waves from the conversion of absorbed photons in GO,[117] and PTT with the NIR radiation-induced heat.[118–121] Yang et al. synthesized nanographene-sheet–PEG (NGS–PEG) by conjugating PEG to GO (Figure 5b). The NGS–PEG solution showed a rapid raise of temperature during 808 nm laser irradiation, enabling ultraefficient PTT.

2.3.4. Carbon Dots

C-dots, called carbon nanodots or carbon quantum dots, are an emerging class of carbon nanomaterials. C-dots are usually quasispherical carbon nanoparticles less than 10 nm with adequate surface passivation.[75,122] C-dots are composed of sp^2 and sp^3 carbon atoms with other heterogeneous atoms such as hydrogen, oxygen, and nitrogen in the form of sp^2 carbon embedded in amorphous sp^3 carbon atoms.[122] High-resolution transmission electron microscopy (TEM) has shown the crystalline lattices of sp^2 carbon atoms. Since the first discovery of C-dots during the purification of SWCNTs,[123] many scientists have investigated the synthetic methods and characteristics of C-dots. C-dots can be synthesized with various precursors of graphite,[124,125] CNT,[123,126] glycerol,[127] glucose,[128] citric

acid,[129] and aromatic compounds[130] by laser ablation,[131] oxidative acid treatment,[124,132] hydrothermal treatment,[128] electrochemical oxidation,[125] and organic synthesis.[129,130] C-dots can be surface modified to control their chemical, optical, and electrical properties.[133,134]

The optical properties of C-dots are extraordinary among carbon materials with a light emission range from deep UV to NIR depending on the excitation.[135–137] The fluorescence of C-dots can be enhanced by the quantum-confinement effect, surface energy traps, and energy states with edge defects.[138] The various energy states in C-dots enable several fluorescence emissions, such as normal one-photon down-conversion fluorescence, two-photon and multiphoton fluorescence,[139–141] and upconversion fluorescence.[138,142] C-dots with a large surface area show outstanding optical properties with biocompatibility for theranostic applications. One such application is the combination of one-photon fluorescence imaging and PDT.[143,144] Others include two-photon fluorescence imaging and drug delivery.[139,145] Tang et al. demonstrated the facilitated real-time monitoring of drug release using Förster resonance energy transfer (FRET) signals of C-dots (Figure 5c).

2.3.5. Nanodiamonds

Nanodiamonds are colloidal diamond particles with a size of 2–10 nm.[76] Compared with other carbon nanomaterials, nanodiamonds, which contain a rack of sp^2 carbon atoms, are photoresponsive in different ways. The origin of fluorescence in nanodiamonds is the defect center frequently found in diamonds. The nitrogen vacancy center, as one type of defect centers, consists of a substitutional nitrogen atom with an adjacent carbon vacancy.[146,147] Nanodiamonds are known to be relatively less toxic than other carbon materials and highly resistant to photobleaching[147] with a high fluorescence quantum efficiency of 0.7–1.0.[148,149] With these promising characteristics, nanodiamonds can be used for the fluorescent imaging of subcellular structures and certain biomarkers,[150,151] drug and gene delivery,[152,153] and tissue engineering.[154]

2.4. Polymeric Melanoidin

Melanoidin is generally known as a nonenzymatic browning product obtained by the Maillard reaction.[17,155–157] Melanoidin is a heterogeneous polymer that is relatively hydrophilic and negatively charged. However, melanoidins obtained by the complex condensation process between proteins and polysaccharides in protein-rich foods are largely insoluble and possess a dense network structure with a high molecular weight. The Maillard reaction is a heat-based food transformation or the condensation process between amino acids and the aldehydes of reducing saccharides.[17,155–157] In the early stage, glucose or fructose reacts with a free amino group to produce the condensation product, an N-substituted glycosylamine. This product immediately makes the Amadori rearrangement product (ARP). ARP is degraded by 1,2-enolization to produce furfural or hydroxymethylfurfural at pH values below 7. Above pH 7, ARP is mainly degraded by 2,3-enolization. All these chemical products are highly reactive and participate in further reactions. The final products, the so-called melanoidins, are synthesized by cyclization, dehydration, retroaldolization, rearrangement, isomerization, and further condensation (**Figure 6**). Melanoidin can be found in processed foods such as coffee, dried fruit, and soy sauce.[158–160] The type of melanoidins is dependent on the sugar and amino acid including glucose–glycine, glucose–histidine, glucose–alanine, and coffee melanoidins. Melanoidin has no precisely defined chemical structure and size due to various starting materials and synthesis methods. The basic structure of glucose melanoidin was suggested as shown in Figure 1. Melanoidin has remarkable functional properties of antioxidant activity, biodegradability, biocompatibility, light absorption, and metal-binding affinity.[17,158,159]

Many studies on melanoidins are related to the antioxidant properties, antimicrobial properties, or chelating metals.[161] Recently, melanoidins have been applied to biomedical photonic research.[17,155] First, an N-doped C-dot was synthesized using melanoidins.[155] Because the starting materials to synthesize melanoidins are glucose and various amino acids, the physicochemical properties of C-dots can be controlled by changing the type of used amino acids. C-dots have high photoluminescence, water solubility, and biocompatibility with easy functionalization. In addition, C-dots have the potential for multicolor luminescence and long-term cellular imaging. Melanoidin has also been applied to PA imaging and PTT using light-responsive and biodegradable properties.[2] Unlike other synthetic methods, melanoidin was synthesized with glucose and glycine (GG) at body temperature and physiological pH. To enhance the light-responsive heat-generation effect, GG-melanoidin was chelated with Fe^{3+}. GG-melanoidin generated enough heat for PTT depending on the light wavelength, power, and illumination time. Using the property, GG-melanoidin was applied to PA tomography for lymph-node imaging, and PTT for tumor ablation and lipolysis.[17]

2.5. Transition-Metal Dichalcogenides

Following the extensive research into graphene, other 2D materials have attracted great attention in recent years. In particular, layered TMDs have lattices of metal atoms (M), such as Mo and W, sandwiched between two chalcogen atoms (X), such as S and Se, with an MX_2 stoichiometry such as MoS_2, TiS_2, TaS_2, WS_2, and $MoSe_2$. The typical structure is shown in **Figure 7**a.[162] In nature, while the M—X bonds are covalent within the layer, these layered TMDs usually have a stacked 3D bulk crystal structure with van der Waals' forces between each layer. Accordingly, bulk TMDs can be exfoliated to single or a few layers by physical or chemical methods to produce layers with a thickness of 6–7 Å as shown in Figure 7b.[163–166] TMDs have been exploited for biomedical applications to biosensors, bioimaging, drug delivery, and cancer therapy.[167]

Originally, mechanical exfoliation using an adhesive Scotch tape was a popular method to fabricate monolayer 2D nanosheets. This method was regarded as the most efficient way to produce highly crystalline clean thin nanosheets of layered materials. However, this technique suffered from limited scale-up and difficult size control.[168] To utilize nanosheets in

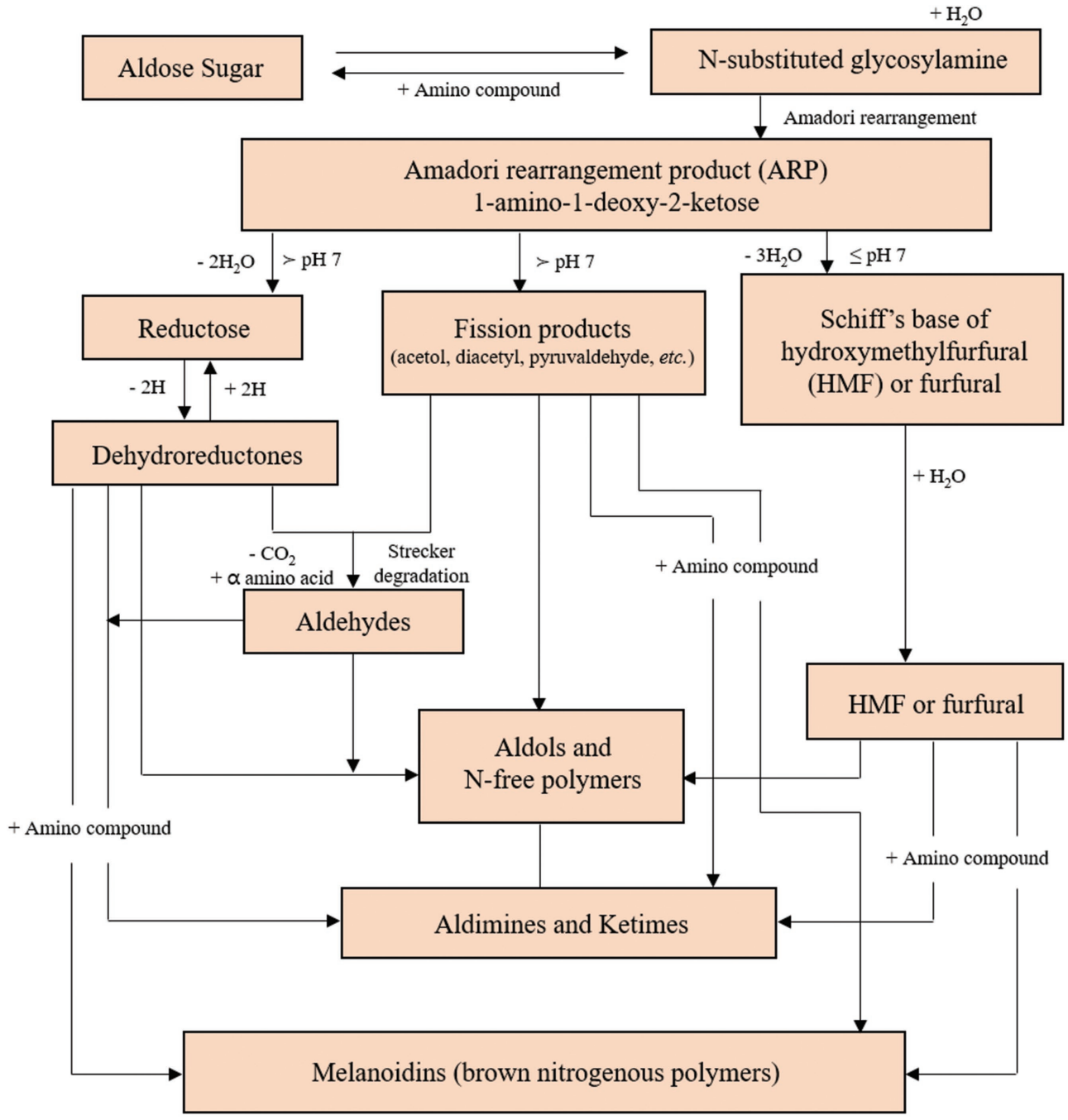

Figure 6. The Maillard reaction scheme. Adapted with permission.[160] Copyright 2001, Elsevier.

biomedicine, chemical exfoliation has been widely explored to produce uniform monolayer TMD nanosheets through bulk production for further applications. Lithium-ion (Li^+)-based intercalation of bulk TMD materials has been regarded as an effective method for the high-yield production of TMD nanosheets.[169] Recently, simple exfoliation methods have been reported, using organic solutions including *N*-methylpyrrolidone or dimethyl sulfoxide.[170] To reduce its size by the strong quantum-confinement and edge effects, several exfoliation processes have been reported, such as the ultrasonication of bulk crystal,[171] thermal ablation of nanosheets in organic solvents,[172] and the electrochemically induced Fenton reaction of nanosheets.[173] However, for the large-scale production of monolayers, aqueous exfoliation has advantages over exfoliation in organic solvents. Sodium cholate as a surfactant was reported to prevent aggregation by the large surface energy, enabling the exfoliation of WS_2, $MoTe_2$, $MoSe_2$, $NbSe_2$, and $TaSe_2$ to monolayers in aqueous solution.[174]

Several recent studies have found that many TMDs have a transition from an indirect bandgap to a direct bandgap from

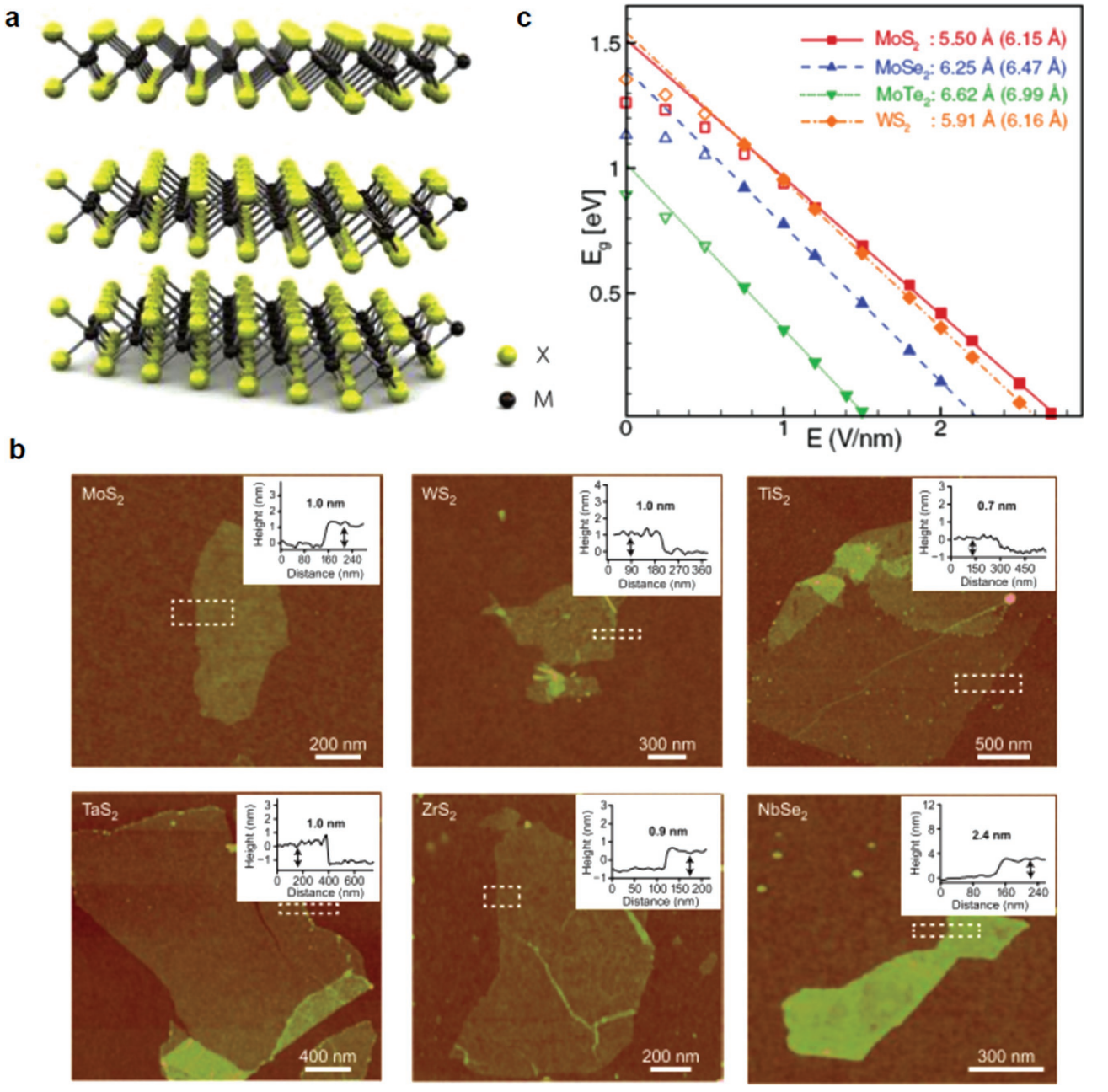

Figure 7. a) 3D schematic representation of a typical MX_2 structure with the metal atoms (M) in gray and the chalcogen atoms (X) in yellow. Reproduced with permission.[162] Copyright 2011, Nature Publishing Group. b) Atomic force microscopy images of TMDs on SiO_2 substrates. The insets represent the height profiles of the nanosheets. Reproduced with permission.[194] Copyright 2013, Nature Publishing Group. c) Plots of bandgap E_g versus applied electric field E for MoS_2, $MoSe_2$, $MoTe_2$, and WS_2. Reproduced with permission.[177] Copyright 2011, American Physical Society.

the bulk to monolayer states. The change of layer number causes a quantum-confinement effect of charge carriers only in the *X*- and *Y*-directions, which results in extraordinary photoluminescence.[175,176] In the case of MoS_2, the indirect bandgap of 1.3 eV in the bulk becomes 1.8 eV in the monolayer state. The 3.16 eV bandgap of bulk WS_2 becomes 2.1 eV in the monolayer state. The bandgap energies (E_g) of some materials are shown in Figure 7c.[177] Several studies have shown that other MoX_2 or WX_2 compounds have similar indirect-to-direct transitions at the monolayer from the bulk, resulting in an extraordinary enhancement of photoluminescence.[178,179] This unique feature has opened new applications of TMDs to optoelectronics. However, there have been limited studies using TMDs in the biomedical fields. Recently, among the numerous kinds of TMD nanosheets, monolayer quantum-sized MoS_2 nanosheets have shown high photoluminescence by the indirect-to-direct-bandgap transition based on hybridization between the d orbitals of the Mo atoms and the p_z orbitals of the S atoms. In addition, size-dependent photoluminescence was reported from red to blue light.[180]

Similar to MoS_2, WS_2 also shows strong fluorescence at the nanoscale with a quantum yield of ≈4%.[181]

Recently, TMDs have been investigated for diagnostic and therapeutic applications. They have been used for fluorescence imaging, PA tomography, and computed tomography (CT).[182] They have also been used for drug delivery, PTT, and PDT. To optimize the therapeutic treatment and monitor the response, image-guided therapy has been proposed as an emerging strategy for personalized theranostics.[183] Owing to their high absorbance in the NIR region, these materials can be utilized as photothermal agents for cancer therapy. With a large surface-area-to-volume ratio and a strong hydrophobic interaction with chemical drugs, TMD materials have been investigated as a drug-delivery platform for combined chemo- and photothermal cancer therapy.[184–186] Several TMDs, such as WS_2 and Bi_2Se_3, which have high-Z elements, have been exploited as X-ray CT imaging agents. Recent studies have also demonstrated that magnetic nanoparticles or radioactive metal ions (e.g., Fe^{3+}, Co^{2+}, Ni^{2+}, and Gd^{3+}) can be used with TMDs for magnetic resonance or nuclear imaging.[187] In addition, in the NIR range, TMDs show a high light-to-heat conversion efficiency. Chou et al. reported that MoS_2 nanosheets showed a higher NIR absorption capacity than graphene or gold nanorods.[188]

The biocompatibility, toxicity, and physiological stability are important factors for further applications of TMDs to the biomedical fields. Similar to other nanoparticles, toxicity of TMDs is highly influenced by their physicochemical properties, including sheet size, morphology, zeta potential, and hydrophilicity.[182,189,190] Although their safety is unconfirmed, a feasibility study is in progress to assess their potential for clinical applications. It has been demonstrated that several TMD materials have lower toxicity to living cells than GO.[191] In particular, TMD nanosheets containing sulfur (e.g., MoS_2 and WS_2) have intrinsic sulfur vacancies and defects. These sites were reported to show high molecular affinity for thiol ligand modification.[192] With the inclusion of thiol edge absorption, chitosan, PEG, or other protein-functionalized TMD nanosheets have shown no obvious in vitro or in vivo toxicity.[184] Although the application of TMD nanomaterials to biomedical fields is still in an early stage, it is believed that TMDs will provide a great opportunity to overcome the technological barriers of 2D materials for diagnostic, therapeutic, and theranostic applications.[193,194]

2.6. Upconversion Nanoparticles

For most luminescence nanomaterials, the emission spectrum is always located at a longer wavelength position than the excitation spectrum. In other words, the excitation energy of photons is higher than the emission energy. This rule is defined as Stokes' law and the energy loss during fluorescence emission is known as the Stokes shift. Most fluorophores, including organic dyes and QDs, typically follow Stokes' law. In some particular cases, the emission energy is higher than the excitation energy. This is anti-Stokes-type luminescence, which occurs through three nonlinear optical processes of second-harmonic generation (SHG), simultaneous two-photon absorption (STPA), and upconversion (**Figure 8**).[195] SHG is a process in which photons with the same frequency are effectively combined to produce new photons with twice the energy (Figure 8a). STPA is a process in which two long-wavelength photons are simultaneously absorbed and excited by two-photon absorption (Figure 8b). In comparison to the SHG and STPA processes in which the intermediate excited states are virtual, upconversion involves the real long-lived intermediate excited states and efficiently converts low-energy photons to high-energy photons.[196] This concept was first proposed by Nicolaas Bloembergen, the Dutch–American physicist, in 1959.[197] Along with their unique optical properties, UCNPs eliminate autofluorescence and light scattering in biological specimens under NIR excitation, enabling deep tissue bioimaging.[198,199] The optical properties are caused by photon upconversion, which is the nonlinear process of sequential absorbance and energy transfer with two or more NIR photons.[200] Photonic nanomaterials that can undergo upconversion phenomena include

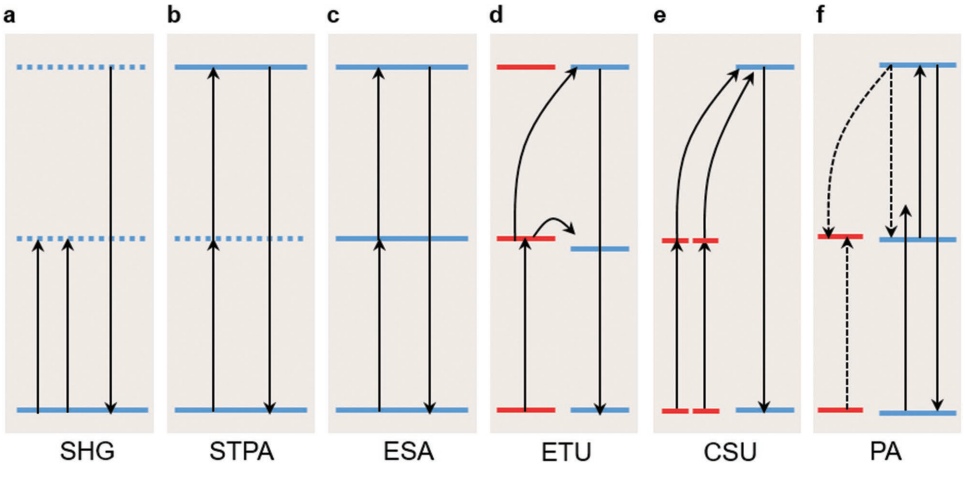

Figure 8. Principal anti-Stokes processes for a) second harmonic generation and b) simultaneous two-photon absorption. c) Upconversion for excited states absorption, d) energy-transfer upconversion, e) cooperative sensitization upconversion, and f) photon avalanche. Reproduced with permission.[195] Copyright 2015, Springer. Reproduced with permission.[196] Copyright 2013, Royal Society of Chemistry. Reproduced with permission.[201] Copyright 2015, Nature Publishing Group.

multienergy levels in accordance with the d orbitals of transition metal ions or the f orbitals of lanthanide ions (Ln^{3+}). The optical properties have indicated that upconversion-nanomaterial systems are a promising light-delivery nanoplatform for bioimaging, PDT, and PTT applications.

The physical energy transfer mechanism for the upconversion luminescence includes excited-state absorption (ESA), energy-transfer upconversion (ETU), cooperative sensitization upconversion (CSU), and photon avalanche (PhA).[201] Energy upconversion is usually dominated by either the ESA or ETU process, in which long-lived intermediate excited states store the energy. In the case of the ESA process in Figure 8c, the energy transition happens after the absorbance of a low-energy photon from the ground state to a metastable intermediate excited state. Then, the second pump photon is absorbed and promotes the excited electrons from intermediate excited states to higher excited states. Consequently, upconversion luminescence occurs by the drop-back of the electrons to the ground state. The ESA process requires an adequate population of the metastable intermediate states to capture the second photon with a high efficiency. Thus, the energy upconversion of ESA takes place in the case of lanthanide-based UCNPs (Er^{3+}, Ho^{3+}, Tm^{3+}, and Nd^{3+}) with sources of high pumping power. Photon upconversion strongly occurs from the contribution of the ETU process, which is based on a sensitizer–activator system such as Yb^{3+}–X^{3+} (where X = Er, Tm, or Ho) couples doped in an inorganic host matrix. In the typical process of ETU (Figure 8d), an electron of the sensitizer ion is excited from the ground state to the intermediate state by the absorbance of photons. Then, the energy of the electrons is transferred to the activator ions during the relaxation of the sensitizer ions and promotes the ions to excited states. Thus, the dopant concentration strongly affects the upconversion efficiency of the ETU process. In comparison with the ETU process, the upconversion efficiency of the ESA process does not depend on the dopant concentration because of the single-ion characteristics. The CSU is a process that involves the interaction of three center ions, and some involved ions can be recognized as sensitizers in the ETU process (Figure 8e). The upconversion efficiency of the CSU process is commonly lower than that of the ESA or ETU process. In addition, the PhA process has a special pump mechanism that requires a pump intensity above a specific threshold (Figure 8f).[195]

Especially, lanthanide-ion-doped upconversion nanomaterials with photophysical stability have been extensively investigated for biophotonic applications. Upconversion luminescence nanoparticles can be classified in terms of their energy-transfer mechanisms, chemical compositions, and synthesis conditions. Typical UCNPs are composed of an inorganic crystalline host matrix and trivalent doped lanthanide ions (sensitizer ions and activator ions). The $4f^n$ electronic configurations of the lanthanide ions are divided by electronic repulsion and spin–orbit coupling, which induces a rich energy-level pattern and photon upconversion.[201] The 4f electrons of the lanthanide ions are partially filled and shielded by the completely filled outer $5s^2$ and $5p^6$ subshells, which results in weak electron–phonon coupling and leads to sharp and narrow f–f transition emission lines.[195,202] A crystalline host matrix may offer significant advantages for photon upconversion due to the low-phonon-energy environment. The optical properties and luminescence quality of UCNPs can be controlled by changing the synthesis methods, the compositions of the host matrix and dopant ions, and additional ion doping.

There have been intensive efforts to obtain highly efficient upconversion luminescence by using diverse methods of thermal decomposition, hydro(solvo)thermal synthesis, coprecipitation, and microwave-assisted synthesis.[203,204] In the typical thermal decomposition method, rare-earth precursors of lanthanide trifluoroacetate [$Ln(CF_3COO)_3$] and fluoride precursors of ammonium fluoride (NH_4F) are prepared in an organic solvent at a high boiling temperature over 300 °C in the presence of a surfactant, either oleic acid or oleylamine. The nanocrystal phase, size, and morphologies of UCNPs can be precisely controlled by varying the synthesis reaction parameters, such as the amount of surfactant and solvent, the composition and amount of precursors, and the reaction temperature and time. This synthesis method is advantageous for the production of nanoparticles with a uniform size and crystallinity. Hydro(solvo)thermal synthesis is a chemical reaction in which precursors in either aqueous or organic solvents are sealed and heated in an autoclave at high pressure and a temperature generally below 200 °C. In comparison with the thermal-decomposition method, it can be conducted at lower temperature, and hydrophilic final products can be produced by the addition of hydrophilic surfactants such as poly(acrylic acid) and PEG.[205]

A variety of UCNPs have been synthesized by changing the composition of the host matrix and dopant lanthanide ions (sensitizers and activators) to achieve various physical and optical properties. The crystalline host matrix affects the distance between the dopant ions, spatial arrangement, the type of anions surrounding the dopant ions, and the coordination numbers, which all strongly influence upconversion luminescence. Host matrices based on cations such as Na^+, Ca^{2+}, and Y^{3+} with similar ionic radii to lanthanide dopant ions can prevent crystal defects and lattice stress. Thus, Na^+ and Ca^{2+} fluorides, which have a low phonon energy and long lifetime (≈350 cm^{-1}) in the excited states, are the most desirable materials for the host matrix.[200,206] According to Blasse and Grabmaier,[207] the upconversion luminescence efficiency of $NaYF_4$:Yb/Er is 20 times higher than that of La_2O_3:Yb/Er and six times higher than that of $La_2(MoO_4)_3$:Yb/Er. The crystal structure of the host materials also influences the optical properties of UCNPs. Kramer et al.[208] reported that the upconversion luminescence efficiency of hexagonal phase $NaYF_4$:Yb/Er is 10 times higher than that of the cubic phase because the dopant ions are located on different lattice sites.[209]

The doped ions of sensitizer–activator systems, as well as the host matrix, are the main determinants for the photon upconversion of nanoparticles. The Yb^{3+} ion is the most widely used sensitizer in favor of various activator ions, such as Er^{3+}, Tm^{3+}, Ho^{3+}, and Pr^{3+}, because the matching of the transition energy between the excited states of the sensitizers and the activators allows efficient resonant energy transfer between the ions. A variety of emission wavelengths from ultraviolet to NIR can be obtained by different combinations of sensitizer–activator ions. Deng et al. showed that the multicolor emission of $NaYF_4$-based UCNPs according to excitation pulses can be temporally

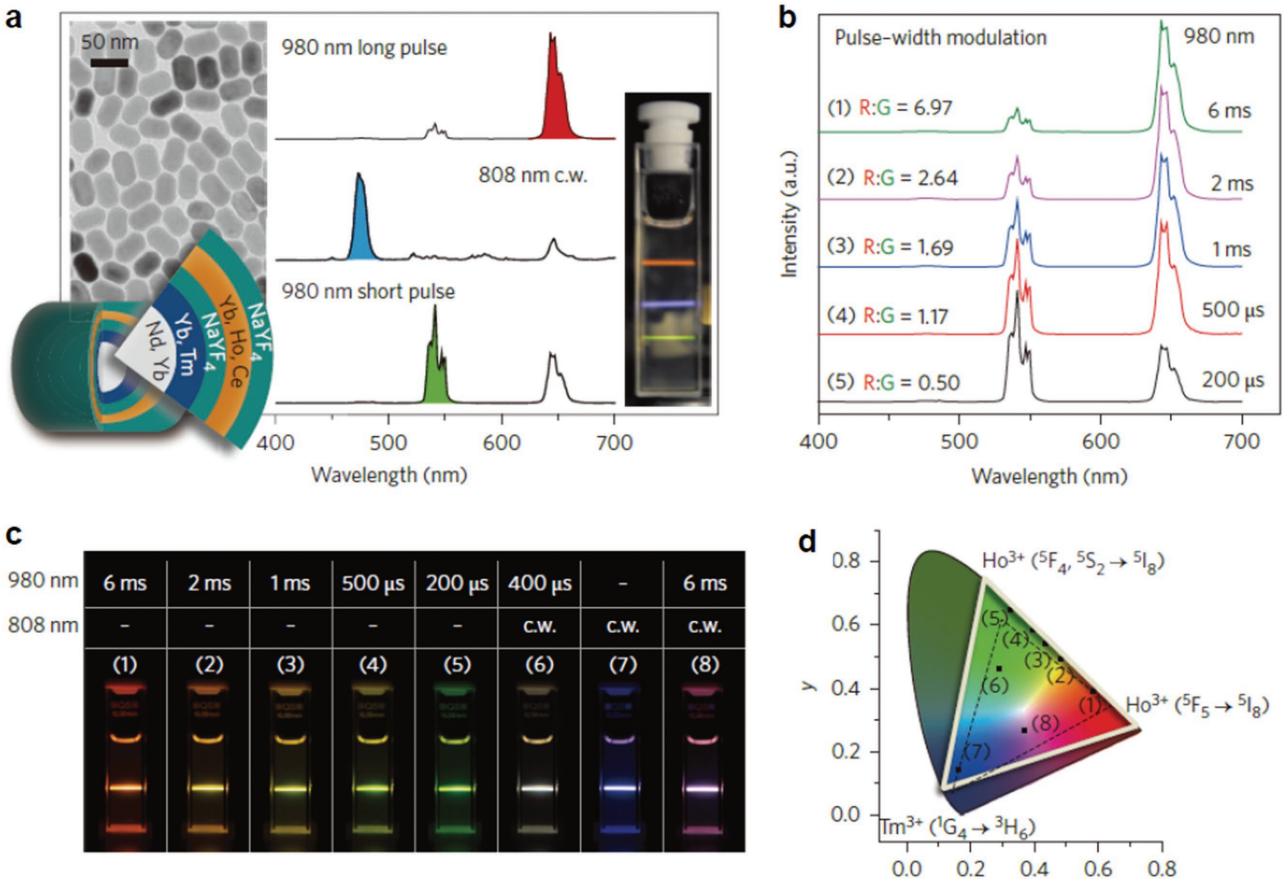

Figure 9. a) Design of $NaYF_4$-based core–shell nanocrystals capable of emitting tunable colors when irradiated with NIR lasers. b) Upconversion emission spectra of the nanocrystals obtained by using different pulse durations, demonstrating the temporal tuning of red and green emission intensities. c) Luminescence images showing multicolor tuning (1–8) of the sample through combined use of 980 and 808 nm lasers. d) The corresponding color gamut of the emission colors (marked by the outer triangle) from the sample shown in (c), compared to the color spaces (marked by the inner triangle) accessible by conventional high-definition televisions. Reproduced with permission.[210] Copyright 2015, Nature Publishing Group.

tuned by the combination of dopant ions,[210] demonstrating various emission luminescences from red to violet (**Figure 9**). To increase the luminescence efficiency and modifiability of photon upconversion, further dopant ions have been added, in addition to lanthanide dopant ions, such as alkali metals or transition metals of Cs^{2+}, Mo^{3+}, and Os^{4+}. For example, Tian et al.[211] showed that the upconversion ratio between red and green light of $NaYF_4$:Yb/Er nanoparticles can be controlled by doping the transition metal of Mn^{2+} at concentrations of 0, 3, 5, and 30 mol% dopant ions. The presence of Mn^{2+} ions interfered with the transition possibilities between the red and green emissions of Er^{3+} ions, and facilitated the occurrence of red emission, resulting in the controlled red to green ratio from 0.83 to 163.78.

Many different approaches have been performed for the synthesis of UCNPs to meet diverse challenges for biomedical applications, such as multimodal bioimaging, drug and gene delivery, PDT, PTT, and also other applications toward solar cells, photocatalysis, RGB displays, security, and barcoding.[201] In contrast to the dominant photonic research focusing on the optical properties of UCNPs, approaches in the biomedical fields have been actively pursued to improve tissue transparency and biostability of NIR light. UCNPs have been surface modified with bioderived and synthetic polymers to increase the biocompatibility. For further in vivo applications, the quantum efficiency of upconversion nanomaterials should be improved significantly with more detailed studies on the retention time, the metabolic pathway, and the clearance from the body.

2.7. Summary and Comparison of Photonic Nanomaterials

A wide variety of photonic nanomaterials have been investigated over the past decade. Their biomedical applications rely on two representative optical properties: fluorescence and light-to-heat conversion. First, QDs are considered as a promising fluorescent material due to their high quantum yield, long fluorescence lifetime, and narrow and tunable emission bands. Despite these outstanding optical properties, some detrimental components of QDs have posed a substantial obstacle for their clinical application. In this context, biocompatible gold nanostructures have attracted great attention as a highly efficient light-to-heat conversion material.[212] Gold nanostructures have a distinct advantage in synthesis simplicity of forming various shapes and of conjugating with biological ligands.[213]

However, the high cost and nonbiodegradability of gold nanostructures limit their practical applications.[214]

The toxicological issues associated with conventional nanomaterials have prompted further investigation on biocompatible organic nanomaterials. As one of the alternatives to QDs, C-dots have attracted much attention due to their biodegradability.[215] In the early stage of research, the optical properties of C-dots were inferior to those of QDs. However, many recent studies have suggested that C-dots can have not only high quantum yield comparable to QDs, but also unique optical properties such as multiphoton and upconversion fluorescence. Polymeric melanoidins composed of sugar and amino acid are another strong candidate for clinical trials in terms of safety issues.[17] They are known to generate intense heat under laser irradiation. Further investigations on their chemical structure will pave the way to optimized applications in photoacoustic tomography and photothermal therapy.

Recently, 2D nanomaterials including GO and TMDs have attracted great interest, with unique optical properties. They can serve as either a fluorophore for bioimaging and/or a heat generator for photothermal applications. Their properties can be controlled by varying the layer structure and the chemical composition.[182,216] UCNPs that emit the light at a shorter wavelength than the excitation wavelength have a strong potential for deep tissue bioimaging, particularly by eliminating the autofluorescence and light scattering in biological samples.[217] For further applications of the aforementioned emerging nanomaterials, their biocompatibility and safety should be improved greatly with optimized performance in the clinic.

3. Biomedical Applications

3.1. Diagnostics

3.1.1. Fluorescence Imaging

Fluorescence is a type of luminescence in which light is emitted from a substance that has absorbed light or other electromagnetic radiation. Fluorescence imaging is one of the most versatile and widely used optical visualization methods. Recently, diverse fluorescent proteins, dyes, and probes have enabled fluorescence imaging of various biological phenomena, such as gene expression, protein functions and interactions, and cellular processes.[218,219] In conjunction with the development of multifunctional imaging agents, the development of imaging techniques for in vivo target-specific visualization has become one of the major goals for diagnostic applications. The visualization methodologies for fluorescence imaging have been changed from the macroscale to the micro- or nanoscale. Currently, fluorescence microscopy can offer super- or high-resolution and video-rate scans for the exploration of structures and dynamics in the biomedical systems.[220,221] In 2014, the Nobel Prize in chemistry was awarded to Eric Betzig, William Moerner, and Stefan Hell for the development of superresolved fluorescence microscopy.[222]

The majority of fluorescence microscopes are "epifluorescence" microscopes, where the fluorescence is produced by reflected rather than transmitted light. The excitation and detection of fluorescence are performed through the objective, which occurs on the same path of light.[223] A typical fluorescence microscope comprises a light source (typically, a laser), an excitation filter, a dichroic filter (a beamsplitter), and an emission filter. The filters are chosen to match the specific wavelengths of excitation or emission for fluorescence imaging, identifying one fluorophore (color) in the image. The images in each color are then combined to produce multicolor images of fluorophores. These multicolor fluorescence-imaging methods are widely used for the development of advanced microscope designs in biomedical research. The confocal microscope uses optical sectioning to improve the resolution of fluorescence images.[224] They have been widely used as effective microscopic imaging tools for the detailed investigation of biological systems.

Many kinds of fluorescent nanomaterials have been investigated as imaging agents for biological processes. Among them, the multicolor emission and nontoxic nature of C-dots suggest their potential for biomedical applications. The confocal imaging of C-dots has been performed for the investigation of cellular uptake, the development of zebrafish embryos,[225] and the assessment of gene expression.[226] A recent paper described the preparation of surface-modified C-dots to reduce the toxicity and increase the quantum yield for in vivo bioimaging.[227] UCNPs with a longer excitation wavelength than the emission wavelength can be effectively used for fluorescence imaging, as the signal of UCNPs is insensitive to autofluorescence from biological samples.[228] In addition, low-energy and NIR excitation reduces scattering from the tissue and photodamage, allowing deep tissue imaging[229,230] and zero-background imaging of cancer cells.[231,232]

However, the major disadvantages of multicolor fluorescence microscopy (such as confocal microscopy) are the low penetration depth of light and the phototoxicity. Hence, thick and living tissue cannot be visualized clearly. Multiphoton microscopy, which uses an NIR laser to excite fluorescent dyes and minimize scattering in the tissue, has shown superiority as an alternative to confocal microscopy. The background signal (noise) was efficiently suppressed, which enabled the imaging of living tissue up to a depth of ≈2 mm (**Figure 10**a–c).[233] The two-photon microscope is a popular form of multiphoton microscope. The difference between two-photon microscopy and traditional fluorescence microscopy is the excitation method. In traditional fluorescence microscopy, the excitation wavelength is shorter than the emission wavelength. However, in the case of two-photon microscopy, the wavelengths of the two exciting photons are longer than that of the emitted light.[234] Recently, intravital imaging using multiphoton microscopy has emerged as an extremely powerful bioimaging technique to visualize biomolecules and biological processes in live animals. As the galvanomirror is installed in the intravital system, biological dynamics,[235] such as gene expression, protein localization,[236] and the detection of biomolecules in vivo, can be monitored with video-rate scans. In addition, subcellular intravital imaging in live animals was carried out to study the molecular biology and physiology of cells.[237]

A variety of C-dots have been prepared that are suitable for multiphoton imaging.[140] The upconversion photoluminescence of C-dots appears to result from a multiphoton activation

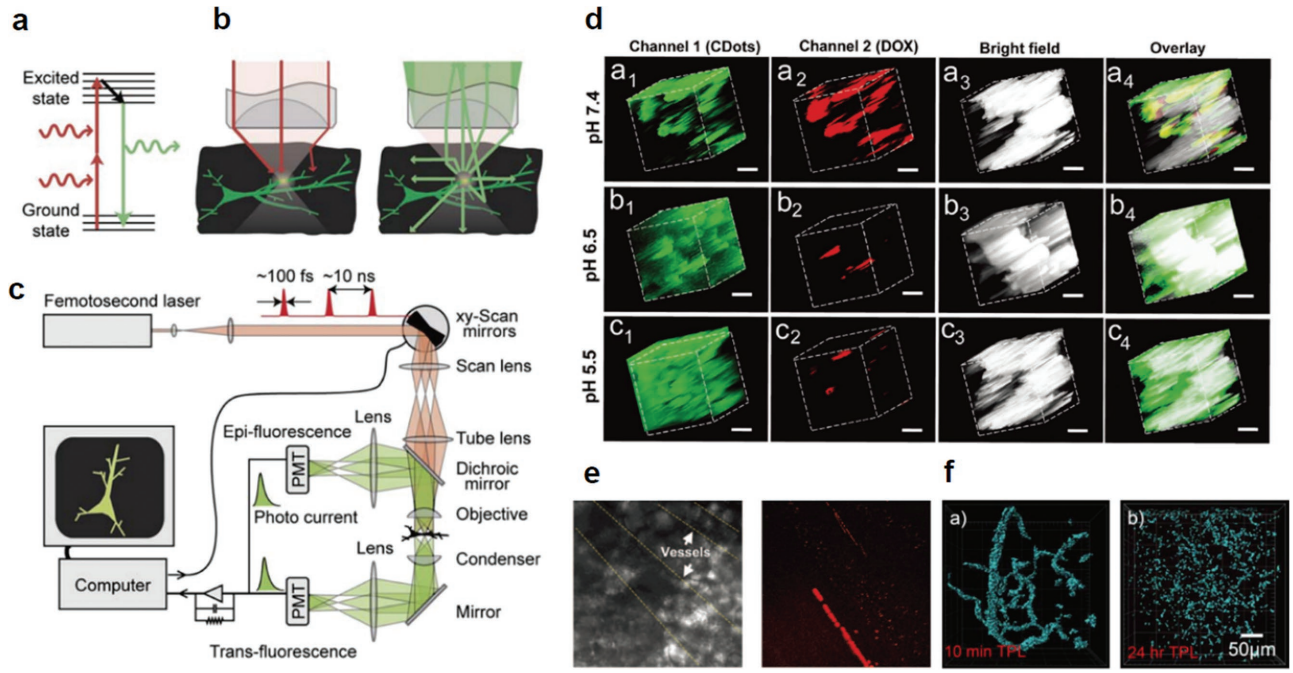

Figure 10. a) Simplified Jablonski diagram of the two-photon excitation (2PE) process. b) Localized excitation in the scattering medium (left) and fluorescence collection in the scattering medium (right). c) A schematic illustration for the 2PE microscope with epifluorescence and transfluorescence detection. a–c) Reproduced with permissions.[252] Copyright 2006, Cell Press. d) 3D two-photon confocal fluorescence images and corresponding bright-field images of glomerular tissues incubated with C-dot–FA–DOX at pH 7.4, 6.5, and 5.5, respectively (scale bars: 60 μm). Reproduced with permissions.[139] Copyright 2013, John Wiley&Sons. e) In vivo imaging of gold nanorods in mouse ear blood vessels. The transmission image of two blood vessels is indicated (left). Two-photon luminescence image of gold nanorods (red dots) flowing through the blood vessels (right). Reproduced with permissions.[246] Copyright 2005, National Academy of Sciences. f) Two-photon 3D reconstructed image of precancerous (dysplastic) lesion labeled with gold nanorods 10 min (left) and 24 h (right) postinoculation, showing a dense and tortuous network of blood vessels. Reproduced with permissions.[251] Copyright 2011, The Optical Society.

process.[238] Water-dispersible and biocompatible C-dots have been used for biosensors, cellular tracking,[139,239–241] and deep-tissue imaging.[141] Amorphous C-dots with high two-photon fluorescence were prepared by using citric acid for two-photon cellular imaging,[242] and water-soluble C-dots with high sensitivity and selectivity have been developed to monitor the pH gradient in living tissue (Figure 10d).[243] In the case of gold nanostructures, multiphoton-absorption-induced luminescence imaging has been performed to monitor the distribution of gold nanostructures in the cell or body.[244] Multiphoton imaging has successfully visualized the uptake of targeted gold nanostructures into human umbilical vein endothelial cells,[245] cancer cells,[246] lymphoma cells,[247] *Dictyostelium discoideum* cells, and murine embryonic stem cells[248] in vitro, as well as mouse ear blood vessels[246] and also the 3D microvasculature to investigate tumor targeting and cancer genesis in vivo[247,249–252] (Figure 10e,f).

3.1.2. Plasmon Resonance Sensing and Imaging

When light is irradiated to materials, the light is absorbed, reemitted, and scattered either elastically (Mie or Rayleigh scattering) or inelastically (Raman scattering). As described in Section 2.2, in the case of noble-metal nanomaterials, free electrons collectively oscillate at the same frequency with the incident light, which is a phenomenon called SPR.[44] The SPR of noble-metal nanoparticles can greatly enhance the Rayleigh and Raman scattering of the nanomaterials. The resulting optical properties have been used for biosensing and bioimaging applications. By adorning metal nanoparticles with biological ligands such as aptamers, antibodies, and peptides, various kinds of biosensors have been developed for the detection of small molecules, DNA, and proteins. One of the most popular types is the colorimetric sensor. A solution of metal nanostructures usually exhibits unique colors based on their SPR properties, which can be changed by the assembly of the nanostructures.[253] The electric field of one particle generated by plasmon oscillation can interact with that of a neighboring particle in close proximity. This interaction influences the frequency of the surface plasmon oscillation. On the basis of this phenomenon, Liu and Lu reported the development of adenosine-sensitive gold nanoparticles for colorimetric sensing.[254] The sensor was composed of two kinds of nanoparticles functionalized with two different DNA strands by gold–thiol chemistry and a linker DNA sequence (**Figure 11**a). Without adenosine, the nanoparticles were aggregated at room temperature and showed a purple color. However, in the presence of adenosine, the DNA on the nanoparticles was bound to adenosine, resulting in the dissociation of the aggregates and the formation of red-colored individual gold nanoparticles (Figure 11b). The colorimetric change was adenosine-specific and dependent on the concentration of adenosine, enabling quantitative analysis (Figure 11c).

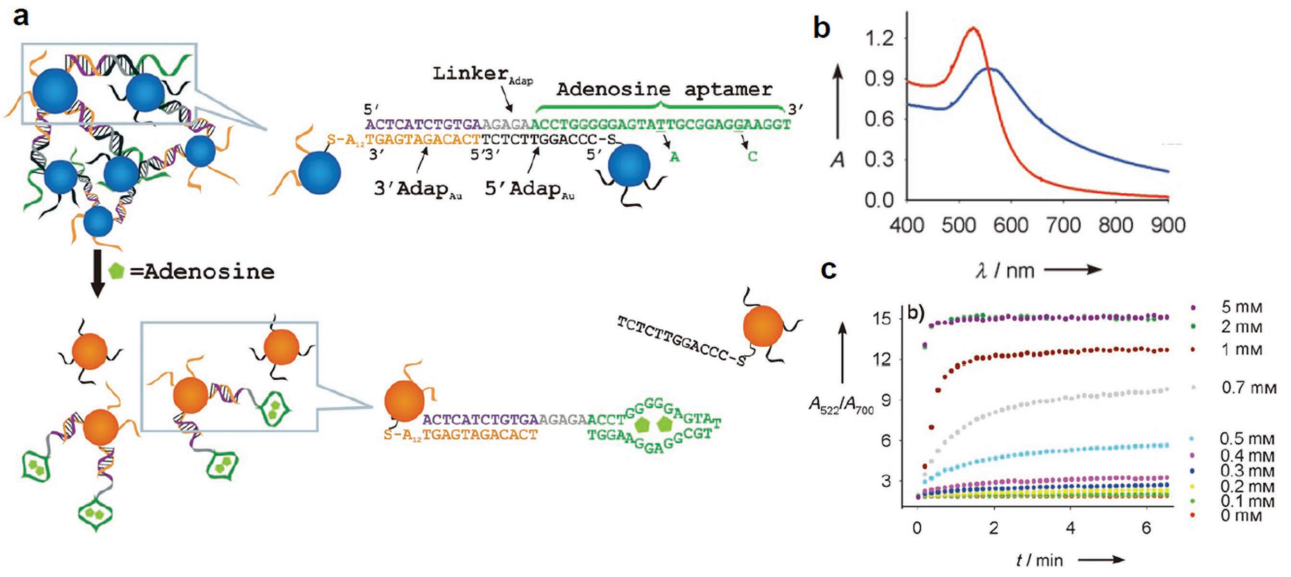

Figure 11. a) Schematic representation for adenosine-sensitive gold-nanoparticle aggregates for colorimetric sensing. Nanoparticles functionalized with two different DNA molecules are linked by Linker$_{Ade}$ to form aggregates. In the presence of adenosine, the aggregates disassemble to give dispersed red nanoparticles. b) Ultraviolet–visible spectra of dispersed (red) and aggregated (blue) gold nanoparticles. c) The color-change kinetics with varying adenosine concentrations. Reproduced with permission.[254] Copyright 2005, John Wiley&Sons.

Another type of sensor is based on SPR sensitivity, which depends on the local dielectric environment surrounding the nanomaterials. An increase in the dielectric constant of the surrounding environment results in a corresponding increase of the SPR wavelength, causing a redshift of the SPR band.[255] The sensitivity of the SPR property is dependent on the metal type and shape of the nanomaterials.[256] The most commonly used metals for SPR are gold and silver. Although the SPR sensitivity of silver is higher than that of gold, in principle, gold nanostructures have the advantage of long-term stability.[257] The dependence of SPR on the shape of nanostructures has also been actively investigated. In general, the higher aspect ratio leads to the higher sensitivity. Furthermore, a triangular shape has also been reported to demonstrate high SPR sensitivity to the dielectric environment. Yonzon et al. reported the SPR sensing of concanavalin A using silver nanotriangles functionalized with mannose. Sherry et al. reported single silver triangular prisms to exhibit an SPR shift in response to the alkanethiol chain length.[258,259] Moreover, Zijlstra et al. reported a single gold nanorod coated with biotin receptors to detect the binding of single proteins in real time using the photothermal microscopy.[260]

Surface-enhanced Raman scattering has also been considered for biosensing applications. In comparison with normal materials, the Raman scattering cross-section of nanomaterials can be enhanced by 3–8 orders of magnitude.[261] There are two types of SERS-based detection: label-free assay and Raman reporter assay. In label-free assay, the SERS substrates are individual nanostructures or their aggregates. The nanoscale junctions in the aggregates can provide strong Raman enhancement by the formation of hot spots.[262] Various platforms have been used for SERS biosensors, including nanoaggregates, nanowire bundles, aligned rafts, 2D close-packed nanoparticles, and metal films.[263] For example, gold–silica core–shell nanoparticles have been reported for glucose detection[264] and silicon nanowires coated with silver nanoparticles have been reported for ultrasensitive DNA detection.[265] "Turn-off" strategies to detect thrombin have also been developed based on the decrease of the Raman signal after the enzymatic cleavage of the nanoaggregates.[266] In the Raman reporter assay, Raman-active molecules with particular nanostructures enhance the signal. In one study, the SERS reporter of rhodamine 6G was used with peptide-nucleic-acid-coated silver nanoparticles to selectively detect single-stranded DNA.[267] Furthermore, an SERS aptasensor composed of gold-nanorod–nanoparticle composites was used with a Raman reporter of mercaptobenzoic acid to detect thrombin at sub-nanomolar concentrations.[268]

Rayleigh scattering greatly enhanced by SPR can be detected with a conventional optical microscope under dark-field illumination conditions. The individual nanoparticles can be clearly distinguished from each other in the colored image.[255] Gold nanomaterials have shown their high stability as a bioimaging agent in the biological environment. El-Sayed et al. conjugated gold nanoparticles with anti-EGFR antibodies, which were used for dark-field imaging to distinguish nonmalignant and malignant cell lines.[56] The antibody-conjugated nanoparticles accumulated in cancerous cells showed strong SPR scattering. However, in the case of noncancerous cells, the nanoparticles were randomly distributed in the extracellular matrix. SPR scattering can also be used for the tracking of nanoparticles in biological samples. Lee et al. visualized the enhanced cellular uptake of HA-coated gold nanoparticles into HA receptor-positive cells via dark-field imaging.[269]

SERS imaging can be performed by using the same method. Gold nanorods have been established as efficient SERS substrates with large Raman scattering cross-sections. El-Sayed et al. performed similar experiments with the abovementioned SPR imaging[56] to distinguish cancerous cells using

anti-EGFR-antibody-conjugated gold nanorods.[270] The dark-field image showed the strongly scattered red light of the gold nanorods bound to the surface of cancerous cells, whereas gold nanorods were randomly distributed in normal cells. The Raman spectra showed a more distinct difference. Gold nanorods treated in cancerous cells showed greatly enhanced, sharp, and polarized Raman spectra due to the homogeneous and aligned assembly of nanorods with a high surface plasmon field. In addition, Ando et al. reported dynamic SERS imaging with gold nanoparticles in live cells to monitor the intracellular motion of the particle over time.[271] While previous SERS studies were mostly performed in vitro, recent studies include in vivo SERS detection. Zhang et al. synthesized gold nanorods functionalized for both SERS and fluorescence imaging, injected the multifunctional nanorods into tumor-bearing mice, and detected SERS intensities from the nanorods accumulated in the tumor tissues.[272]

3.1.3. Photoacoustic Imaging

Photoacoustic imaging is a burgeoning biomedical imaging technique that has been utilized for in vitro and in vivo diagnostic imaging of single cells, tissue structures, and small-animal whole-body systems.[273–275] PA imaging can provide an image with high optical contrast and reasonable imaging depth using acoustic wave emission from optically excited imaging agents. When a pulsed laser is used as the light source and the pulse duration is shorter than the sample thermal stress confinement times, the energy is deposited by an isochoric heating pathway without thermal-energy exchange to the surroundings. Such isochoric heating causes a pressure rise within the sample, which induces thermoelastic expansion and generates a wide-band ultrasound pressure wave, the so-called PA wave. The conversion from optical to ultrasonic energy allows PA imaging to have the combined strength of optical and ultrasonic imaging with excellent selectivity and high penetration.

There are several endogenous contrast agents used in PA imaging, including hemoglobin, melanin, cytochromes, DNA, and RNA. Such agents enable PA imaging to perform powerful label-free analysis. However, when a detection depth reaches the limit, or endogenous contrast is not available, exogenous contrast agents should be used to increase the sensitivity and contrast of bioimaging.[276,277] Among the exogenous contrast agents, gold nanostructures have attracted great attention for nanoparticle-based PA imaging due to the SPR effect. The SPR of gold nanostructures has amplified the light absorbance at certain resonance wavelengths, and the resonance wavelengths can be tuned by changing the nanostructures. Gold nanoparticles, nanorods, nanocages, and nanoshells have been used in PA imaging with their tunable and strong SPR in the NIR region.[278–286] El-Brolossy et al. reported the optical absorption properties of gold nanoparticles with different shapes and sizes using the PA method.[278] Wang et al. demonstrated the feasibility of gold nanoshells as an in vivo contrast-enhancing agent for PA imaging.[279] They successfully visualized the dynamic distribution of gold nanoshells as a nanoparticle contrast agent with a tunable absorption spectrum in a rat brain with high spatial resolution and satisfactory sensitivity. Zhang et al. evaluated the ability of systemically administered PEGylated gold nanoparticles as a photoacoustic contrast agent for in vivo tumor imaging.[280] After subcutaneous injection, gold nanoparticles (20 and 50 nm) could be visualized in mice by PA imaging. In addition, after intravenous injection of PEGylated gold nanoparticles to tumor-bearing mice, the accumulation of gold nanoparticles in tumors could be clearly visualized by PA imaging. Yang et al. demonstrated that gold nanocages could be used for in vivo PA imaging to enhance the contrast between blood and the surrounding tissues.[281]

Gold nanostructures with targeting molecules have also been developed for PA imaging. Agarwal et al. demonstrated PA imaging for cancer-cell targeting using gold nanorods conjugated with an antibody.[282] By changing the aspect ratio of the gold nanoparticles, their plasmon peak absorption wavelengths could be tuned to NIR wavelengths (700–900 nm) to increase the penetration depth into biological tissues. Kim et al. demonstrated the feasibility of PA imaging for inflammatory responses using bioconjugated gold nanorods.[283] To target the stimulated cells, gold nanorods were conjugated with antiintercellular adhesion molecule-1 (ICAM-1), which binds to cell surfaces overexpressing ICAM-1. The bioconjugated gold-nanorod contrast agents showed high-contrast PA images and clearly differentiated the targeted inflamed cells from the control of unstimulated cells. Li et al. reported gold nanorods for multiple targeted PA imaging.[284] Antibodies and blockers (e.g., PEG) were conjugated to gold nanorods with different aspect ratios to form various types of nanoprobes. The optical absorption wavelength of the gold nanorods was maximally increased with their aspect ratios. Consequently, different types of cancer cells could be recognized, and multiple characteristics could be visualized with appropriate wavelength laser irradiation. Kim et al. used gold nanocages as a contrast agent for the quantitative molecular PA imaging of melanomas in vivo (**Figure 12**).[285] When gold nanocages were bioconjugated with [Nle^4-D-Phe^7]-α-melanocyte-stimulating hormone for active targeting to melanoma, the PA signal was approximately three times higher than that for the PEGylated gold nanocages used for passive targeting. Lee et al. recently developed an HA–gold-nanorod/death receptor 5 antibodycomplex for the transdermal theranosis of skin cancer.[286] In this case, gold nanorods absorbing NIR laser light were harnessed as a PA imaging platform for diagnostic applications.

Carbon nanomaterials have also been utilized as contrast agents for PA imaging. SWNTs are the most widely used carbon contrast agent for PA imaging.[287–290] Pramanik et al. showed that SWCNTs provided more than sixfold signal enhancement in PA imaging at a wavelength of 1064 nm in comparison with the blood.[287] Zerda et al. showed that SWCNTs conjugated with cyclic Arg–Gly–Asp (RGD) peptides could be used as a contrast agent for PA imaging of tumors.[288] The intravenous injection of targeted SWCNTs in mice led to an eightfold increase in the PA signal in the tumor compared to the mice injected with nontargeted SWCNTs (**Figure 13**). Other carbon-nanomaterial contrast agents have also been developed, including GO nanoribbons, graphene nanosheets, carbon nanospheres, carbon nanodots, and nanodiamonds.[117,291–295] Lalwani et al. investigated graphene nanoribbons as contrast agents for PA imaging and showed that oxidized single- and multiwalled GO nanoribbons exhibited

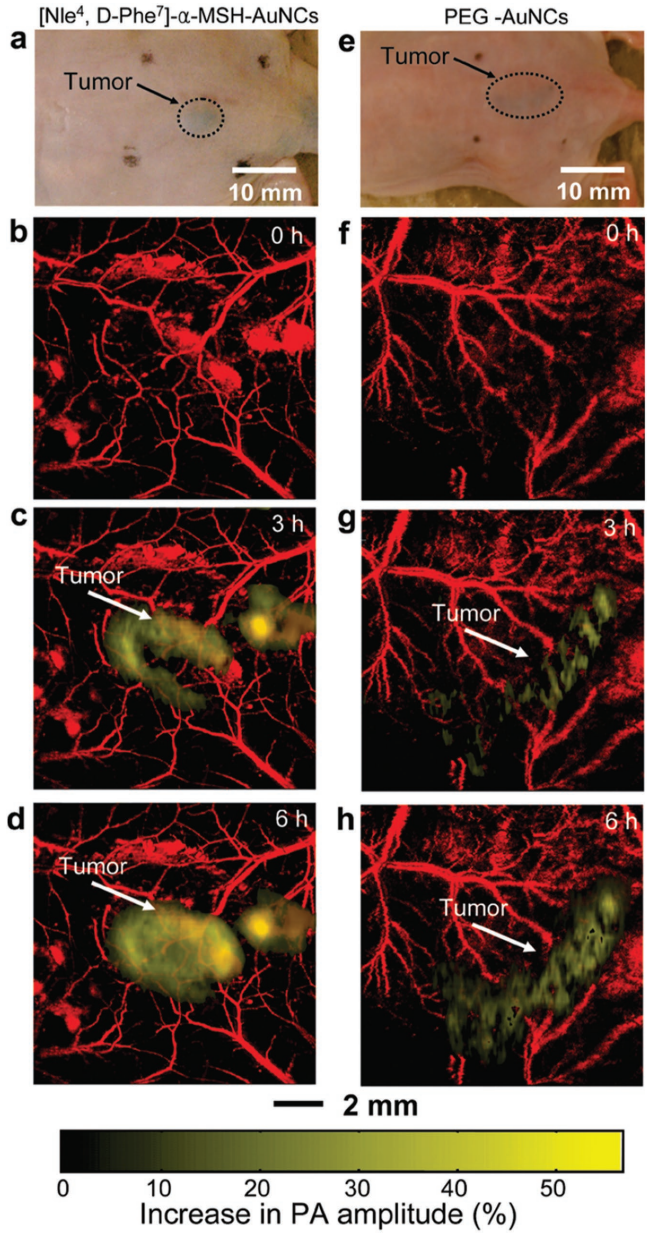

Figure 12. In vivo noninvasive PA time-course coronal images of B16 melanomas using [Nle^4-D-Phe^7]-α-melanocyte-stimulating hormone-conjugated gold nanocages ([Nle^4-D-Phe^7]-MSH-AuNCs) and PEGylated gold nanocages (PEG-AuNCs). Photographs of nude mice transplanted with B16 melanomas before injection of a) [Nle^4-D-Phe^7]-MSH-AuNCs and e) PEG-AuNCs. Time-course PA images of the B16 melanomas after intravenous injection with 100 µL of b–d) 10×10^{-9} M [Nle^4-D-Phe^7]-MSH-AuNCs and f–h) PEG-AuNCs via the tail vein. The background vasculature images were obtained using a PA microscope at 590 nm (ultrasonic frequency = 50 MHz) and the melanoma images were obtained using the PA macroscope at 778 nm (ultrasonic frequency = 10 MHz). Reproduced with permission.[285] Copyright 2010 American Chemical Society.

about 5–10-fold signal enhancement for PA imaging in comparison with the blood at the wavelength of 755 nm.[291] Sheng et al. showed that intravenous injection of nanosized reduced GO (rGO) in tumor-bearing mice showed rapid and significant PA signal enhancement in the tumor region by passive targeting.[292] Miao et al. demonstrated that glucose-derived carbon nanospheres could be employed as a novel NIR-light-absorbing agent for PA imaging.[293] The PA signal amplitude generated by the carbon-nanosphere dispersion was ≈8.5 times higher than that of deionized water. Lee et al. demonstrated that nitrogen-doped carbon nanodots could be utilized as an effective PA contrast agent for in vivo and ex vivo noninvasive PA imaging of sentinel lymph nodes after local delivery.[295]

2D TMDs have also been implemented in PA imaging.[185,296] Qian et al. synthesized TiS_2–PEG nanosheets, which offered a strong contrast in PA imaging due to their high absorbance in the NIR region, showing the high tumor uptake and retention of these nanosheets after systemic administration into tumor-bearing mice.[296] Similarly, Cheng et al. demonstrated that PEGylated WS_2 nanosheets with high NIR-absorbance appeared to be a strong contrast agent for PA imaging.[185] In addition, MoS_2/WS_2 QDs have been used for the same application.[172] Melanoidin is a rarely investigated material for PA imaging. Recently, Lee et al. demonstrated a wide range of biomedical photonic applications of melanoidins, including in vivo PA mapping of sentinel lymph nodes and PA tracking of gastrointestinal tracts.[17] Remarkably, melanoidin appears to be a biocompatible and biodegradable PA imaging contrast agent, showing great feasibility for further clinical applications.

3.2. Therapeutics

3.2.1. Photothermal Therapy

Cancer is one of the most threatening diseases in humans.[297] Current cancer therapy includes surgical dissection, chemotherapy, and radiotherapy. However, physical surgery cannot remove all cancerous cells and tissues. In the cases of chemo- and radiotherapies, significant side effects have been reported, requiring additional medical treatment. As an alternative method, minimally invasive thermal therapies have been investigated, such as PTT, microwave and radiofrequency ablation, magnetic thermal ablation, and focused ultrasonography.[187,298,299] However, such therapeutic approaches are limited due to their nonspecific damage to target tissues, which usually results in injury to normal tissues. To enhance the selectivity of the radiation to tumor tissues, researchers have tried to develop nanoparticles as a light-to-heat converter for the PTT of tumors.[297] Light absorbing nanomateirals can generate heat by optical excitation, especially in the NIR region. Due to the absence of NIR-absorbing chromophores in the body, light can penetrate the skin with little interaction and minimal damage.[297] When a continuous-wave laser is applied as a light source, the heat generated from nanomaterials can be used for PTT. After injection of light-responsive nanoparticles, specific tumor sites can be treated by laser irradiation.[17] This approach can provide greatly enhanced benefits over traditional cancer therapies, such as minimal invasion, ease of treatment, and possible cancer treatment without surgery.[192,300,301]

A wide range of nanomaterials have been investigated as a contrast agent for PTT. Recently, light-absorbing gold nanomaterials, carbon-based nanomaterials, melanoidin, UCNPs, and even TMDs have been explored as PTT agents with their excellent

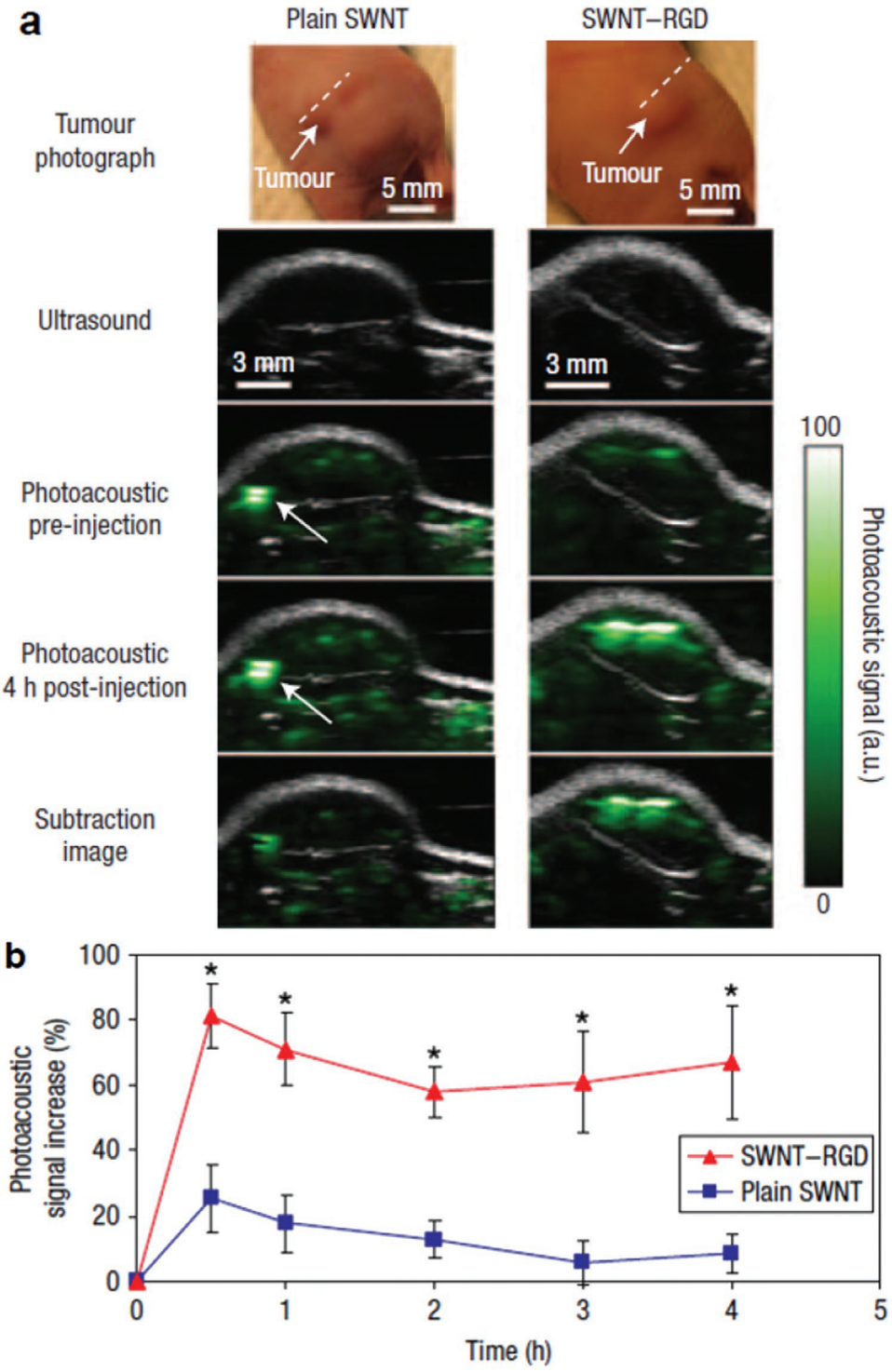

Figure 13. Single-walled carbon nanotube targeting tumors in live mice. a) Ultrasound (gray) and photoacoustic (green) images of one vertical slice (white dotted line) through the tumor. b) Mice injected with SWNT-RGD showed a significantly higher photoacoustic signal than those injected with plain single-walled carbon nanotubes ($P < 0.001$). The error bars represent standard errors ($n = 4$). *$P < 0.05$. Reproduced with permission.[288] Copyright 2008, Nature Publishing Group.

NIR-light-absorbing characteristics.[169,185,186,190,295,302–304] The electron–phonon and phonon–phonon interactions of nanomaterials have resulted in significant heat generation when irradiated with NIR light.[305] The aforementioned nanomaterials are well known as effective light-to-heat converting materials in the tissue-transparent NIR optical window, making them excellent candidates for PTT.[304] The most well-known nanomaterials for PTT are gold-based nanomaterials with their biocompatibility,

easy surface functionalization, high photothermal conversion rate, and photostability. Gold nanoparticles and other shaped gold nanomaterials, including gold nanoshells, nanocages, and nanorods, have been exploited for biomedical applications. A safe water-soluble tricarbocyanine dye of ICG was conjugated to gold nanoparticles and gold nanorods. Both ICG-tethered gold nanoparticles and gold nanorods showed remarkable photostability for PTT.[306] Loo et al. reported gold nanoshells for the PTT of carcinoma cells. Gold nanoshells are composed of a dielectric silica core covered with a thin bioinert gold shell. The optical property of this material can be tuned by modulating the core radius and shell thickness.[299] Chen et al. demonstrated that gold nanocages with a size less than 50 nm showed a central wavelength of ≈810 nm. The gold nanocages, with a hollow interior and a thin and porous but robust wall, resulted in effective carcinoma PTT.[66] In addition, low-molecular-weight chitosan-coated gold nanorods were developed as a synergetic therapeutic system with anticancer drugs. Gold nanorods were used as a PTT agent and fluorescein isothiocyanate for fluorescence imaging with loading the anticancer drug, cisplatin, into the nanocomplex.[307]

Carbon-based nanomaterials are also promising for PTT. The most well-known example of this class is SWCNTs with their strong NIR absorption. SWCNTs functionalized with targeting ligands have been explored to selectively target tumor tissues with minimal side effects to normal tissues. McDevitt et al. demonstrated that SWCNTs conjugated with monoclonal antibody of CD20, radiometal ion chelates, and fluorescent probes selectively targeted tumor tissues.[308] Other groups have demonstrated the selective treatment of tumor cells using SWCNTs conjugated with a folate moiety.[300] MWCNTs have also been used to demonstrate PTT. It was reported that MWCNTs show three times more absorbance of NIR light than SWCNTs due to the greater availability of electrons for light absorption per particle.[297] Graphene and its derivatives, including GO and rGO, have also been widely investigated as more efficient PTT agents than gold nanomaterials and CNTs.[186] As shown in recent studies, rGO has approximately sixfold stronger NIR absorption than GO, resulting in significantly higher photothermal efficiency. With an ultrahigh surface-to-volume ratio, it can be used as an efficient chemical drug carrier with surface functionalization. PEGylated GO with an ultrahigh PTT effect has been reported to have a lower clearance from reticuloendothelial systems than PEGylated CNTs.[308] A PEGylated GO– iron oxide (IO) nanocomposite containing doxorubicin (DOX) was synthesized for magnetically targeted therapy. Tumor tissues were clearly visualized by PA imaging and magnetic resonance imaging (MRI). In addition, the same group reported a chlorin-e6 (Ce6)-loaded PEG–GO for combined PDT and PTT. As shown in **Figure 14**, we reported HA-conjugated GO for transdermal PTT of skin cancers. The noninvasive PTT agents appeared to be transdermally delivered via HA receptors on the skin, especially in the leaky skin-cancer tissues.[190]

UCNP–Ag nanocomposites were synthesized and utilized for the photothermal ablation of tumor tissues under irradiation of 980 nm NIR light.[309] Another group reported self-assembled UCNP–IONP–Au nanocomposites (IONP: iron oxide nanoparticle) for magnetically targeted therapy. When a magnet was placed near the tumor site, the composites were accumulated in the tumor site by magnetic attraction. After that, NIR light was applied for photothermal ablation.[303] Chou and co-workers developed chemically exfoliated MoS_2 nanosheets, for the first time, as a PTT agent. Although MoS_2 nanosheets have a similar 2D morphology with GO and rGO, they showed an excellent physiological stability with a zeta potential of about −45 mV. Furthermore, they showed 7.8 times higher absorbance in the NIR than GO and gold nanorods. With a comparable extinction coefficient, MoS_2 is water dispersible, unlike rGO, which is a great benefit for biomedical applications.[188] Other TMD nanosheets, including WS_2 and Bi_2Se_3, have also been used as PTT agents. Both materials showed strong absorbance in the NIR region for bioimaging and photothermal ablation of tumor tissues in model mice. In the case of WS_2 nanosheets, the surface was easily functionalized with PEG using thiol chemistry. The conjugation of Bi_2Se_3 with poly(vinylpyrrolidone) resulted in drastically enhanced stability and biocompatibility.[185,302]

3.2.2. Photodynamic Therapy

PDT has been widely investigated for the treatment of cancer and ocular diseases to overcome the limitations of conventional therapy.[310] PDT has several advantages of noninvasiveness, localized therapy, and minimized side effect.[311] PDT requires three elements of light, oxygen, and a photosensitizer. PDT is performed by the administration of the PS to target tissues followed by light irradiation with a specific wavelength to stimulate the PS. The excited electron of the PS transfers energy to the oxygen in tissues, thus generating cytotoxic ROS, including singlet oxygen ($^1O_2$). Singlet oxygen can lead to tumor-cell necrosis and apoptosis by oxidizing the key cellular components.[312] **Figure 15** shows the generation mechanism of singlet oxygen using the Jablonski diagram. After light irradiation at an adequate wavelength, the ground singlet state (S_0) of the PS is transformed into an excited triplet state (T_1). The excited triplet can participate in two kinds of reactions, as shown in Figure 15. First, the excited triplet can undergo electron-transfer processes in the biological tissues to form radicals, which produce oxygenated products like the superoxide ion of O^{2-}. Second, it can participate in the photochemical process, that is, the conversion of stable triplet oxygen ($^3O_2$) to highly reactive singlet oxygen ($^1O_2$). For PDT, oxygen is necessary in the tumors. The key component of PS requires a high production rate of singlet oxygen and a high absorption coefficient in the NIR region (660–800 nm). The most widely used PSs are porphyrins, chlorins, and bacteriochlorins.[313] These compounds have an aromatic structure that generates a strong absorption band between 600 and 800 nm, a so-called Q-band. For biomedical applications, the PS must be water soluble, stable, and chemically pure. In addition, the light-penetration depth should be seriously considered for effective PDT. Singlet oxygen has a short diffusion range of about 45 nm in cellular media. Thus, the light-penetration depth to tissues is an important issue for successful PDT. As the wavelength of light decreases, the absorption and scattering increase. The tissue components, including hemoglobin and melanin, have strong

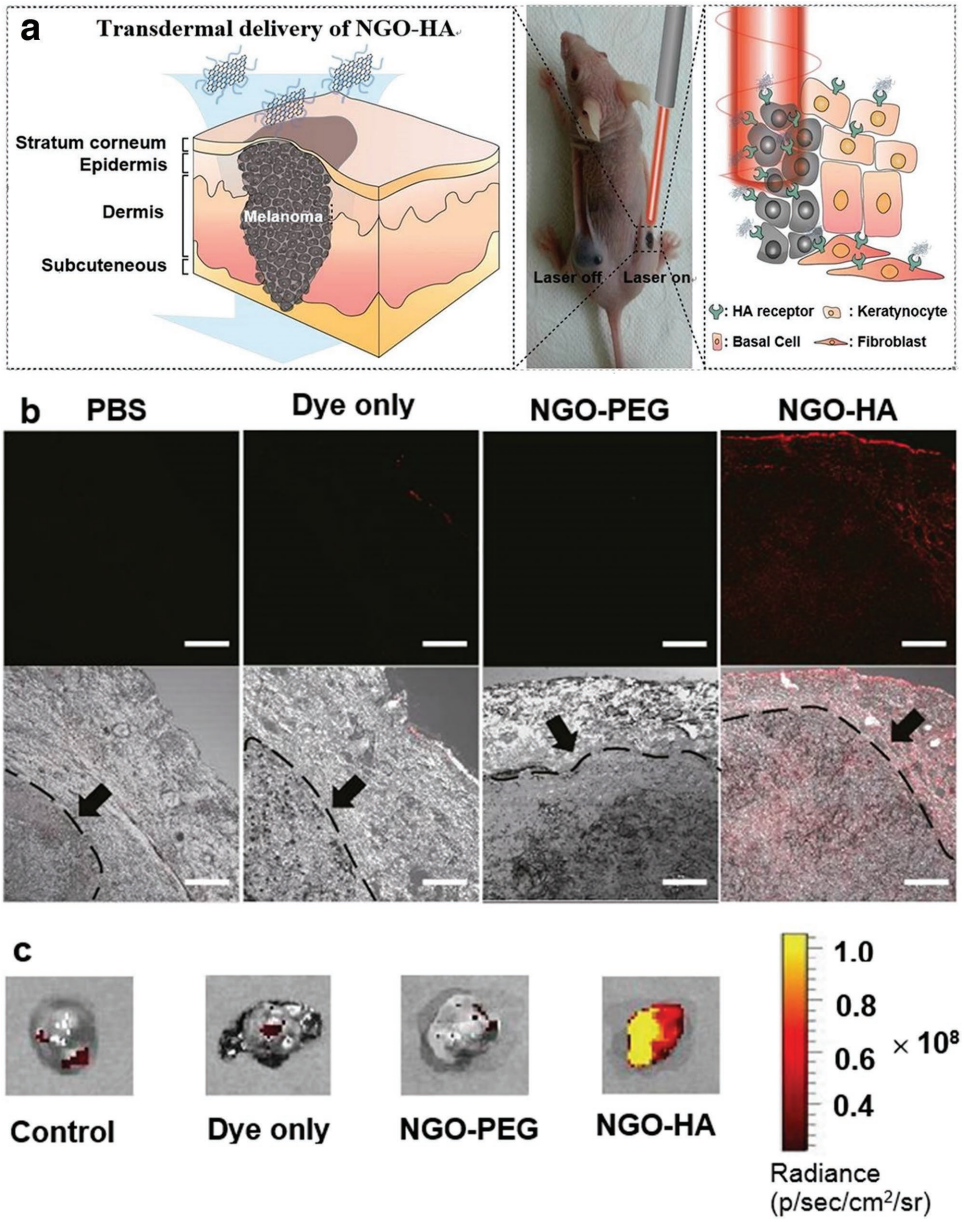

Figure 14. a) Schematic illustration for the transdermal delivery of nanographene oxide–hyaluronic acid (NGO–HA) conjugates into melanoma skin cancers and the subsequent photothermal therapy using NIR light. b) Confocal microscopy analysis and c) ex vivo bioimaging of dissected tumors after transdermal delivery of PBS, Hilyte dye only, NGO–PEG–Lissamine, and NGO–HA–Hilyte conjugates (scale bar: 200 µm). Reproduced with permission.[190] Copyright 2014, American Chemical Society.

absorption peaks at wavelengths shorter than 620 nm.[314] This makes the NIR range the desired optical window for PDT.

Several PSs, including Photofrin, aminolevulinic acid (ALA), 2-(1-hexyloxyethyl)2-devinyl pyropheophorbride-a, phthalocyanines, Ce6, and Visudyne, have been investigated for various clinical applications.[315] PSs can be classified into three groups by generation. The first-generation PSs are porphyrin-based PSs such as hematoporphyrin (Hp) and hematoporphyrin derivatives (HpD). The second-generation PSs were developed to surpass the drawbacks of the first-generation PSs. They are composed of various structures with porphyrin and chlorine. The third-generation PSs were developed by modifying the first- and the second-generation PSs via conjugating biological antibodies and nanoparticles.[316] Photofrin is the first-generation PS, which is a chromatographically purified HpD. HpD is synthesized by the addition of sulfuric and acetic acids to Hp. HpD has more target-specific localization to the tumor than Hp. However, Photofrin has several drawbacks, including impurities and low absorbance in the NIR region. Compared with first-generation PSs, second-generation PSs have higher purity, a higher singlet-oxygen generation rate, and stronger absorption in the wavelength range of 650–850 nm. Additionally, they have a short photosensitivity time, which ensures patient compliance after laser treatment.[317] Several second-generation PSs, including Npe6 (mono-*N*-aspartyl Ce6), hypericin, $AlpCS_n$, Ce6 derivative, and ALA, are recently under

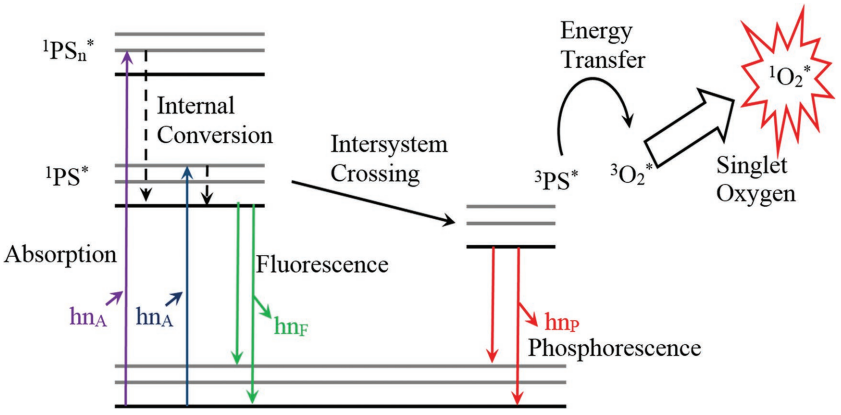

Figure 15. Modified Jablonski diagram illustrating the formation of singlet oxygen. Reproduced with permission.[311] Copyright 2011, Royal Society of Chemistry.

clinical development stages. ALA is a protoporphyrin IX which is converted to heme. It can be administered via oral, intravenous, or topical routes. Excluding the topical administration of ALA, other injection routes have demonstrated a photosensitivity time of about 48 h. Using ALA, preliminary research for the treatment of skin malignancies has achieved a worldwide success.[318] The third-generation PSs have attracted great attention owing to their target-specific delivery. The design of new PSs includes antibodies, aptamers, and photoresponsive nanomaterials. QDs, graphene quantum dots (GQDs), and C-dots have been investigated as third-generation PSs for applications toward PDT.[312,319,320]

QDs possess unique optical properties depending on their sizes. The emission wavelength of QDs can be controlled by tuning their sizes and altering their compositions. In addition, QDs have a large transition dipole moment to strongly absorb light. A QD linked to a silicon phthalocyanine 4 PS (SiPc4) was successfully synthesized and investigated for PDT.[319] The QD was reacted as the preliminary energy donor and indirectly excited Pc4 via the FRET mechanism. Ge et al. reported GQD as a PDT agent, which could produce singlet oxygen through a multistate sensitization process. GQDs were demonstrated as a good agent for imaging and highly efficient cancer PDT.[312] C-dots have also been applied to PDT for the treatment of skin melanoma.[320] C-dots have a particle size range of 1–10 nm. C-dots were used to improve the solubility of the PS Ce6 and the local delivery efficiency with their small sizes. HA was conjugated to C-dot–Ce6 to enhance the transdermal delivery efficiency. Two-photon fluorescence imaging confirmed the high transdermal delivery efficiency of C-dot–Ce6–HA conjugates. The C-dot–Ce6–HA conjugate showed a high PDT efficacy for the treatment of skin melanoma (**Figure 16**).

Many researchers have attempted to apply PDT for the treatment of head, neck, brain, lung, pancreas, breast, prostate, and skin cancers.[321] The photoresponsive materials of carbon nanomaterials, gold nanomaterials, and UCNPs have the following advantageous properties: large surface-to-volume ratio, low nonspecific accumulation in normal tissues, water-soluble properties, and ease of surface modification with targeting agents. Gold nanomaterials have unique photoresponsive properties of the SPR and the ability to convert light to heat energy. In addition, through the FRET mechanism, gold nanomaterials increase the excitation efficiency of the PS.[322] Cheng et al. reported the difference in drug-release period and drug efficacy between covalent and noncovalent binding of SiPc4 on PEGylated gold nanoparticles. They observed that SiPc4 molecules were accumulated preferentially in the tumor site compared with free SiPc4. In their study, gold nanoparticles acted as a PS delivery carrier and a PDT agent. Gold nanomaterials can be used for synergistic PTT and PDT. However, in many reports, the wavelengths for PTT and PDT are different. For example, a gold-nanorod–$AlPcS_4$ complex developed for PTT and PDT was excited at 810 and 670 nm, respectively.[323] Recently, PTT and PDT could be performed using one laser at a single wavelength. Gao et al. developed gold nanocages covered with lipid-loaded hypocrellin B that could be excited at the wavelength of 790 nm. The system simultaneously converted light energy to heat energy and generated ROS.[324]

Graphene is composed of carbon atoms with an sp^2 bond and has many attractive features, including excellent electronic, optical, thermal, and mechanical properties.[325] Huang et al. developed folic-acid- and sulfonic-acid-conjugated GO loaded with PS for target-specific PDT.[325] Ce6 was loaded into the GO via hydrophobic interactions and π–π stacking. This system enhanced the accumulation of PS in tumor tissues, which led to high PDT efficacy in cancer cells following laser irradiation. MoS_2 is a member of the family of TMDs and has been extensively studied due to its ultrathin structure. MoS_2 nanosheets have an excellent fluorescence quenching effect. Jia et al. designed an MoS_2 nanoprobe for controlled PDT via the ATP-mediated release of $^1O_2$.[326] A Ce6-labeled ATP aptamer was assembled on MoS_2 nanoplates, showing good biocompatibility, strong affinity to single-strand DNA, and quenching the fluorescence of chlorin-e6. The nanoprobe was internalized into the cells. After that, under 660 nm laser irradiation, ATP in the cell led to the release of the aptamer from the MoS_2 surface, which restored the fluorescence of the Ce6 and generated singlet oxygen. UCNPs have the potential to convert low-energy light to high-energy light through an anti-Stokes emission process. The excitation in the NIR range appeared to improve the PDT efficacy for the treatment of solid and large tumors compared with conventional PSs. UCNPs used in PDT require three components: a host, dopant, and PS. Recently, Xu et al. developed an anti-cAngptl4-antibody-conjugated nanocomposite using titanium dioxide (TiO_2) covalently attached to $NaYF_4$:Yb^{3+},Tm^{3+} UCNPs.[327,328] After NIR irradiation, the UCNPs emitted visible light, which excited TiO_2 for the reaction of water and oxygen to generate ROS. This system showed remarkable in vitro PDT efficacy, demonstrating light-triggered drug release and targeted cancer-cell apoptosis under NIR irradiation.

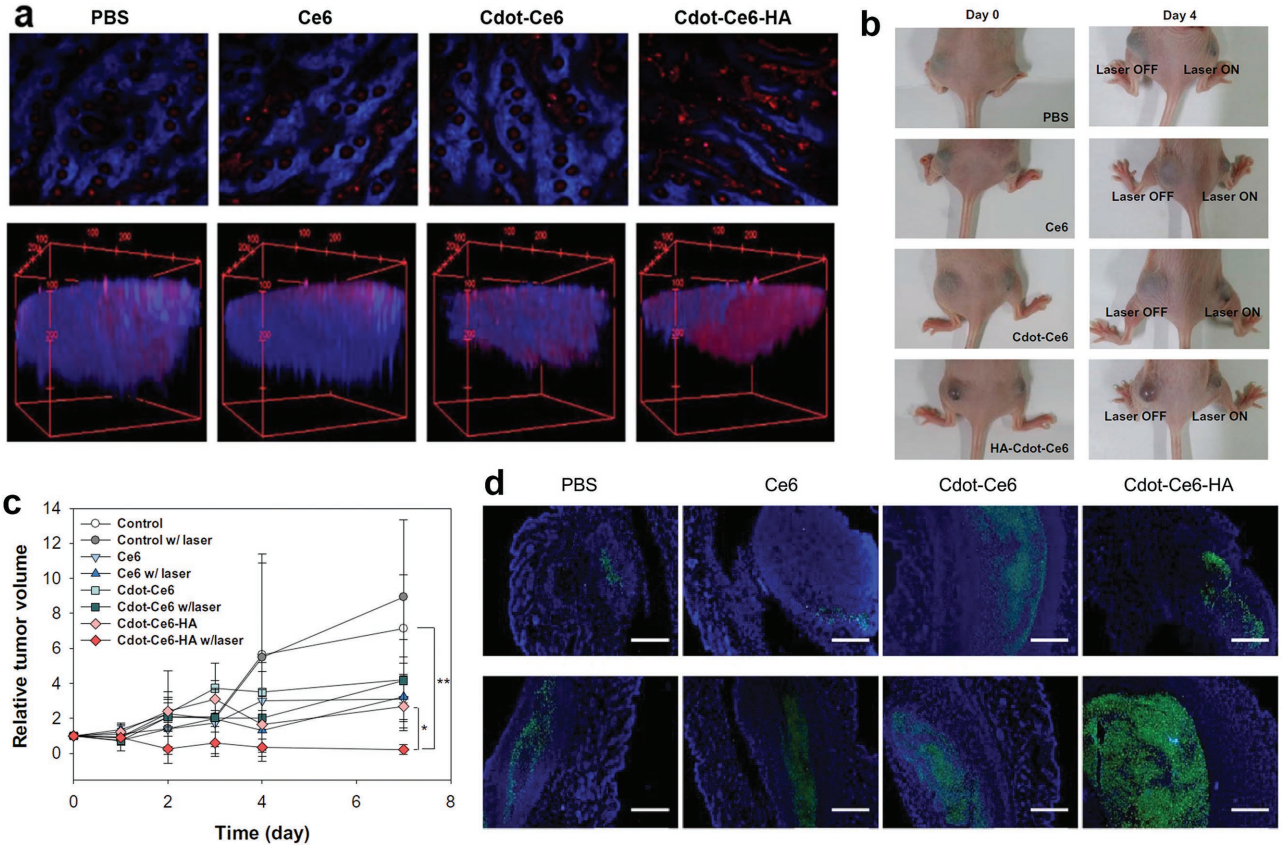

Figure 16. a) Two-photon microscopic cross-sectional views of skin cancers after the administration of four samples. Photographs showing the therapeutic effect of b) photodynamic therapy and c) the relative tumor volume (V/V_0) for up to 7 d after photodynamic therapy. d) TUNEL assays of cancerous skin tissues after treatment with the samples in the absence (top) and presence (bottom) of laser irradiation (scale bar: 500 μm; green: TUNEL-positive area). Reproduced with permission.[320] Copyright 2015, Elsevier.

3.2.3. Optogenetic Therapy

Optogenetics refers to the combination of optics and genetics for the optical control of cells in living tissues, typically neurons, which are genetically modified to have light-sensitive ion channels. Opsins are light-sensitive proteins that can be activated for light-triggered cell functions. The representative opsins are channelrhodopsin-2 (ChR2) and *Natronomonas pharaonis* halorhodopsin (NpHR), which are bioderived proteins and naturally occurring light-responsive effectors. Moreover, engineered synthetic rhodopsin/GPCR chimeras like OptoXR have also been developed for the optical control of intracellular biochemical signaling.[329] Diverse opsin genes can be expressed using various targeting strategies, such as transgenic technology, electroporation, lentivirus or adeno-associated viral expression.[329,330] In the case of transgenic technology, functional opsin genes were introduced into cell-type specific promoters to produce transgenic animal lines. Viral vectors can be applied to a wide range of subjects from rodents to primates, which require a relatively short time of less than 5 weeks for opsin gene expression and induce high expression of the opsin gene by the insertion of multiple gene copies into the target cells. For the case of specific cell types, in utero electroporation can be used to deliver DNA on a specific embryonic day of mice and express opsin genes in the striatum or hippocampal inhibitory neurons.[329] The neuronal activities can be measured by optogenetic sensors for calcium (GCaMP), neurotransmitters (GluSnFRs), vesicular release (synaptopHluorin), or membrane voltage (Arc Lightning, ASAP1).[331,332]

The advantage of optogenetics is that it can target probes to genetically defined cells and subcellular compartments. This ability allows the probes to be used for investigation of the different levels of nervous systems, as shown in **Figure 17**a.[333] This system can be used for the exploration of brain circuits, facilitating applications to control the underlying behaviors for health and disease. Optogenetics has been considered as a promising technology especially for neuroscience by using light to manipulate defined neurons within the range of 1 ms.[334] Genetically targeted neurons can be controlled with light, enabling diverse regenerative approaches, such as vision restoration, neural circuitry control, neuronal disease treatment, and cardiac and skeletal muscle control. Retinitis pigmentosa (RP) is a hereditary and degenerative retinal disease that causes severe vision impairment and incurable blindness. Busskamp et al. reported that the light-sensitive ion channel or pumps expressed by opsin gene delivery triggered the restoration of vision in RP animal models.[335] The restoration of photosensitivity in the RP model was performed in several ways by conducting ChR2 or NpHR opsin expression into either ganglion cells, bipolar

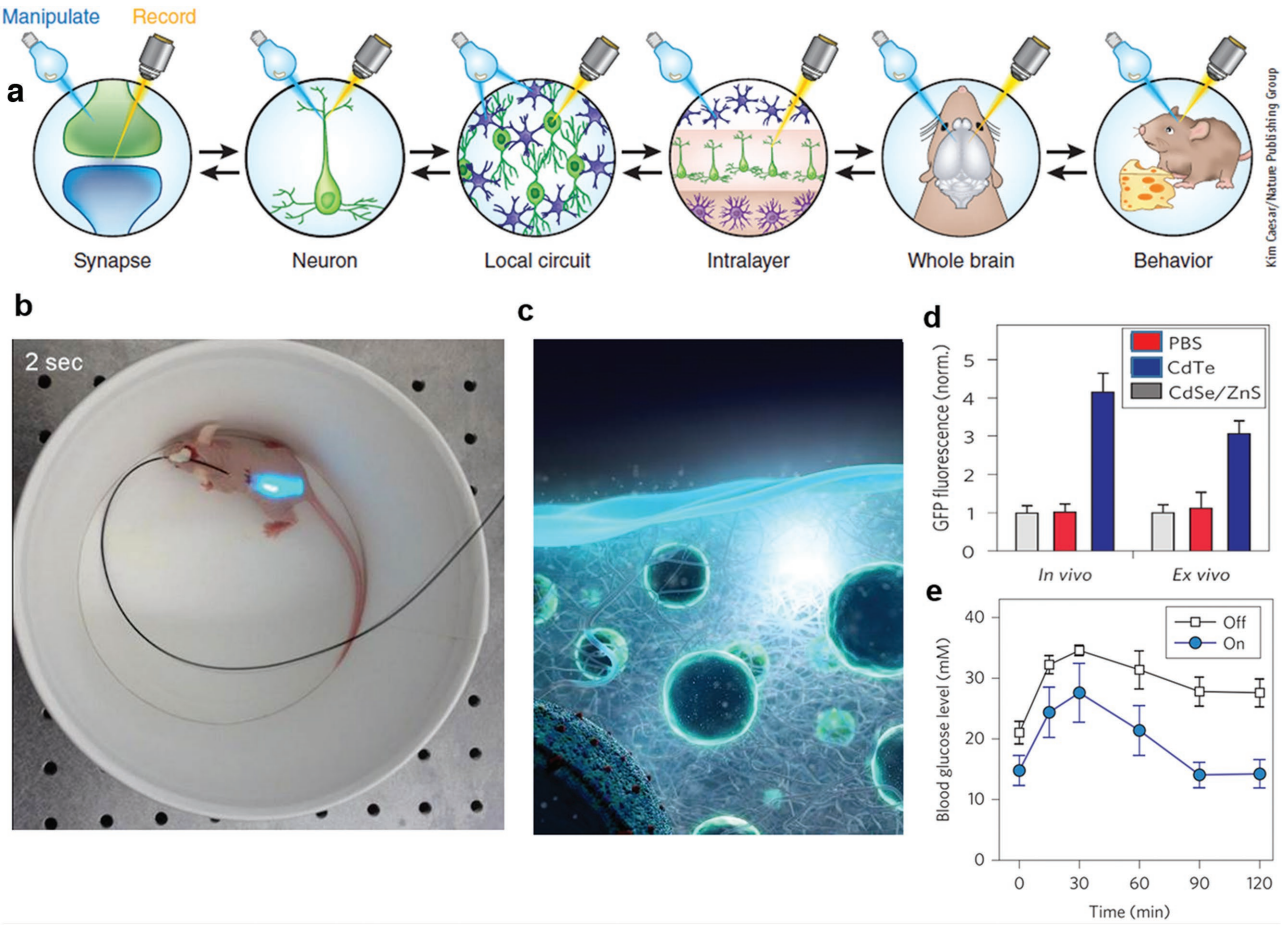

Figure 17. a) Schematic illustration for optogenetics applied at all levels from synapse to behaviors. Specificity can be achieved either by targeting probe expression to relevant cellular compartments and network elements or by targeting light to these elements. Reproduced with permission.[333] Copyright 2014, Nature Publishing Group. b) The freely moving mouse, c) implanted with optogenetic cell-containing transparent waveguide hydrogels. d) The comparison of green fluorescent protein (GFP) fluorescence for nanotoxicity analysis of QDs by the fiber-optical system in vivo (left) and fluorescence microscopy ex vivo (right). e) The change of blood glucose levels according to light irradiation through optogenetic cell-containing waveguide hydrogels in chemically induced diabetic model mice. Reproduced with permission.[349] Copyright 2013, Nature Publishing Group.

cells, amacrine cells, or cone cells for the reactivation of light-insensitive retinas.[336,337]

Optogenetics has been applied to study and control the neural circuitry of fear memory recall,[338] depression modification,[339] and schizophrenic intervention,[340] resulting in novel findings in psychiatry and neurobiology. In addition, optogenetics has been investigated to reveal the critical factors and the mechanisms of neuronal actions for neuronal disorders in Parkinson's disease[341] and Alzheimer's disease.[342] Yamamoto et al. reported the effect of chronic synaptic activation on Aβ pathology in Alzheimer's disease.[342] The transduction of ChR2 induced long-lasting neuronal hyperexcitability into the hippocampal region. They observed that hippocampal Aβ42 levels were immediately increased by ≈24% after acute light activation. The results revealed functional abnormalities of specific neural circuits in Aβ pathology and Alzheimer's disease. However, the most current studies related to the brain involve the identification of neuronal circuits. In conjunction with the identification of neuronal mechanisms, optogenetics can contribute to the phototherapy of psychical and neurological disorders. Moreover, optogenetics have also been investigated to control the cardiac and skeletal muscles,[343] and the chronic pain.[344]

Conventional optogenetics requires invasive light delivery to the brain via a hole in the skull using optical fibers with the risk of infection. The optical fibers and light-emitting diode (LED) sources are unsuitable for applications to animal-behavior experiments and ultimately medical treatment. To deliver light effectively and noninvasively, approaches have been made to stimulate opsin-modified cells using gold nanomaterials, QDs, and UCNPs.[345] According to Carvalho-de-Souza et al.,[346] neurons can be depolarized by cell-targeted gold nanoparticles with exposure to light pulses. They observed that gold nanoparticles, conjugated with high-avidity ligands, bound to target neurons and converted light pulses to heat, which enabled the change in membrane capacitance, depolarization of the cell, and induction of action potentials. Ligand-conjugated gold nanoparticles increased the photothermal stimulation of cells with a high resistance to washout. They revealed that considerable depolarization of target cells was made possible by rapid heating in a

short period without cell damage because the depolarizing current was depending on the rate of temperature change.

Lugo et al. successfully switched the voltage-gated K^+ and Na^+ ion channels in the membrane of prostate cancer (LnCap) cells and cortical neurons that were integrated with CdTe and CdSe QDs.[347] The excitation of QDs by light irradiation resulted in electrical dipole moments and disturbed the cell membrane potential by the dipole-induced electric field. The LnCap cells were cultured on the QD films, which were fabricated with electrostatic layers by self-assembly. The CdTe QD film activated with 430 nm light hyperpolarized LnCap cells by stimulating the K^+ ion channels. The cortical neurons were cultured on a CdSe QD film drop-cast on an ITO substrate. The cortical neurons were depolarized by the excited QDs and 550 nm light irradiation induced multiple action potentials. These approaches showed that the stimulation of electrical signaling was affected by the proximity of the cells to the QD films.

According to Hososhima et al.,[348] photoreactive UCNPs activated ChR2 by 975 nm NIR irradiation. The UCNPs ($NaYF_4$:Sc/Yb/Er) emitted visible green light (543 nm) after irradiation with an NIR laser, which stimulated the chimeric variants of VChR1, such as C1V1 or mVChR1 expressed on the cortical neurons (ND7/23 cell) and generated action potentials. In addition, for optogenetic diagnosis and therapy, biocompatible and flexible light-guiding hydrogels were developed to deliver light into the deep tissues, as shown in Figure 17b,c.[349] The PEG-based hydrogels were prepared by the photo-crosslinking of PEG diacrylate with a molecular weight of 5 kDa. The PEG waveguide hydrogels were transparent and mechanically flexible, propagating the light of the optical fiber all the way. The PEG waveguide hydrogels containing optogenetic cells were applied to detect the nanotoxicity of QDs by measuring green fluorescent protein which was expressed by cytotoxic stress (Figure 17d). In addition, optogenetic diabetes therapy was performed by light triggering to synthesize glucagon-like peptide-1 (GLP-1) (Figure 17e). Upon light irradiation, the secreted GLP-1 induced low blood glucose level and showed a therapeutic effect on diabetes. Moreover, a polymer waveguide was developed to deliver light into the deep tissue for photochemical tissue bonding (**Figure 18**).[350] Nizamoglu et al. demonstrated that the delivered light effectively activated the PS of Rose Bengal, inducing wound closure of porcine skin by crosslinking the disconnected collagen in the damaged skin.

3.3. Theranostics

As described above, photonic nanomaterials have been utilized for various diagnostic and therapeutic applications. Recently, it has been found that some photonic nanomaterials have multiple functionalities for both diagnosis and therapy simultaneously. One of the representative examples is light-to-heat-converting nanomaterials. Light-to-heat-converting nanomaterials, including gold nanorods and CNTs, can generate intense heat under laser irradiation for PTT of cancer, as well as PA waves under pulsed laser irradiation for PA imaging. For example, polymeric melanoidins and carbon-based nanomaterials have been developed for PA imaging and PTT.[17] The GG-melanoidin was synthesized with glucose and glycine, and a GG-melanoidin/Fe^{3+} complex was prepared by chelating Fe ions to enhance the photothermal effect. The melanoidin was employed for PA imaging of lymph node (**Figure 19**a) and the gastrointestinal tract, and for PTT of cancer (Figure 19b) and photothermal lipolysis (Figure 19c). As shown in Figure 19d, GG-melanoidin disappeared from the injection site, but accumulated in the bladder 4 h postinjection, demonstrating effective renal clearance of the biocompatible GG-melanoidin. Furthermore, some TMD nanomaterials for PTT, such as Bi_2Se_3 nanoplates[302] and WS_2 nanosheets,[351] have been found to show a strong X-ray attenuation property due to their high atomic numbers. Thus, these nanomaterials have been developed as theranostic agents for X-ray CT imaging and for PTT of cancer. Light-to-heat-converting nanomaterials can realize image-guided PTT to maximize therapeutic effects on cancer tissues and minimize side effects to healthy tissues.[352]

Fluorescent nanoparticles generally used for in vivo bioimaging have been investigated for PDT.[353] For example, light irradiation can produce excitons in QDs, and the excitons can be transferred from the triplet state to nearby oxygen molecules, which results in reactive singlet oxygen species causing cell damage.[319] Fluorescent nanoparticle-based PSs have the advantages of stability and water solubility, but they have one major drawback of low quantum yield of less than 5%. To overcome this drawback, most nanoparticle-based PDT agents are in the form of a conjugate of nanoparticle carriers and small-molecule-based PSs. Various kinds of nanomaterials such as QDs, GQDs, C-dots, gold nanomaterials, MoS_2 nanomaterials, and UCNPs have been used as a carrier for the small-molecule-based PSs. These nanoparticle–small-molecule conjugates have realized efficient PDT on cancer cells under light irradiation. Related efforts to develop more efficient theranostic agents are now actively in progress.

Remarkably, photonic nanomaterials have been used as carriers of both drug molecules and imaging agents to achieve a synergistic effect. In several systems that combine photonic nanomaterials with drug molecules, drug release can be triggered by light irradiation and the following heat generation.[354] You et al. reported DOX-loaded PEG-coated HAuNSs (DOX@PEG-HAuNS) for NIR-light-triggered drug delivery.[67] DOX was adsorbed onto both the inner and the outer surfaces of HAuNSs via electrostatic interaction and released under irradiation of NIR laser for photothermal conversion. The DOX@PEG-HAuNS showed a significantly enhanced antitumor effect on MDA-MB-213 cells under laser irradiation due to the synergistic effect of the cytotoxic DOX and photothermal ablation. Volodkin et al. developed liposome–gold-nanoparticle complexes using electrostatic interactions.[355] Aggregated gold nanoparticles surrounded by liposomes exhibited high NIR absorption, and the corresponding local heating of nearby liposomes resulted in releasing the encapsulated molecules under focused laser beam. These nanoparticles for light-triggered drug delivery can also be used for diagnosis, such as PA imaging and dark-field light-scattering imaging. Especially, such light-sensitive nanoparticles can be effectively utilized for transdermal applications because the skin can be readily exposed to light.

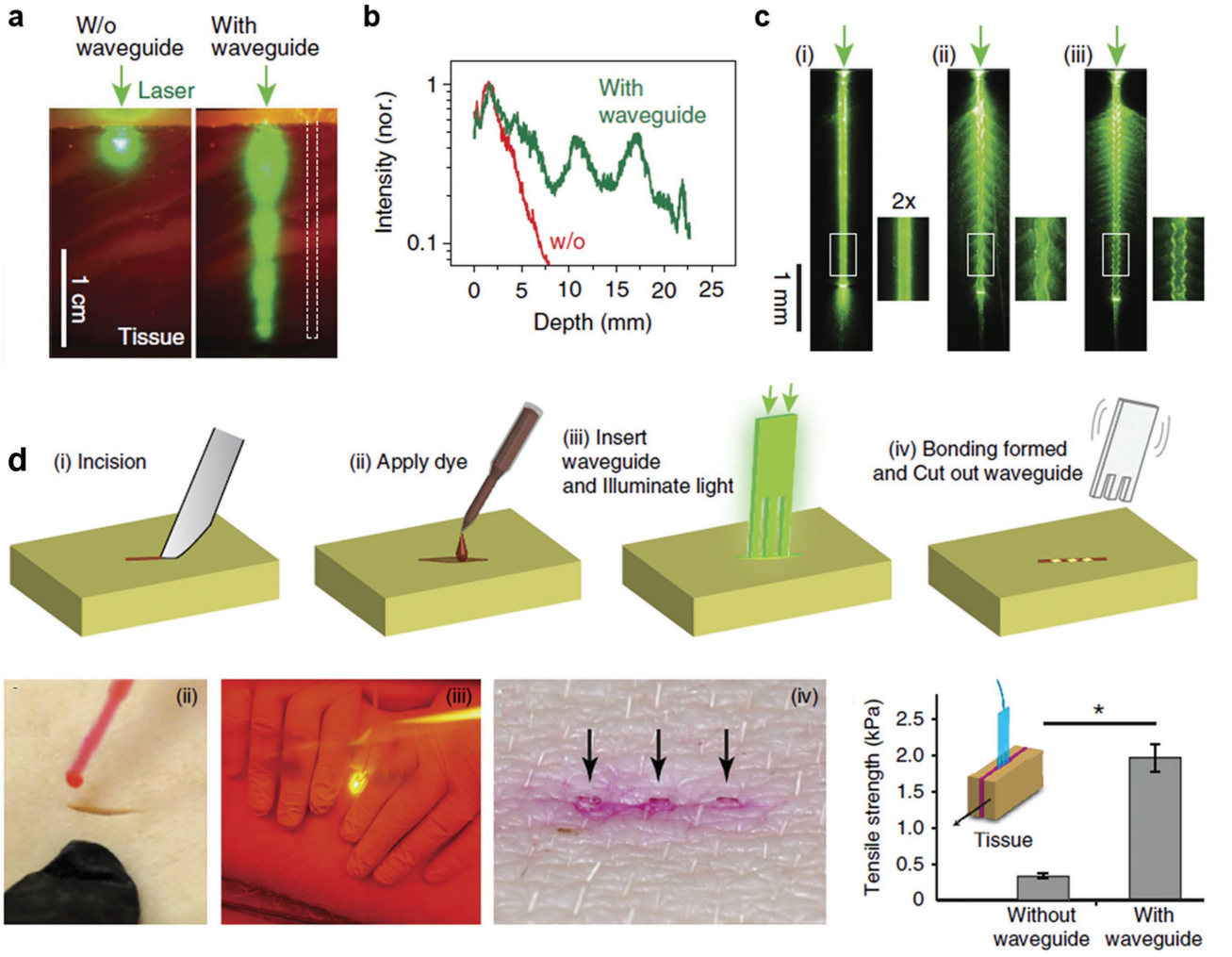

Figure 18. a) The propagation of light in bovine tissue without a waveguide (left) and with a waveguide (right). b) The profile of the light decay. c) The propagation of light in different surface patterns. d) Wound closure by using a light-guiding biodegradable polymer waveguide for photochemical tissue bonding in porcine skin and the resulting enhanced tensile strength ex vivo. Reproduced with permission.[350] Copyright 2016, Nature Publishing Group.

Moreover, multifunctional photonic nanomaterials for theranostic applications can be used together with additional contrast agents for multimodal imaging. For example, hybrid theranostic agents have been developed in combination of photothermal and magnetic nanomaterials. Yang et al. reported rGO–IONP nanocomposite for in vivo multimodal imaging and image-guided PTT.[356] The nanocomposite was applied to the triple-modal imaging of fluorescence imaging, T_2-weighted MRI, and PA imaging. Liu et al. reported IONPs and chelator-molecule-free ^{64}Cu-decorated MoS_2 nanosheets for multimodal image-guided PTT.[189] This nanoplatform was prepared with *meso*-2,3-dimercaptosuccinnic-acid-modified IONPs self-assembled on the defect site of MoS_2. Then, both MoS_2 and IONPs were PEGylated to enhance the biological stability. Subsequently, the ^{64}Cu radioisotope could be labeled without any chelating linkers with a high loading yield of about 70%. PA tomography, MRI, and positron emission tomography were conducted in tumor-model mice. After bioimaging, PTT was conducted with an excellent photothermal effect on the tumor site under 808 nm NIR irradiation. Fullerene has also attracted great attention as a multifunctional theranostic agent because it can generate ROS in a high yield under visible light. Liu et al. introduced Gd^{3+} ions to the PEG terminal of fullerene–PEG conjugates via metal chelation, and demonstrated MRI imaging and PDT of the tumor tissues.[357]

4. Conclusion and Perspectives

We have reviewed multifunctional photonic nanomaterials for a wide variety of biomedical applications, such as fluorescence imaging, SPR imaging, PA imaging, PTT, PDT, and optogenetics. The photonic nanomaterials include semiconductor nanomaterials of QDs and TMDs, metallic nanomaterials of gold nanoparticles, gold nanorods, gold nanocages, and emerging UCNPs, and organic nanomaterials of fullerene, carbon nanotubes, graphene, C-dots, nanodiamonds, and polymeric melanoidin. They have been used for diagnostic applications taking advantages of their fluorescence, surface plasma resonance, photoacoustic effect, and so on. In addition, they have been exploited for therapeutic applications of PTT, PDT,

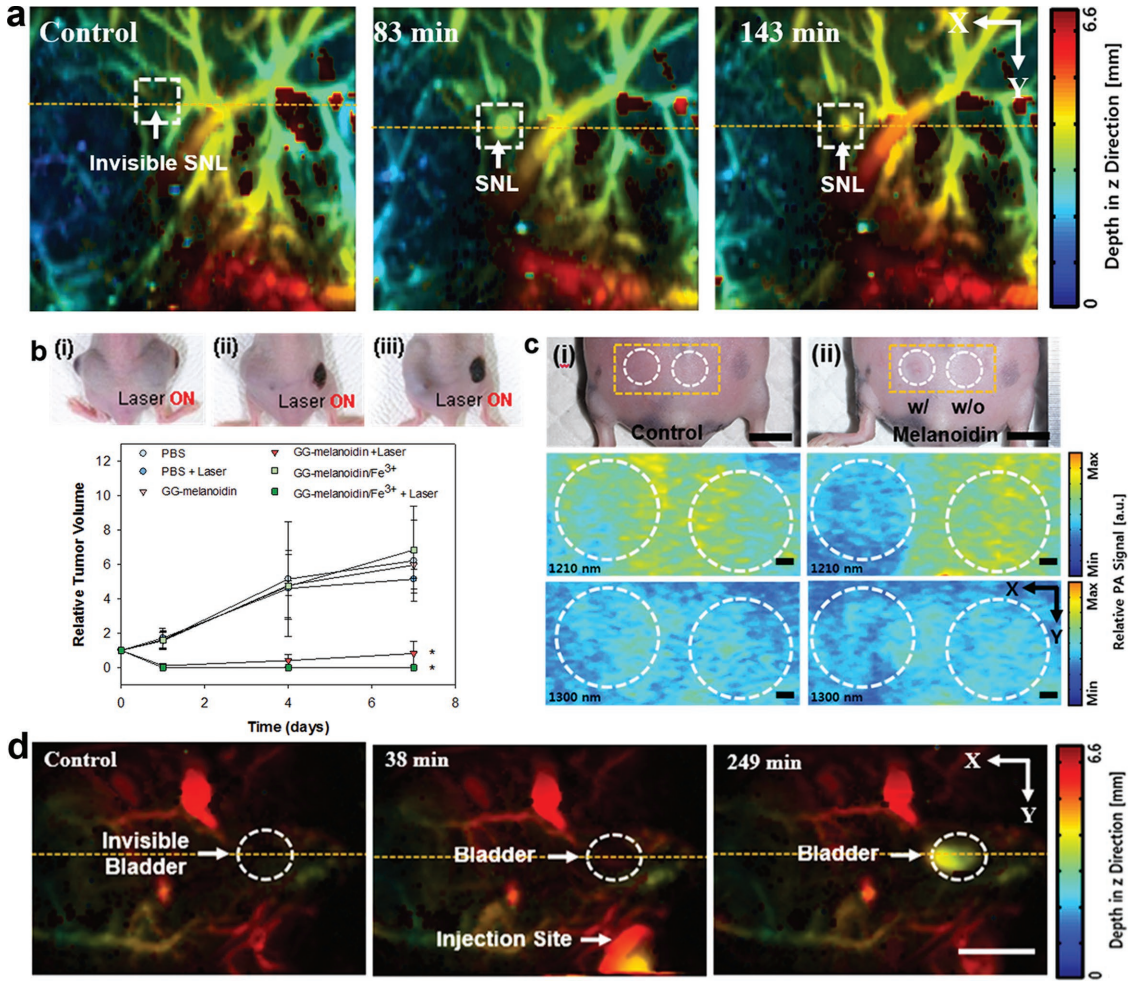

Figure 19. a) Depth-encoded photoacoustic maximum amplitude projection (MAP) images of sentinel lymph nodes (SLNs) after intradermal injection of GG-melanoidin (scale bar: 5 mm). b) Photographs showing the photothermal cancer therapy using i) PBS, ii) GG-melanoidin, and iii) GG-melanoidin/Fe^{3+} complex (scale bar: 1 cm), and the relative tumor volume (V/V_0) (*$P < 0.05$ vs PBS). c) Photographs (scale bar: 1 cm) and PA images (scale bar: 1 mm) at 1210 nm (top) and 1300 nm (bottom) for the lipolysis of subcutaneous fat i) before and ii) after photothermal treatment with and without subcutaneous injection of melanoidin. d) Whole-body depth-encoded PA MAP images showing the renal clearance of GG-melanoidin (scale bar: 10 mm). Reproduced with permission.[17] Copyright 2016 American Chemical Society.

and optogenetic therapy. Furthermore, photonic nanomaterials have shown great feasibility for theranostic applications.

Currently, the most important issue is the safety of photonic nanomaterials for further clinical applications. Recent studies have shown that the clinical feasibility of nanomaterials is strongly dependent on several factors. First, biocompatible materials should be used for the preparation of photonic nanomaterials. In this context, various gold nanomaterials, carbon nanomaterials, and polymeric melanoidins have been extensively investigated for biophotonic applications. Although gold nanomaterials offer many advantages for biomedical applications, they are limited in their clinical usage due to the accumulation in the reticuloendothelial system (liver, spleen, kidney, etc.) possibly causing long-term toxicity. Letfullin et al. reported the laser-induced explosion of gold nanoparticles to minimize toxicity.[358] Second, the size and surface characteristics of photonic nanomaterials should be considered for effective body clearance. Globular proteins have a hydrodynamic size of ≈5–6 nm. Nanomaterials with a size of this range have potential to be cleared in the body by renal filtration.[359] In terms of surface charge, zwitterionic or neutrally coated q-dots resulted in rapid renal excretion due to the low surface adsorption of serum protein. Third, photonic nanomaterials prepared with biodegradable materials have a great advantage in terms of safety, like polymeric melanoidin. Although carbon nanomaterials have shown a great potential as a theranostic agent with their feasible photophysical property, biocompatibility, and water solubility, the biodegradability of carbon nanomaterials is a critical issue for further clinical applications. Lee et al. developed nitrogen-doped C-dots for PA imaging and PTT.[295] In vitro serum tests confirmed the biodegradability of C-dots. The renal clearance of the C-dots was also confirmed by PA imaging.

Among the various diagnostic systems, PA imaging seems to have a great feasibility, providing an image with high optical contrast and reasonable imaging depth. PTT, PDT, and optogenetics using photonic nanomaterials are currently in the development stage, but their clinical trials are strongly expected to

improve patient compliance and the cure rate of skin cancer, age-related macular degeneration, and Parkinson's disease. Moreover, in line with the progress of material properties and functionalities, target-specific phototherapy can be achieved by the addition of targeting moiety without causing side effects in normal tissues. Many studies into new applications are in progress, including ocular phototherapy using PTT,[360] PDT,[361] and optogenetics.[362] Taken together, the endeavored multidisciplinary research on photonic materials should pave a new way to further technological advances, allowing their practical applications toward futuristic photomedicine.

Acknowledgements

H.K. and S.B. contributed equally to this work. This research was supported by the Center for Advanced Soft-Electronics (Global Frontier Project, CASE-2015M3A6A5072945), the Nano·Material Technology Development Program (Grant No. 2017M3A7B8065278), and the Basic Science Research Program (Grant Nos. NRF-2016R1C1B1011830 and 2017R1E1A1A03070458) of the National Research Foundation (NRF) funded by the Ministry of Science, ICT & Future Planning, Korea. This work was also supported by the World Class 300 Project (R&D) (Grant No. S2482887) of the Small and Medium Business Administration (SMBA), Korea.

Conflict of Interest

The authors declare no conflict of interest.

Keywords

diagnostics, nanomaterials, photonics, theranostics, therapeutics

Received: March 15, 2017
Revised: October 20, 2017
Published online:

[1] H. Kobayashi, M. Ogawa, R. Alford, P. L. Choyke, Y. Urano, *Chem. Rev.* **2010**, *110*, 2620.
[2] J. W. Lichtman, J.-A. Conchello, *Nat. Methods* **2005**, *2*, 910.
[3] Z. Guo, S. Park, J. Yoon, I. Shin, *Chem. Soc. Rev.* **2014**, *43*, 16.
[4] L. M. Wysocki, L. D. Lavis, *Curr. Opin. Chem. Biol.* **2011**, *15*, 752.
[5] J. Yu, X. Zhang, X. Hao, X. Zhang, M. Zhou, C.-S. Lee, X. Chen, *Biomaterials* **2014**, *35*, 3356.
[6] J. O. Escobedo, O. Rusin, S. Lim, R. M. Strongin, *Curr. Opin. Chem. Biol.* **2010**, *14*, 64.
[7] J. Chan, S. C. Dodani, C. J. Chang, *Nat. Chem.* **2012**, *4*, 973.
[8] U. Resch-Genger, M. Grabolle, S. Cavaliere-Jaricot, R. Nitschke, T. Nann, *Nat. Methods* **2008**, *5*, 763.
[9] T. Kitai, T. Inomoto, M. Miwa, T. Shikayama, *Breast Cancer* **2005**, *12*, 211.
[10] R. Kiesslich, J. Fritsch, M. Holtmann, H. H. Koehler, M. Stolte, S. Kanzler, B. Nafe, M. Jung, P. R. Galle, M. F. Neurath, *Gastroenterology* **2003**, *124*, 880.
[11] G. Hong, A. L. Antaris, H. Dai, *Nat. Biomed. Eng.* **2017**, *1*, 10.
[12] P. Alivisatos, *Nat. Biotechnol.* **2004**, *22*, 47.
[13] P. C. Ray, *Chem. Rev.* **2010**, *110*, 5332.
[14] F. Pinaud, X. Michalet, L. A. Bentolila, J. M. Tsay, S. Doose, J. J. Li, G. Iyer, S. Weiss, *Biomaterials* **2006**, *27*, 1679.
[15] X. Yang, M. Yang, B. Pang, M. Vara, Y. Xia, *Chem. Rev.* **2015**, *115*, 10410.
[16] N. W. S. Kam, M. O'Connell, J. A. Wisdom, H. Dai, *Proc. Natl. Acad. Sci. USA* **2005**, *102*, 11600.
[17] M.-Y. Lee, C. Lee, H. S. Jung, M. Jeon, K. S. Kim, S. H. Yun, C. Kim, S. K. Hahn, *ACS Nano* **2016**, *10*, 822.
[18] K. Kalantar-zadeh, J. Z. Ou, T. Daeneke, M. S. Strano, M. Pumera, S. L. Gras, *Adv. Funct. Mater.* **2015**, *25*, 5086.
[19] F. Wang, D. Banerjee, Y. Liu, X. Chen, X. Liu, *Analyst* **2010**, *135*, 1839.
[20] W. C. W. Chan, D. J. Maxwell, X. Gao, R. E. Bailey, M. Han, S. Nie, *Curr. Opin. Biotechnol.* **2002**, *13*, 40.
[21] D. Bera, L. Qian, T.-K. Tseng, P. H. Hollway, *Materials* **2010**, *3*, 2260.
[22] Y. Shirasaki, G. J. Supran, M. G. Bawendi, V. Bulovic, *Nat. Photonics* **2013**, *7*, 13.
[23] M. A. Hines, P. Guyot-Sionnest, *J. Phys. Chem.* **1996**, *100*, 468.
[24] H. Zhu, M. Z. Hu, L. Shao, K. Yu, R. Dabestani, Md. B. Zaman, S. Liao, *J. Nanomater.* **2014**, *2014*, 324972.
[25] S. Hinds, S. Myrskog, L. Levina, G. Koleilat, J. Yang, S. O. Kelley, E. H. Sargent, *J. Am. Chem. Soc.* **2007**, *129*, 7218.
[26] X. Michalet, F. F. Pinaud, L. A. Bentolilla, J. M. Tsay, S. Doose, J. J. Li, G. Sundaresan, A. M. Wu, S. S. Gambhir, S. Weiss, *Science* **2005**, *307*, 538.
[27] M. Bruchez Jr., M. Moronne, P. Gin, S. Weiss, A. P. Alivisatos, *Science* **1998**, *281*, 2013.
[28] I. L. Medintz, H. T. Uyeda, E. R. Goldman, H. Mattoussi, *Nat. Mater.* **2005**, *4*, 435.
[29] C. B. Murray, D. J. Norris, M. G. Bawendi, *J. Am. Chem. Soc.* **1993**, *115*, 8706.
[30] B. O. Dabbousi, J. Rodriguez-Viejo, F. V. Mikulec, J. R. Heine, H. Mattoussi, R. Ober, K. F. Jensen, M. G. Bawendi, *J. Phys. Chem. B* **1997**, *101*, 9463.
[31] K. Susumu, H. T. Uyeda, I. L. Medintz, T. Pons, J. B. Delehanty, H. Mattoussi, *J. Am. Chem. Soc.* **2007**, *129*, 13987.
[32] D. Gerion, F. Pinaud, S. C. Williams, W. J. Parak, D. Zanchet, S. Weiss, A. P. Alivisatos, *J. Phys. Chem. B* **2001**, *105*, 8851.
[33] X. Wu, H. Liu, J. Liu, K. N. Haley, J. A. Treadway, J. P. Larson, N. Ge, F. Peale, M. P. Bruchez, *Nat. Biotechnol.* **2003**, *21*, 41.
[34] D. J. Bharali, D. W. Lucey, H. Jayakumar, H. E. Pudavar, P. N. Prasad, *J. Am. Chem. Soc.* **2005**, *127*, 11364.
[35] X. Gao, Y. Cui, R. M. Levenson, L. W. K. Chung, S. Nie, *Nat. Biotechnol.* **2004**, *22*, 969.
[36] P. K. Chattopadhyay, D. A. Price, T. F. Harper, M. R. Betts, J. Yu, E. Gostick, S. P. Perfetto, P. Goepfert, R. A. Koup, S. C. De Rosa, M. P. Bruchez, M. Roederer, *Nat. Med.* **2006**, *12*, 972.
[37] D. Geißler, L. J. Charbonnière, R. F. Ziessel, N. G. Butlin, H.-G. Löhmannsröben, N. Hildebrandt, *Angew. Chem., Int. Ed.* **2010**, *49*, 1396.
[38] J. L. Stein, E. A. Mader, B. M. Cossairt, *J. Phys. Chem. Lett.* **2016**, *7*, 1315.
[39] A. M. Dertus, W. C. W. Chan, S. N. Bhatia, *Nano Lett.* **2004**, *4*, 11.
[40] M. Bottrill, M. Green, *Chem. Commun.* **2011**, *47*, 7039.
[41] P. J. Sadler, M. Bottrill, M. Green, *Adv. Inorg. Chem.* **1991**, *36*, 1.
[42] J. W. Sigler, G. B. Bluhm, H. Duncan, J. T. Sharp, D. C. Ensign, W. R. McCrum, *Ann. Intern. Med.* **1974**, *80*, 21.
[43] M. Faraday, *Philos. Trans. R. Soc. London* **1857**, *147*, 145.
[44] E. Hutter, J. H. Fendler, *Adv. Mater.* **2004**, *16*, 1685.
[45] D. A. Giljohann, D. S. Seferos, W. L. Daniel, M. D. Massich, P. C. Patel, C. A. Mirkin, *Angew. Chem., Int. Ed.* **2010**, *49*, 3280.
[46] M.-C. Daniel, D. Astruc, *Chem. Rev.* **2004**, *104*, 293.
[47] T. Niidome, M. Yamagata, Y. Okamoto, Y. Akiyama, H. Takahashi, T. Kawano, Y. Katayama, Y. Niidome, *J. Controlled Release* **2006**, *114*, 343.
[48] H. Xu, X. Mao, Q. Zeng, S. Wang, A.-N. Kawde, G. Liu, *Anal. Chem.* **2009**, *81*, 669.

[49] A. G. Tkachenko, H. Xie, D. Coleman, W. Glomm, J. Ryan, M. F. Anderson, S. Franzen, D. L. Feldheim, *J. Am. Chem. Soc.* **2003**, *125*, 4700.
[50] X.-M. Jiang, L.-M. Wang, J. Wang, C.-Y. Chen, *Appl. Biochem. Biotechnol.* **2012**, *166*, 1533.
[51] J. Turkevich, P. C. Stevenson, J. Hillier, *Discuss. Faraday Soc.* **1951**, *11*, 55.
[52] G. Frens, *Nat. Phys. Sci.* **1973**, *241*, 20.
[53] M. Brust, M. Walker, D. Bethell, D. J. Schiffrin, R. Whyman, *J. Chem. Soc., Chem. Commun.* **1994**, 801.
[54] P. N. Njoki, I.-I. S. Lim, D. Mott, H.-Y. Park, B. Khan, S. Mishra, R. Sujakumar, J. Luo, C.-J. Zhong, *J. Phys. Chem. C* **2007**, *111*, 14664.
[55] J. Liu, Y. Lu, *J. Am. Chem. Soc.* **2003**, *125*, 6642.
[56] I. H. El-Sayed, X. Huang, M. A. El-Sayed, *Nano Lett.* **2005**, *5*, 829.
[57] X. Huang, P. K. Jain, I. H. El-Sayed, M. A. El-Sayed, *Nanomedicine* **2007**, *2*, 681.
[58] N. R. Jana, L. Gearheart, C. J. Murphy, *Adv. Mater.* **2001**, *13*, 1389.
[59] B. Nikoobakht, M. A. El-Sayed, *Chem. Mater.* **2003**, *15*, 1957.
[60] X. Huang, M. A. El-Sayed, *J. Adv. Res.* **2010**, *1*, 13.
[61] X. Huang, I. H. El-Sayed, W. Qian, M. A. El-Sayed, *J. Am. Chem. Soc.* **2006**, *128*, 2115.
[62] I. Pastoriza-Santos, R. A. Alvarez-Puebla, L. M. Liz-Marzán, *Eur. J. Inorg. Chem.* **2010**, *2010*, 4288.
[63] Y. Zhai, J. S. DuChene, Y.-C. Wang, J. Qiu, A. C. Johnston-Peck, B. You, W. Guo, B. DiCiaccio, K. Qian, E. W. Zhao, F. Ooi, D. Hu, D. Su, E. A. Stach, Z. Zhu, W. D. Wei, *Nat. Mater.* **2016**, *15*, 889.
[64] C. Wang, C. Kan, J. Zhu, X. Zeng, X. Wang, H. Li, D. Shi, *J. Nanomater.* **2010**, 969030.
[65] Y. Shao, Y. Jin, S. Dong, *Chem. Commun.* **2004**, 1104.
[66] J. Chen, D. Wang, J. Xi, L. Au, A. Siekkinen, A. Warsen, Z.-Y. Li, H. Zhang, Y. Xia, X. Li, *Nano Lett.* **2007**, *7*, 1318.
[67] J. You, G. Zhang, C. Li, *ACS Nano* **2010**, *4*, 1033.
[68] S. Preciado-Flores, D. Wang, D. A. Wheeler, R. Newhouse, J. K. Hensel, A. Schwartzberg, L. Wang, J. Zhu, M. Barboza-Flores, J. Z. Zhang, *J. Mater. Chem.* **2011**, *21*, 2344.
[69] A. M. Schwartzberg, T. Y. Olson, C. E. Talley, J. Z. Zhang, *J. Phys. Chem. B* **2006**, *110*, 19935.
[70] J. Chen, M. Yang, Q. Zhang, E. C. Cho, C. M. Cobley, C. Kim, C. Glaus, L. V. Wang, M. J. Welch, Y. Xia, *Adv. Funct. Mater.* **2010**, *20*, 3684.
[71] J. Chen, F. Saeki, B. J. Wiley, H. Cang, M. J. Cobb, Z.-Y. Li, L. Au, H. Zhang, M. B. Kimmey, X. Li, Y. Xia, *Nano Lett.* **2005**, *5*, 473.
[72] H. W. Kroto, J.R. Heath, S. C. O'Brien, R. F. Curl, R. E. Smalley, *Nature* **1985**, *318*, 162.
[73] S. Iijima, *Nature* **1991**,*354*, 56.
[74] K. S. Novoselov, A. K. Geim, S. V. Morozov, D. Jiang, Y. Zhang, S. V. Dubonos, I. V. Grigorieva, A. A. Firsov, *Science* **2004**, *306*, 666.
[75] S. N. Baker, G. A. Baker, *Angew. Chem., Int. Ed.* **2010**, *49*, 6726.
[76] V. N. Mochalin, O. Shenderova, D. Ho, Y. Gogotsi, *Nat. Nanotechnol.* **2012**, *7*, 11.
[77] Z. Liu, S. Tabakman, K. Welsher, H. J. Dai, *Nano Res.* **2009**, *2*, 85.
[78] Y. Liang, Y. Li, H. Wang, H. Dai, *J. Am. Chem. Soc.* **2013**, *135*, 2013.
[79] H. L. Wang, H. J. Dai, *Chem. Soc. Rev.* **2013**, *42*, 3088.
[80] G. Otero, G. Biddau, C. Sánchez-Sánchez, R. Caillard, M. F. López, C. Rogero, F. J. Palomares, N. Cabello, M. A. Basanta, J. Ortega, J. Méndez, A. M. Echavarren, R. Pérez, B. Gómez-Lor, J. A. Martín-Gago, *Nature* **2008**, *454*, 865.
[81] A. Bianco, M. Maggini, G. Scorrano, C. Toniolo, G. Marconi, C. Villani, M. Prato, *J. Am. Chem. Soc.* **1996**, *118*, 4072.
[82] M. Brettreich, A. Hirsch, *Tetrahedron Lett.* **1998**, *39*, 2731.
[83] T. Andersson, K. Nilsson, M. Sundahl, G. Westman, O. Wennerstrom, *J. Chem. Soc., Chem. Commun.* **1992**, 604.
[84] J. Jeong, J. Jung, M. Choi, J. W. Kim, S. J Chung, S. Lim, H. Lee, B. H. Chung, *Adv. Mater.* **2012**, *24*, 1999.
[85] J. Bernholc, D. Brenner, M. B. Nardelli, V. Meunier, C. Roland, *Annu. Rev. Mater. Res.* **2002**, *32*, 347.
[86] T. Guo, P. Nikolaev, A. G. Rinzler, D. Tomanek, D. T. Colbert, R. E. Smalley, *J. Phys. Chem.* **1995**, *99*, 10694.
[87] O. Smiljanic, B. L. Stansfield, J. P. Dodelet, A. Serventi, S. Désilets, *Chem. Phys. Lett.* **2002**, *356*, 189.
[88] N. Ishigami, H. Ago, K. Imamoto, M. Tsuji, K. Iakoubovskii, N. Minami, *J. Am. Chem. Soc.* **2008**, *130*, 9918.
[89] M. S. Dresselhaus, G. Dresselhaus, P. C. Eklund, *Science of Fullerenes and Carbon Nanotubes*, Academic Press, San Francisco, CA **1996**, p. 761.
[90] J. W. G. Wildoer, L. C. Venema, A. G. Rinzler, R. E. Smalley, C. Dekker, *Nature* **1998**, *391*, 59.
[91] T. W. Odom, J. L. Huang, P. Kim, C. M. Lieber, *Nature* **1998**, *391*, 62.
[92] M. J. O'Connell, S. M. Bachilo, C. B. Huffman, V. C. Moore, M. S. Strano, E. H. Haroz, K. L. Rialon, P. J. Boul, W. H. Noon, C. Kittrell, J. P. Ma, R. H. Hauge, R. B. Weisman, R. E. Smalley, *Science* **2002**, *297*, 593.
[93] A. M. Smith, M. C. Mancini, S. M. Nie, *Nat. Nanotechnol.* **2009**, *4*, 710.
[94] J. T. Robinson, K. Welsher, S. M. Tabakman, S. P. Sherlock, H. L. Wang, R. Luong, H. J. Dai, *Nano Res.* **2010**, *3*, 779.
[95] T. Murakami, H. Nakatsuji, M. Inada, Y. Matoba, T. Umeyama, M. Tsujimoto, S. Isoda, M. Hashida, H. Imahori, *J. Am. Chem. Soc.* **2012**, *134*, 17862.
[96] K. Welsher, S. P. Sherlock, H. J. Dai, *Proc. Natl. Acad. Sci. USA* **2011**, *108*, 8943.
[97] G. S. Hong, J. C. Lee, J. T. Robinson, U. Raaz, L. M. Xie, N. F. Huang, J. P. Cooke, H. J. Dai, *Nat. Med.* **2012**, *18*, 1841.
[98] K. Welsher, Z. Liu, S. P. Sherlock, J. T. Robinson, Z. Chen, D. Daranciang, H. J. Dai, *Nat. Nanotechnol.* **2009**, *4*, 773.
[99] Z. Liu, A. C. Fan, K. Rakhra, S. Sherlock, A. Goodwin, X. Y. Chen, Q. W. Yang, D. W. Felsher, H. J. Dai, *Angew. Chem., Int. Ed.* **2009**, *48*, 7668.
[100] Z. Liu, X. M. Sun, N. Nakayama-Ratchford, H. J. Dai, *ACS Nano* **2007**, *1*, 50.
[101] Z. Liu, K. Chen, C. Davis, S. Sherlock, Q. Z. Cao, X. Y. Chen, H. J. Dai, *Cancer Res.* **2008**, *68*, 6652.
[102] Y. Liu, Y. Zhao, B. Sun, C. Chen, *Acc. Chem. Res.* **2013**, *46*, 702.
[103] M. Lotya, Y. Hernandez, P. J. King, R. J. Smith, V. Nicolosi, L. S. Karlsson, F. M. Blighe, S. De, Z. M. Wang, I. T. McGovern, G. S. Duesberg, J. N. Coleman, *J. Am. Chem. Soc.* **2009**, *131*, 3611.
[104] S. Park, R. S. Ruoff, *Nat. Nanotechnol.* **2009**, *4*, 217.
[105] L. Y. Jiao, L. Zhang, X. R. Wang, G. Diankov, H. J. Dai, *Nature* **2009**, *458*, 877.
[106] D. V. Kosynkin, A. L. Higginbotham, A. Sinitskii, J. R. Lomeda, A. Dimiev, B. K. Price, J. M. Tour, *Nature* **2009**, *458*, 872.
[107] K. S. Kim, Y. Zhao, H. Jang, S. Y. Lee, J. M. Kim, K. S. Kim, J. H. Ahn, P. Kim, J. Y. Choi, B. H. Hong, *Nature* **2009**, *457*, 706.
[108] D. L. Ma, Y. F. Zhang, M. X. Liu, Q. Q. Ji, T. Gao, Y. Zhang, Z. F Liu, *Nano Res.* **2013**, *6*, 671.
[109] J. M. Cai, P. Ruffieux, R. Jaafar, M. Bieri, T. Braun, S. Blankenburg, M. Muoth, A. P. Seitsonen, M. Saleh, X. L. Feng, K. Mullen, *Nature* **2010**, *466*, 470.
[110] K. Nakada, M. Fujita, G. Dresselhaus, M. S. Dresselhaus, *Phys. Rev. B* **1996**, *54*, 17954.
[111] K. I. Bolotin, K. J. Sikes, Z. Jiang, M. Klima, G. Fudenberg, J. Hone, P. Kim, H. L. Stormer, *Solid State Commun.* **2008**, *146*, 351.
[112] X. Du, I. Skachko, A. Barker, E. Y. Andrei, *Nat. Nanotechnol.* **2008**, *3*, 491.
[113] E. Pop, V. Varshney, A. K. Roy, *MRS Bull.* **2012**, *37*, 1273.
[114] K. S. Novoselov, Z. Jiang, Y. Zhang, S. V. Morozov, H. L. Stormer, U. Zeitler, J. C. Maan, G. S. Boebinger, P. Kim, A. K. Geim, *Science* **2007**, *315*, 1379.

[115] J. Z. Shang, L. Ma, J. W. Li, W. Ai, T. Yu, G. G. Gurzadyan, *Sci. Rep.* **2012**, *2*, 792.
[116] X. M. Sun, Z. Liu, K. Welsher, J. T. Robinson, A. Goodwin, S. Zaric, H. J. Dai, *Nano Res.* **2008**, *1*, 203.
[117] M. A. Patel, H. Yang, P. L. Chiu, D. D. T. Mastrogiovanni, C. R. Flach, K. Savaram, L. Gomez, A. Hemnarine, R. Mendelsohn, E. Garfunkel, H. B. Jiang, H. X. He, *ACS Nano* **2013**, *7*, 8147.
[118] K. Yang, S. A. Zhang, G. X. Zhang, X. M. Sun, S. T. Lee, Z.A. Liu, *Nano Lett.* **2010**, *10*, 3318.
[119] J. T. Robinson, S. M. Tabakman, Y. Y. Liang, H. L. Wang, H. S. Casalongue, D. Vinh, H. J. Dai, *J. Am. Chem. Soc.* **2011**, *133*, 6825.
[120] R. Romero-Aburto, T. N. Narayanan, Y. Nagaoka, T. Hasumura, T. M. Mitcham, T. Fukuda, P. J. Cox, R. R. Bouchard, T. Maekawa, D. S. Kumar, S. V. Torti, S. A. Mani, P. M. Ajayan, *Adv. Mater.* **2013**, *25*, 5632.
[121] K. Yang, J. M. Wan, S. Zhang, B. Tian, Y. J. Zhang, Z. Liu, *Biomaterials* **2012**, *33*, 2206.
[122] H. T. Li, Z. H. Kang, Y. Liu, S. T. Lee, *J. Mater. Chem.* **2012**, *22*, 24230.
[123] X. Y. Xu, R. Ray, Y. L. Gu, H. J Ploehn, L. Gearheart, K. Raker, W. A. Scrivens, *J. Am. Chem.Soc.* **2004**, *126*, 12736.
[124] Y. P. Sun, B. Zhou, Y. Lin, W. Wang, K. A. S. Fernando, P. Pathak, M. J. Meziani, B. A. Harruff, X. Wang, H. F. Wang, P. J. G Luo, H Yang, M. E. Kose, B. L. Chen, L. M. Veca, S. Y. Xie, *J. Am. Chem. Soc.* **2006**, *128*, 7756.
[125] Q. L. Zhao, Z. L. Zhang, B. H. Huang, J. Peng, M. Zhang, D. W. Pang, *Chem. Commun.* **2008**, 5116.
[126] J. G. Zhou, C Booker, R. Y. Li, X. T. Zhou, T. K. Sham, X. L Sun, Z. F. Ding, *J. Am. Chem. Soc.* **2007**, *129*, 744.
[127] C. J. Liu, P. Zhang, F. Tian, W. C. Li, F. Li, W. G. Liu, *J. Mater. Chem.* **2011**, *21*, 13163.
[128] Z. C. Yang, M. Wang, A. M. Yong, S. Y. Wong, X. H. Zhang, H. Tan, A. Y. Chang, X. Li, J. Wang, *Chem. Commun.* **2011**, *47*, 11615.
[129] W. Kwon, G. Lee, S. Do, T. Joo, S. Rhee, *Small* **2014**, *10*, 506.
[130] X. Yan, X. Cui, L. S. Li, *J. Am. Chem. Soc.* **2010**, *132*, 5944.
[131] S. L. Hu, K. Y. Niu, J. Sun, J. Yang, N. Q. Zhao, X. W. Du, *J. Mater. Chem.* **2009**, *19*, 484.
[132] J. Peng, W. Gao, B. K. Gupta, Z. Liu, R. Romero-Aburto, L. H. Ge, L. Song, L. B. Alemany, X. B. Zhan, G. H. Gao, S. A. Vithayathil, B. A. Kaipparettu, A. A. Marti, T. Hayashi, J. J. Zhu, P. M. Ajayan, *Nano Lett.* **2012**, *12*, 844.
[133] Y. Park, J. Yoo, B. Lim, S. Rhee, W. Kwon, *J. Mater. Chem. A* **2016**, *4*, 11582.
[134] W. Kwon, Y. H. Kim, J.-H. Kim, T. Lee, S. Do, Y. Park, M. S. Jeong, T.-W. Lee, S.-W. Rhee, *Sci. Rep.* **2016**, *6*, 24205.
[135] L. B. Tang, R. B. Ji, X. K. Cao, J. Y. Lin, H. X. Jiang, X. M. Li, K. S. Teng, C. M. Luk, S. J. Zeng, J. H. Hao, S. P. Lau, *ACS Nano* **2012**, *6*, 5102.
[136] L. B. Tang, R. B. Ji, X. M. Li, G. X. Bai, C. P. Liu, J. H. Hao, J. Y. Lin, H. X. Jiang, K. S. Teng, Z. B. Yang, S. P. Lau, *ACS Nano* **2014**, *8*, 6312.
[137] M. Nurunnabi, Z. Khatun, G. R. Reeck, D. Y. Lee, Y. K. Lee, *Chem. Commun.* **2013**, *49*, 5079.
[138] S. J. Zhu, J. H. Zhang, S. J. Tang, C. Y. Qiao, L. Wang, H. Y. Wang, X. Liu, B. Li, Y. F. Li, W. L. Yu, X. F. Wang, H. C. Sun, B. Yang, *Adv. Funct. Mater.* **2012**, *22*, 4732.
[139] J. Tang, B. Kong, H. Wu, M. Xu, Y. C. Wang, Y. L. Wang, D. Y. Zhao, G. F. Zheng, *Adv. Mater.* **2013**, *25*, 6569.
[140] L. Cao, X. Wang, M. J. Meziani, F. S. Lu, H. F. Wang, P. J. G. Luo, Y. Lin, B. A. Harruff, L. M. Veca, D. Murray, S. Y. Xie, Y. P. Sun, *J. Am. Chem. Soc.* **2007**, *129*, 11318.
[141] Q. Liu, B. D. Guo, Z. Y. Rao, B. H. Zhang, J. R. Gong, *Nano Lett.* **2013**, *13*, 2436.
[142] A. Salinas-Castillo, M. Ariza-Avidad, C. Pritz, M. Camprubi-Robles, B. Fernandez, M. J. Ruedas-Rama, A. Megia-Fernandez, A. Lapresta-Fernandez, F. Santoyo-Gonzalez, A. Schrott-Fischer, L. F. Capitan-Vallvey, *Chem. Commun.* **2013**, *49*, 1103.
[143] P. Huang, J. Lin, X. S. Wang, Z. Wang, C. L. Zhang, M. He, K. Wang, F. Chen, Z. M. Li, G. X. Shen, D. X. Cui, X. Y. Chen, *Adv. Mater.* **2012**, *24*, 5104.
[144] Z. M. Markovic, B. Z. Ristic, K. M. Arsikin, D. G. Klisic, L. M. Harhaji-Trajkovic, B. M. Todorovic-Markovic, D. P. Kepic, T. K. Kravic-Stevovic, S. P. Jovanovic, M. M. Milenkovic, D. D. Milivojevic, V. Z. Bumbasirevic, M. D. Dramicanin, V. S. Trajkovic, *Biomaterials* **2012**, *33*, 7084.
[145] M. Thakur, S. Pandey, A. Mewada, V. Patil, M. Khade, E. Goshi, M. Sharon, *J. Drug Delivery* **2014**, *2014*, 282193.
[146] A. Gruber, A. Drabenstedt, C. Tietz, L. Fleury, J. Wrachtrup, C. von Borczyskowski, *Science* **1997**, *276*, 2012.
[147] I. Aharonovich, A. D. Greentree, S. Prawer, *Nat. Photonics* **2011**, *5*, 397.
[148] S. J. Yu, M. W. Kang, H. C. Chang, K. M. Chen, Y. C. Yu, *J. Am. Chem. Soc.* **2005**, *127*, 17604.
[149] T. Gaebel, I. Popa, A. Gruber, M. Domhan, F. Jelezko, J. Wrachtrup, *New J. Phys.* **2004**, *6*, 98.
[150] A. Krueger, Y. J. Liang, G. Jarre, J. Stegk, *J. Mater. Chem.* **2006**, *16*, 2322.
[151] Y. R. Chang, H. Y. Lee, K. Chen, C. C. Chang, D. S. Tsai, C. C. Fu, T. S. Lim, Y. K. Tzeng, C. Y. Fang, C. C. Han, H. C. Chang, W. Fann, *Nat. Nanotechnol.* **2008**, *3*, 284.
[152] X. Q. Zhang, R. Lam, X. Y. Xu, E. K. Chow, H. J. Kim, D. Ho, *Adv. Mater.* **2011**, *23*, 4770.
[153] E. K. Chow, X. Q. Zhang, M. Chen, R. Lam, E. Robinson, H. J. Huang, D. Schaffer, E. Osawa, A. Goga, D. Ho, *Sci. Transl. Med.* **2011**, *3*, 73ra21.
[154] Q. W. Zhang, V. N. Mochalin, I. Neitzel, I. Y. Knoke, J. J. Han, C. A. Klug, J. G. Zhou, P. I. Lelkes, Y. Gogotsi, *Biomaterials* **2011**, *32*, 87.
[155] W. Wei, C. Xu, L. Wu, J. Wang, J. Ren, X. Qu, *Sci. Rep.* **2014**, *4*, 3564.
[156] A. Cossu, A. M. Posadino, R. Giordo, C. Emanueli, A. M. Sanguinetti, A. Piscopo, M. Poiana, G. Capobianco, A. Piga, G. Pintus, *PLoS One* **2012**, *7*, e48817.
[157] X. Wang, Y. Zhang, C. Zhi, X. Wang, D. Tang, Y. Xu, Q. Weng, X. Jiang, M. Mitome, D. Golberg, Y. Bando, *Nat. Commun.* **2013**, *4*, 2905.
[158] H. Wang, A. M. Jenner, C.-Y. J. Lee, G. Shui, S. Y. Tang, M. Whiteman, M. R. Wenk, B. Halliwell, *Free Radical Res.* **2007**, *41*, 479.
[159] J. A. Vignoli, D. G. Bassoli, M. T. Benassi, *Food Chem.* **2011**, *124*, 863.
[160] S. I. F. S. Martins, W. M. F. Jongen, M. A. J. S. V. Boekel, *Trends Food Sci. Technol.* **2001**, *11*, 364.
[161] S. Pastoriza, J. A. Rufian-Henares, *Food Chem.* **2014**, *164*, 438.
[162] B. Radisavljevic, A. Radenovic, J. Brivio, V. Giacometti, A. Kis. *Nat. Nanotechnol.* **2011**, *6*, 147.
[163] Z. Zeng, T. Sun, J. Zhu, X. Huang, Z. Yin, G. Lu, Z. Fan, Q. Yan, H. H. Hng, H. Zhang, *Angew. Chem., Int. Ed.* **2012**, *51*, 9052.
[164] Z. Zeng, Z. Yin, X. Huang, H. Li, Q. He, G. Lu, F. Body, H. Zhang, *Angew. Chem., Int. Ed.* **2011**, *50*, 11093.
[165] M. Xu, T. Liang, M. Shi, H. Chen, *Chem. Rev.* **2013**, *113*, 3766.
[166] J. He, K. Hummer, C. Franchini, *Phys. Rev. B* **2014**, *89*, 1.
[167] G. Yang, C. Zhu, D. Du, Y. Lin, *Nanoscale* **2015**, *7*, 14217.
[168] H. Li, J. Wu, Z. Yin, H. Zhang, *Acc. Chem. Res.* **2014**, *47*, 1067.
[169] S. S. Chou, B. Kaehr, J. Kim, B. M. Foley, M. De, P. E. Hopkins, J. Huang, C. J. Brinker, V. P. Dravid, *Angew. Chem., Int. Ed.* **2013**, *52*, 4160.

[170] J. N. Coleman, M. Lotya, A. O. Neill, S. D. Bergin, P. J. King, U. Khan, K. Young, A. Gaucher, S. De, R. J. Smith, I. V Shvets, S. K. Arora, G. Stanton, H. Kim, K. Lee, G. T. Kim, G. S. Duesberg, T. Hallam, J. J. Boland, J. J. Wang, J. F. Donegan, J. C. Grunlan, G. Moriarty, A. Shmeliov, R. J. Nicholls, J. M. Perkins, E. M. Grieveson, K. Theuwissen, D. W. Mccomb, P. D. Nellist, V. Nicolosi, *Science* **2011**, *331*, 568.
[171] D. Gopalakrishnan, D. Damien, M. M. Shaijumon, *ACS Nano* **2014**, *5*, 5297.
[172] S. Xu, D. Li, P. Wu, *Adv. Funct. Mater.* **2015**, *25*, 1127.
[173] B. L. Li, L. X. Chen, H. L. Zou, J. L. Lei, H. Q. Luo, N. B. Li, *Nanoscale* **2014**, *6*, 9831.
[174] R. J. Smith, P. J. King, M. Lotya, C. Wirtz, U. Khan, S. De, A. O. Neill, G. S. Duesberg, J. C. Grunlan, G. Moriarty, J. Chen, J. Wang, A. I. Minett, V. Nicolosi, J. N. Coleman, *Adv. Funct. Mater.* **2011**, *23*, 3944.
[175] H. R. Gutie, N. Perea-lo, A. Laura, A. Berkdemir, B. Wang, M. Terrones, *Nano Lett.* **2013**, *13*, 3447.
[176] A. Splendiani, L. Sun, Y. Zhang, T. Li, J. Kim, C. Chim, G. Galli, F. Wang, *Nano Lett.* **2010**, *10*, 1271.
[177] A. Ramasubramaniam, D. Naveh, E. Towe, *Phys. Rev. B* **2011**, *84*, 205325.
[178] Q. H. Wang, K. Kalantar-zadeh, A. Kis, J. N. Coleman, M. S. Strano, *Nat. Nanotechnol.* **2012**, *7*, 699.
[179] R. Severin, A. Mu, C. Janowitz, R. Manzke, T. Bo, *Phys. Rev. B* **2001**, *64*, 1.
[180] H. Lin, C. Wang, J. Wu, Z. Xu, Y. Huang, C. Zhang, *New J. Chem.* **2015**, *39*, 8492.
[181] L. Lin, Y. Xu, S. Zhang, I. M. Ross, A. C. M. Ong, D. A. Allwood, *ACS Nano* **2013**, *9*, 8214.
[182] C. Tan, H. Zhang, *Chem. Soc. Rev.* **2015**, *44*, 2713.
[183] D.-E. Lee, H. Koo, I.-C. Sun, J. H. Ryu, K. Kim, I. C. Kwon, *Chem. Soc. Rev.* **2012**, *41*, 2656.
[184] W. Yin, L. Yan, J. Yu, G. Tian, L. Zhou, X. Zheng, X. Zhang, *ACS Nano* **2014**, *8*, 6922.
[185] L. Cheng, J. Liu, X. Gu, H. Gong, X. Shi, T. Liu, C. Wang, X. Wang, G. Liu, H. Xing, W. Bu, B. Sun, Z. Liu, *Adv. Mater.* **2014**, *26*, 1886.
[186] Z. Zhang, J. Wang, C. Chen, *Adv. Mater.* **2013**, *25*, 3869.
[187] L. Cheng, C. Yuan, S. Shen, X. Yi, H. Gong, K. Yang, Z. Liu, *ACS Nano* **2015**, *9*, 11090.
[188] S. S. Chou, B. Kaehr, J. Kim, B. M. Foley, M. De, P. E. Hopkins, J. Huang, C. J. Brinker, V. P. Dravid, *Angew. Chem., Int. Ed.* **2013**, *125*, 4254.
[189] T. Liu, S. Shi, C. Liang, S. Shen, L. Cheng, C. Wang, X. Song, S. Goel, T. E. Barnhart, W. Cai, Z. Liu, *ACS Nano* **2015**, *9*, 950.
[190] H. S. Jung, W. H. Kong, D. K. Sung, M. Lee, S. E. Beack, D. H. Keum, K. S. Kim, S. H. Yun, S. K. Hahn, *ACS Nano* **2014**, *8*, 260.
[191] W. Z. Teo, E. L. K. Chng, Z. Sofer, M. Pumera, *Chem. Eur. J.* **2014**, *20*, 9627.
[192] S. S. Chou, M. De, J. Kim, S. Byun, C. Dykstra, J. Yu, J. Huang, V. P. Dravid, *J. Am. Chem. Soc.* **2013**, *135*, 4584.
[193] W. T. Cong, Z. Tang, X. G. Zhao, J. H. Chu, *Sci. Rep.* **2015**, *5*, 9361.
[194] M. Chhowalla, H. S. Shin, G. Eda, L. Li, K. P. Loh, H. Zhang, *Nat. Chem.* **2013**, *5*, 263.
[195] F. Zhang, *Photon Upconversion Nanomaterials*, Springer Verlag, Berlin **2015**, p. 1.
[196] H. Dong, L. D. Sun, C. H. Yan, *Nanoscale* **2013**, *5*, 5703.
[197] N. Bloembergen, *Phys. Rev. Lett.* **1959**, *2*, 84.
[198] G. Chen, H. Qiu, P. N. Prasad, X. Chen, *Chem. Rev.* **2014**, *114*, 5161.
[199] S. Wang, L. Zhang, C. Dong, L. Su, H. Wang, J. Chang, *Chem. Commun.* **2015**, *51*, 406.
[200] M. Haase, H. Schäfer, *Angew. Chem., Int. Ed.* **2011**, *50*, 5808.
[201] B. Zhou, B. Shi, D. Jin, X. Liu, *Nat. Nanotechnol.* **2015**, *10*, 924.
[202] K. Binnemans, *Chem. Rev.* **2009**, *109*, 4283.
[203] M. K. Gnanasammandhan, N. M. Idris, A. Bansal, K. Huang, Y. Zhang, *Nat. Protoc.* **2016**, *11*, 688.
[204] S. Hao, G. Chen, C. Yang, *Theranostics* **2013**, *3*, 331.
[205] Y. Ma, M. Chen, M. Li, *Mater. Lett.* **2014**, *139*, 22.
[206] S. Heer, K. Kompe, H. U. Gudel, M. Haase, *Adv. Mater.* **2004**, *16*, 2102.
[207] G. Blasse, B. C. Grabmaier, *Luminescent Materials*, Springer Verlag, Berlin **1994**, p. 1.
[208] K. W. Kramer, D. Biner, G. Frei, H. U. Gudel, M. P. Hehlen, S. R. Luthi, *Chem. Mater.* **2004**, *16*, 1244.
[209] A. Aebischer, M. Hostettler, J. Hauser, K. Kramer, T. Weber, H. U. Gudel, H. B. Burgi, *Angew. Chem., Int. Ed.* **2006**, *118*, 2869.
[210] R. Deng, F. Qin, R. Chen, W. Huang, M. Hong, X. Liu, *Nat. Nanotechnol.* **2015**, *10*, 237.
[211] G. Tian, Z. Gu, L. Zhou, W. Yin, X. Liu, L. Yan, S. Jin, W. Ren, G. Xing, S. Li, Y. Zhao, *Adv. Mater.* **2012**, *24*, 1226.
[212] X. Huang, P. K. Jain, I. H. El-Sayed, M. A. El-Sayed, *Lasers Med. Sci.* **2008**, *23*, 217.
[213] S. Wang, K. J. Chen, T. H. Wu, H. Wang, W. Y. Lin, M. Ohashi, P. Y. Chiou, H. R. Tseng, *Angew. Chem., Int. Ed.* **2010**, *49*, 3777.
[214] J. Oh, H. Yoon, J. H. Park, *Biomed. Eng. Lett.* **2013**, *3*, 67.
[215] E. B. Ehlerding, F. Chen, W. Cai, *Adv. Sci.* **2016**, *3*, 1500223.
[216] X. Sun, Z. Liu, K. Welsher, J. T. Robinson, A. Goodwin, S. Zaric, H. Dai, *Nano Res.* **2008**, *1*, 203.
[217] C. Wang, H. Tao, L. Cheng, Z. Liu, *Biomaterials* **2011**, *32*, 6145.
[218] R. Y. Tsien, *FEBS Lett.* **2005**, *579*, 927.
[219] M. Funovics, R. Weissleder, C. H. Tung, *Anal. Bioanal. Chem.* **2003**, *377*, 956.
[220] R. K. Jain, L. L. Munn, D. Fukumura, *Nat. Rev. Cancer* **2002**, *2*, 266.
[221] T. M. Ragan, H. Huang, P. T. C. So, *Methods Enzymol.* **2003**, *361*, 481.
[222] L. Möckl, D. C. Lamb, C. Bräuchle, *Angew. Chem., Int. Ed.* **2014**, *53*, 13972.
[223] D. J. Webb, C. M. Brown, *Methods Mol. Biol.* **2013**, *931*, 29.
[224] B. Huang, M. Bates, X. Zhuang, *Annu. Rev. Biochem.* **2009**, *78*, 993.
[225] Y.-F. Kang, Y.-H. Li, Y.-W. Fang, Y. Xu, X.-M. Wei, X.-B. Yin, *Sci. Rep.* **2015**, *5*, 11835.
[226] C. Liu, P. Zhang, X. Zhai, F. Tian, W. Li, J. Yang, Y. Liu, H. Wang, W. Wang, W. Liu, *Biomaterials* **2012**, *33*, 3604.
[227] R. Liu, D. Wu, S. Liu, K. Koynov, W. Knoll, Q. Li, *Angew. Chem.* **2009**, *121*, 4668.
[228] H. S. Mader, P. Kele, S. M. Saleh, O. S. Wolfbeis, *Curr. Opin. Chem. Biol.* **2010**, *14*, 582.
[229] G. Chen, J. Shen, T. Y. Ohulchanskyy, N. J. Patel, A. Kutikov, Z. Li, J. Song, R. K. Pandey, H. Ågren, P. N. Prasad, G. Han, *ACS Nano* **2012**, *6*, 8280.
[230] M. Nyk, R. Kumar, T. Y. Ohulchanskyy, E. J. Bergey, P. N. Prasad, *Nano Lett.* **2008**, *8*, 3834.
[231] M. Wang, C.-C. Mi, W.-X. Wang, C.-H. Liu, Y.-F. Wu, Z-.R. Xu, C.-B. Mao, S.-K. Xu, *ACS Nano* **2009**, *3*, 1580.
[232] M. Wang, C. Mi, Y. Zhang, J. Liu, F. Li, C. Mao, S. Xu, *J. Phys. Chem. C* **2009**, *113*, 19021.
[233] F. Helmchen, W. Denk, *Nat. Methods* **2005**, *2*, 932.
[234] P. T. So, C. Y. Dong, B. R. Masters, K. M. Berland, *Annu. Rev. Biomed. Eng.* **2000**, *2*, 399.
[235] P.-Y. Lin, C.-W. Hsieh, M.-L. Kung, S. Hsieha, *Sci. Rep.* **2013**, *3*, 1703.
[236] A. F. Fradkov, Y. Chen, L. Ding, E. V. Barsova, M. V. Matz, S. A. Lukyanov, *FEBS Lett.* **2000**, *479*, 127.
[237] J. D. Orth, R. H. Kohler, F. Foijer, P. K. Sorger, R. Weissleder, T. J. Mitchison, *Cancer Res.* **2011**, *71*, 4608.
[238] T.-M. Liu, J. Conde, T. Lipiński, A. Bednarkiewicz, C.-C. Huang, *NPG Asia Mater.* **2016**, *8*, e295.

[239] J. Wang, Z. H. Zhang, S. Zha, Y. Y. Zhu, P. Y. Wu, B. Ehrenberg, J. Y. Chen, *Biomaterials* **2014**, *35*, 9372.
[240] X. D. Zhang, H. X. Wang, H. Wang, Q. Zhang, J. F. Xie, Y. P. Tian, J. Wang, Y. Xie, *Adv. Mater.* **2014**, *26*, 4438.
[241] B. B. Wang, Y. F. Wang, H. Wu, X. J. Song, X. Guo, D. M. Zhang, X. J. Ma, M. Q. A. Tan, *RSC Adv.* **2014**, *4*, 49960.
[242] G. Tong, J. Wang, R. Wang, X. Guo, L. He, F. Qiu, G. Wang, B. Zhu, X. Zhu, T. Liu, *J. Mater. Chem. B* **2015**, *3*, 700.
[243] B. Kong, A. Zhu, C. Ding, X. Zhao, B. Li, Y. Tian, *Adv. Mater.* **2012**, *24*, 5844.
[244] R. A. Farrer, F. L. Butterfield, V. W. Chen, J. T. Fourkas, *Nano Lett.* **2005**, *5*, 1139.
[245] M. B. Dowling, L. Li, J. Park, G. Kumi, A. Nan, H. Ghandehari, J. T. Fourkas, P. DeShong, *Bioconjgate Chem.* **2010**, *21*, 1968.
[246] H. Wang, T. B. Huff, D. A. Zweifel, W. He, P. S. Low, A. Wei, J. X. Cheng, *Proc. Natl. Acad. Sci. USA* **2005**, *102*, 15752.
[247] X. Qu, J. Wang, Z. Zhang, N. Koop, R. Rahmanzadeh, G. Hüttmann, *J. Biomed. Opt.* **2008**, *13*, 031217.
[248] D. Nagesha, G. S. Laevsky, P. Lampton, R. Banyal, C. Warner, C. DiMarzio, S. Sridhar, *Int. J. Nanomed.* **2007**, *2*, 813.
[249] J. Park, A. Estrada, K. Sharp, K. Sang, J. A. Schwartz, D. K. Smith, C. Coleman, J. D. Payne, B. A. Korgel, A. K. Dunn, J. W. Tunnell, *Opt. Express* **2008**, *16*, 1590.
[250] C. G. England, J. S. Huang, K. T. James, G. Zhang, A. M. Gobin, H. B. Frieboes, *PLoS One* **2015**, *10*, e0129172.
[251] S. Motamedi, T. Shilagard, K. Edward, L. Koong, S. Qui, G. Vargas, *Biomed. Opt. Express* **2011**, *2*, 1194.
[252] K. Svoboda, R. Yasuda, *Neuron* **2006**, *50*, 823.
[253] V. Pavlov, Y. Xiao, B. Shlyahovsky, I. Willner, *J. Am. Chem. Soc.* **2004**, *126*, 11768.
[254] J. Liu, Y. Lu, *Angew. Chem., Int. Ed.* **2005**, *45*, 90.
[255] P. K. Jain, X. Huang, I. H. El-Sayed, M. A. El-Sayed, *Plasmonics* **2007**, *2*, 107.
[256] K.-S. Lee, M. A. El-Sayed, *J. Phys. Chem. B* **2006**, *110*, 19220.
[257] J. Homola, S. S. Yee, G. Gauglitz, *Sens. Actuators, B* **1999**, *54*, 3.
[258] L. J. Sherry, R. Jin, C. A. Mirkin, G. C. Schatz, R. P. Van Duyne, *Nano Lett.* **2006**, *6*, 2060.
[259] C. R. Yonzon, E. Jeoung, S. Zou, G. C. Schatz, M. Mrksich, R. P. Van Duyne, *J. Am. Chem. Soc.* **2004**, *126*, 12669.
[260] P. Zijlstra, P. M. R. Paulo, M. Orrit, *Nat. Nanotechnol.* **2012**, *7*, 379.
[261] S. L. Kleinman, R. R. Frontiera, A.-I. Henry, J. A. Dieringer, R. P. Van Duyne, *Phys. Chem. Chem. Phys.* **2013**, *15*, 21.
[262] D. Cialla, A. März, R. Böhme, F. Theil, K. Weber, M. Schmitt, J. Popp, *Anal. Bioanal. Chem.* **2012**, *403*, 27.
[263] G. Braun, I. Pavel, A. R. Morrill, D. S. Seferos, G. C. Bazan, N. O. Reich, M. Moskovits, *J. Am. Chem. Soc.* **2007**, *129*, 7760.
[264] I. Al-Ogaidi, H. Gou, A. K. A. Al-kazaz, Z. P. Aguilar, A. K. Melconian, P. Zheng, N. Wu, *Anal. Chim. Acta* **2014**, *811*, 76.
[265] Y. He, S. Su, T. Xu, Y. Zhong, J. A. Zapien, J. Li, C. Fan, S.-T. Lee, *Nano Today* **2011**, *6*, 122.
[266] Z. Wu, Y. Liu, X. Zhou, A. Shen, J. Hu, *Biosens. Bioelectron.* **2013**, *44*, 10.
[267] L. Fabris, M. Dante, G. Braun, S. J. Lee, N. O. Reich, M. Moskovits, T.-Q. Nguyen, G. C. Bazan, *J. Am. Chem. Soc.* **2007**, *129*, 6086.
[268] Y. Wang, K. Lee, J. Irudayaraj, *Chem. Commun.* **2010**, *46*, 613.
[269] M.-Y. Lee, S.-J. Park, K. Park, K. S. Kim, H. Lee, S. K. Hahn, *ACS Nano* **2011**, *5*, 6138.
[270] X. Huang, I. H. El-Sayed, W. Qian, M. A. El-Sayed, *Nano Lett.* **2007**, *7*, 1591.
[271] J. Ando, K. Fujita, N. I. Smith, S. Kawata, *Nano Lett.* **2011**, *11*, 5344.
[272] Y. Zhang, J. Qian, D. Wang, Y. Wang, S. He, *Angew. Chem., Int. Ed.* **2013**, *52*, 1148.
[273] E. M. Strohm, M. J. Moore, M. C. Kolios, *IEEE J. Sel. Top. Quantum Electron.* **2016**, *22*, 137.
[274] J. Xia, L. V. Wang, *IEEE Trans. Biomed. Eng.* **2014**, *61*, 1380.
[275] L.V. Wang, S. Hu, *Science* **2012**, *23*, 1458.
[276] D. Wu, L. Huang, M. S. Jiang, H. Jiang, *Int. J. Mol. Sci.* **2014**, *15*, 23616.
[277] S. Mallidi, G. P. Luke, S. Emelianov, *Trends Biotechnol.* **2011**, *29*, 213.
[278] T. A. El-Brolossy, T. Abdallah, M. B. Mohamed, S. Abdallah, K. Easawi, S. Negm, H. Talaat, *Eur. Phys. J.: Spec. Top.* **2008**, *153*, 361.
[279] Y. Wang, X. Xie, X. Wang, G. Ku, K. L. Gill, D. P. O'Neal, G. Stoica, L. V. Wang, *Nano Lett.* **2004**, *4*, 1689.
[280] Q. Zhang, N. Iwakuma, P. Sharma, B. M. Moudgil, C. Wu, J. McNeill, H. Jiang, S. R. Grobmyer, *Nanotechnology* **2009**, *20*, 395102.
[281] X. Yang, S. E. Skrabalak, Z.-Y. Li, Y. Xia, L. V. Wang, *Nano Lett.* **2007**, *7*, 3798.
[282] A. Agarwal, S. W. Huang, M. O'Donnell, K. C. Day, M. Day, N. Kotov, S. Ashkenazi, *J. Appl. Phys.* **2007**, *102*, 064701.
[283] K. Kim, S.-W. Huang, S. Ashkenazi, M. O'Donnell, A. Agarwal, N. A. Kotov, M. F. Denny, M. J. Kaplan, *Appl. Phys. Lett.* **2007**, *90*, 223901.
[284] P.-C. Li, C.-R. C. Wang, D.-B. Shieh, C.-W. Wei, C.-K. Liao, C. Poe, S. Jhan, A.-A Ding, Y.-N. Wu, *Opt. Express* **2008**, *16*, 18605.
[285] C. Kim, E. C. Cho, J. Chen, K. H. Song, L. Au, C. Favazza, Q. Zhang, C. M. Cobley, F. Gao, Y. Xia, L. V. Wang, *ACS Nano* **2010**, *4*, 4559.
[286] H. Lee, J. H. Lee, J. Kim, J. H. Mun, J. Chung, H. Koo, C. Kim, S. H. Yun, S. K. Hahn, *ACS Appl. Mater. Interfaces* **2016**, *8*, 32202.
[287] M. Pramanik, M. Swierczewska, D. Green, B. Sitharaman, L. V. Wang, *J. Biomed. Opt.* **2009**, *14*, 034018.
[288] A. D. L. Zerda, C. Zavaleta, S. Keren, S. Vaithilingam, S. Bodapati, Z. Liu, J. Levi, B. R. Smith, T.-J. Ma, O. Oralkan, Z. Cheng, X. Chen, H. Dai, B. T. Khuri-Yakub, S. S. Gambhir, *Nat. Nanotechnol.* **2008**, *3*, 557.
[289] C. Wang, X. Ma, S. Ye, L. Cheng, K. Yang, L. Guo, C. Li, Y. Li, Z. Liu, *Adv. Funct. Mater.* **2012**, *22*, 2363.
[290] L. Xiang, Y. Yuan, D. Xing, Z. Ou, S. Yang, F. Zhou, *J. Biomed. Opt.* **2008**, *13*, 021008.
[291] G. Lalwani, X. Caib, L. Nieb, L. V. Wang, B. Sitharaman, *Photoacoustics* **2013**, *1*, 62.
[292] Z. Sheng, L. Song, J. Zheng, D. Hu, M. He, M. Zheng, G. Gao, P. Gong, P. Zhang, Y. Ma, L. Cai, *Biomaterials* **2013**, *34*, 5236.
[293] Z.-H. Miao, H. Wang, H. Yang, Z. Li, L. Zhen, C.-Y. Xu, *ACS Appl. Mater. Interfaces* **2016**, *8*, 15904.
[294] T. Zhang, H. Cui, C.-Y. Fang, L.-J. Su, S. Ren, H.-C. Chang, X. Yang, M. L. Forrest, *J. Biomed. Opt.* **2013**, *18*, 026018.
[295] C. Lee, W. Kwon, S. Beack, D. Lee, Y. Park, H. Kim, S. K. Hahn, S.-W. Rhee, C. Kim, *Theranostics* **2016**, *6*, 2196.
[296] X. Qian, S. Shen, T. Liu, L. Cheng, Z. Liu, *Nanoscale* **2015**, *7*, 6380.
[297] J. W. Fisher, S. Sarkar, C. F. Buchanan, C. S. Szot, H. C. Hatcher, S. V Torti, C. G. Rylander, N. Rylander, N. Carolina, *Cancer Res.* **2010**, *70*, 9855.
[298] H. Huang, S. Barua, G. Sharma, S. K. Dey, K. Rege, *J. Controlled Release* **2011**, *155*, 344.
[299] C. Loo, A. Lowery, N. Halas, J. West, R. Drezek, *Nano Lett.* **2005**, *5*, 709.
[300] N. Wong, S. Kam, M. O. Connell, J. A. Wisdom, H. Dai, *Proc. Natl. Acad. Sci. USA* **2005**, *102*, 10600.
[301] J. U. Menon, P. Jadeja, P. Tambe, K. Vu, B. Yuan, K. T. Nguyen, *Theranostics* **2013**, *3*, 152.
[302] J. Li, F. Jiang, B. Yang, X. Song, Y. Liu, H. Yang, D. Cao, W. Shi, G. Chen, *Sci. Rep.* **2013**, *3*, 1998.

[303] L. Cheng, K. Yang, Y. Li, J. Chen, C. Wang, M. Shao, S. T. Lee, Z. Liu, *Angew. Chem., Int. Ed.* **2011**, *123*, 7523.
[304] L. Cheng, C. Wang, Z. Liu, *Nanoscale* **2013**, *5*, 13.
[305] S. Link, M. A. El-sayed, *Int. Rev. Phys. Chem.* **2000**, *19*, 409.
[306] W. Kuo, Y. Chang, K. Cho, K. Chiu, C. Lien, C. Yeh, S. Chen, *Biomaterials* **2012**, *33*, 3270.
[307] R. Guo, L. Zhang, H. Qian, R. Li, X. Jiang, B. Liu, *Langmuir* **2010**, *26*, 5428.
[308] M. R. McDevitt, D. Chattopadhyay, B. J. Kappel, J. S. Jaggi, S. R. Schiffman, C. Antczak, J. T. Njardarson, R. Brentjens, D. A. Scheinberg, *J. Nucl. Med.* **2007**, *48*, 1180.
[309] B. Dong, S. Xu, J. Sun, S. Bi, D. Li, X. Bai, Y. Wang, L. Wang, H. Song, *J. Mater. Chem.* **2011**, *21*, 6193.
[310] S. S. Lucky, K. C. Soo, Y. Zhang, *Chem. Rev.* **2015**, *115*, 1990.
[311] M. Ethiraja, Y. Chen, P. Joshi, R. K. Pandey, *Chem. Soc. Rev.* **2011**, *40*, 340.
[312] J. Ge, M. Lan, B. Zhou, W. Liu, L. Guo, H. Wang, Q. Jia, G. Niu, X. Huang, H. Zhou, X. Meng, P. Wang, C.-S. Lee, W. Zhang, X. Han, *Nat. Commun.* **2014**, *5*, 4596.
[313] A. K. Mandal, T. Sashin, M. Liu, J. S. Lindsey, D. F. Bocian, D. Holten, *New J. Chem.* **2016**, *40*, 9648.
[314] A. Bjorgan, M. Milanic, L. L. Randeberg, *J. Biomed. Opt.* **2014**, *19*, 0660030.
[315] R. R. Allison, C. H. Sibata, *Photodiagn. Photodyn. Ther.* **2010**, *7*, 61.
[316] A. Juzeniene, Q. Peng, J. Moan, *Photochem. Photobiol. Sci.* **2007**, *6*, 1234.
[317] D. Maitra, J. S. Elenbaas, S. E. Whitesall, V. Basrur, L. G. D'Alecy, M. B. Omary, *J. Biol. Chem.* **2015**, *290*, 23711.
[318] J. C. Kennedy, R. H. Pottier, *Photochem. Photobiol. B* **1992**, *14*, 275.
[319] A. C. Samia, X. Chen, C. Burda, *J. Am. Chem. Soc.* **2003**, *125*, 15736.
[320] S. Beack, W. H. Kong, H. S. Jung, I. H. Do, S. Han, H. Kim, K. S. Kim, S. H. Yun, S. K. Hahn, *Acta Biomater.* **2015**, *26*, 295.
[321] D. E. Dolmans, D. Fukumura, R. K. Jain, *Nat. Rev. Cancer* **2003**, *3*, 380.
[322] Y. Cheng, J. D. Meyers, A. M. Broome, M. E. Kenney, J. P. Basilion, C. Burda, *J. Am. Chem. Soc.* **2011**, *133*, 2583.
[323] B. Jang, J.-Y. Park, C.-H. Tung, I.-H. Kim, Y. Choi, *ACS Nano* **2011**, *5*, 1086.
[324] L. Gao, J. Fei, J. Zhao, H. Li, Y. Cui, J. Li, *ACS Nano* **2012**, *6*, 8030.
[325] P. Huang, C. Xu, J. Lin, C. Wang, X. Wang, C. Zhang, X. Zhou, S. Guo, D. Cui, *Theranostics* **2011**, *1*, 240.
[326] L. Jia, L. Ding, J. Tian, L. Bao, Y. Hu, H. Ju, J.-S. Yu, *Nanoscale* **2015**, *7*, 15953.
[327] S. Cui, H. Chen, H. Zhu, J. Tian, X. Chi, Z. Qian, S. Achilefu, Y. Gu, *J. Mater. Chem.* **2012**, *22*, 4861.
[328] Q. C. Xu, Y. Zhang, M. J. Tan, S. Yuan, C. Choong, N. S. Tan, T. T. Y. Tan, *Adv. Healthcare Mater.* **2012**, *1*, 470.
[329] F. Zhang, V. Gradinaru, A. R. Adamantidis, R. Durand, R. D. Airan, L. Lecea, K. Deisseroth, *Nat. Protoc.* **2010**, *5*, 439.
[330] L. Luo, E. M. Callaway, K. Svoboda, *Neuron* **2008**, *57*, 634.
[331] J. J. Mancuso, J. Kim, S. Lee, S. Tsuda, N. B. H. Chow, G. J. Augustine, *Exp. Physiol.* **2010**, *96*, 26.
[332] J. S. Treger, M. F. Priest, F. Bezanilla, *eLife* **2015**, *4*, e10482.
[333] M. Hausser, *Nat. Methods* **2014**, *11*, 1012.
[334] A. M. Packer, B. Roska, M. Hausser, *Nat. Neurosci.* **2013**, *16*, 805.
[335] V. Busskamp, S. Picaud, J. A. Sahel, B. Roska, *Gene Ther.* **2012**, *19*, 169.
[336] V. Busskamp, J. Duebel, D. Balya, M. Fradot, T. J. Viney, S. Siegert, A. C. Groner, E. Cabuy, V. Forster, M. Seeliger, M. Biel, P. Humphries, M. Paques, S. M. Said, D. Trono, K. Deisseroth, J. A. Sahel, S. Picaud, B. Roska, *Science* **2010**, *329*, 413.
[337] P. S. Lagali, D. Balya, G. B. Awatramani, T. A. Münch, D. S. Kim, V. Busskamp, C. L. Cepko, B. Roska, *Nat. Neurosci.* **2008**, *11*, 667.
[338] X. Liu, S. Ramirez, P. T. Pang, C. B. Puryear, A. Govindarajan, K. Deisseroth, S. Tonegawa, *Nature* **2012**, *484*, 381.
[339] C. Belzung, M. Turiault, G. Griebel, *Pharmacol. Biochem., Behav.* **2014**, *122*, 144.
[340] A. Peled, *Med. Hypotheses* **2011**, *76*, 914.
[341] Y. Chen, M. Xiong, S. C. Zhang, *Nat. Biotechnol.* **2015**, *33*, 149.
[342] K. Yamamoto, Z. Tanei, T. Hashimoto, T. Wakabayashi, H. Okumo, Y. Naka, O. Yizhar, L. E. Fenno, M. Fukayama, H. Bito, J. R. Cirrito, D. M. Holtzman, K. Deisseroth, T. Iwatsubo, *Cell Rep.* **2015**, *11*, 859.
[343] T. Bruegmann, T. Bremen, C. C. Vogt, T. Send, B. K. Fleischmann, P. Sasse, *Nat. Commun.* **2015**, *6*, 7153.
[344] S. M. Iyer, K. L. Montgomery, C. Towne, S. Y. Lee, C. Ramakrishnan, K. Deisseroth, S. L. Delp, *Nat. Biotechnol.* **2014**, *32*, 274.
[345] K. Huang, Q. Dou, X. J. Loh, *RSC Adv.* **2016**, *6*, 60896.
[346] J. L. Carvalho-de-Souza, J. S. Treger, B. Dang, S. B. Kent, D. R. Pepperberg, F. Bezanilla, *Neuron* **2015**, *86*, 207.
[347] K. Lugo, X. Miao, F. Rieke, L. Y. Lin, *Biomed. Opt. Express* **2012**, *3*, 447.
[348] S. Hososhima, H. Yuasa, T. Ishizuka, M. R. Hoque, T. Yamashita, A. Yamanaka, E. Sugano, H. Tomita, H. Yawo, *Sci. Rep.* **2015**, *5*, 16533.
[349] M. Choi, J. W. Choi, S. Kim, S. Nizamoglu, S. K. Hahn, S. H. Yun, *Nat. Photonics* **2013**, *7*, 987.
[350] S. Nizamoglu, M. C. Gather, M. Humar, M. Choi, S. Kim, K. S. Kim, S. K. Hahn, G. Scarcelli, M. Randolph, R. W. Redmond, S. H. Yun, *Nat. Commun.* **2016**, *7*, 10374.
[351] X.-Z. Cui, Z.-G. Zhou, Y. Yang, J. Wei, J. Wang, M.-W. Wang, H. Yang, Y.-J. Zhang, S.-P. Yang, *Chin. Chem Lett.* **2015**, *26*, 749.
[352] S. Kim, Y.-S. Chen, G. P. Luke, M. Mehrmohammadi, J. R. Cook, S. Y. Emelianov, *IEEE Int. Ultrason. Symp.* **2010**, 233.
[353] J. Xie, S. Lee, X. Chen, *Adv. Drug Delivery Rev.* **2010**, *62*, 1064.
[354] P. Rai, S. Mallidi, X. Zheng, R. Rahmanzadeh, Y. Mir, S. Elrington, A. Khurshid, T. Hasan, *Adv. Drug Delivery Rev.* **2010**, *62*, 1094.
[355] D. V. Volodkin, A. G. Skirtach, H. Möhwald, *Angew. Chem., Int. Ed.* **2009**, *48*, 1807.
[356] K. Yang, L. Hu, X. Ma, S. Ye, L. Cheng, X. Shi, C. Li, Y. Li, Z. Liu, *Adv. Mater.* **2012**, *24*, 1868.
[357] J. Liu, S. Ohta, A. Sonoda, M. Yamada, M. Yamamoto, N. Nitta, K. Murata, Y. Tabata, *J. Controlled Release* **2007**, *117*, 104.
[358] R. R. Letfullin, C. Joenathan, T. F. George, V. P. Zharov, *Nanomedicine* **2006**, *1*, 473.
[359] H. S. Choi, W. Liu, P. Misra, E. Tanaka, J. P. Zimmer, B. I. Ipe, M. G. Bawendi, J. V. Frangioni, *Nat. Biotechnol.* **2007**, *25*, 1165.
[360] C. L. Wong, M. Olivo, *Plasmonics* **2014**, *9*, 809.
[361] F. Ratto, P. Matteini, F. Rossi, R. Pini, N. Tiwari, S.K. Kulkarni, L. Menabuoni, *Proc. SPIE* **2008**, *6844*, 68441V.
[362] G. H. A. Salomao, A. U. Fernandes, M. S. Baptista, J. P. Tardivo, D. M. Christofolini, J. A. Correa, *Lasers Surg. Med.* **2015**, *47*, 421.

